

Flinders University

NATIONAL CENTRE FOR GROUNDWATER RESEARCH AND TRAINING

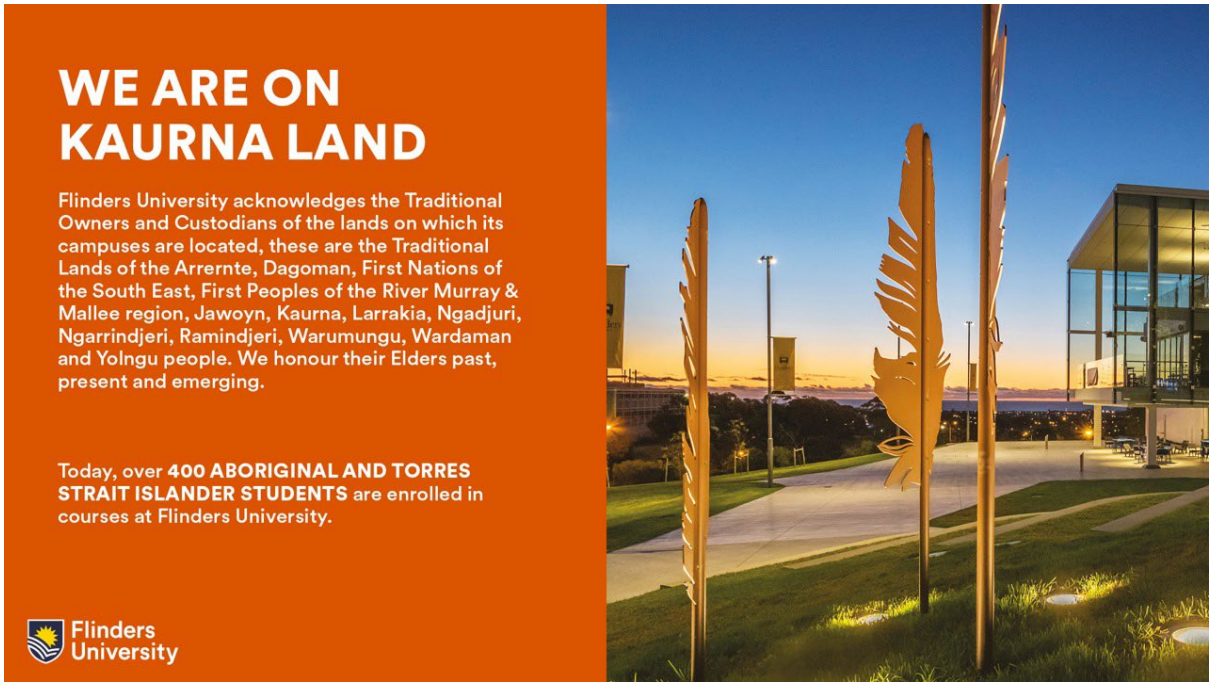
Hydrogeophysical Investigation of the Elliston-Bramfield Groundwater Resource

Aquifer characterisation and seawater intrusion assessment – Final Report

Authors: Eddie Banks, Mike Hatch, Margaret Shanafield and Saskia Noorduijn

Hydrogeophysical Investigation of the Elliston–Bramfield Groundwater Resource
Aquifer characterisation and seawater intrusion assessment – Final Report

Version Number	Date Approved	Approved By	Brief Description
1.0	20/05/2026	Eddie Banks and co−authors	Submitted draft
1.1	18/06/2026	Kent Inverarity and Kate Hyland	Client review
1.2	26/06/2026	Eddie Banks	Final version



ISBN: []

Prepared by: The National Centre for Groundwater Research and Training (NCGRT)
Flinders University
GPO Box 2100
Adelaide SA 5000
+61 8 8201 2193

Copyright: This publication is subject to copyright under the Copyright Act 1968 (Cth). Apart from any use permitted under the Act, no part of this publication may be reproduced, stored, or transmitted in any form or by any means without prior written permission.

Enquiries should be addressed to the National Centre for Groundwater Research and Training, Flinders University.

Disclaimer: This report has been prepared by Flinders University and the National Centre for Groundwater Research and Training and reviewed in accordance with the publication protocols of the South Australian Department for Environment and Water. The report contains independent scientific/technical advice to inform decision−making. The independent findings and recommendations of this report are subject to separate and further consideration and decision−making processes and do not necessarily represent the views of the Australian Government. Flinders University does not warrant or make any representation regarding the use, or results of the use, of the information contained herein about its correctness, accuracy, reliability, currency or otherwise and expressly disclaim all liability or responsibility to any person using the information or advice. Information contained in this document is, to the knowledge of the project partners, correct at the time of writing.To the extent permitted by law, Flinders University (including its employees and consultants) excludes all liability to any person for any consequences arising directly or indirectly from the use of this publication, in whole or in part, and any information or material contained within it.

Citation: Banks, E.W., Hatch, M. A., Shanafield, M. & Noorduijn, S. (2026) Hydrogeophysical Investigation of the Elliston–Bramfield Groundwater Resource. Aquifer characterisation and seawater intrusion assessment – Final Report. Flinders University, South Australia.



Acknowledgements

This work was undertaken as part of the ‘Ensuring water security, economic prosperity and nature positive outcomes for the small coastal township of Elliston’ project. The project is jointly funded by the Australian and South Australian governments, with Australian Government funding provided through the National Water Grid Fund.

A huge thanks to South Australian Department for Environment and Water (DEW) staff Kate Hyland, Christina Fawns, Kent Inverarity, Claire Faulkner and Courtney Sanders for fieldwork assistance and support dragging geophysics gear across the paddocks around Elliston and Bramfield. We are grateful to Kate and Kent for their assessment of the activities throughout the project and review of this final report. Thanks to DEW staff Lara Lanigan, Cameron Wood and Peter Baker, and Eyre Peninsula Landscape Board member Andrew Solomon for providing other hydrogeological data sets and for constructive discussions about the project findings to improve the science to underpin the water allocation planning review. Thanks to Flinders students Phanumat (Aye) Kullaboot, Jan Schultz and Christy Songola for assistance and support in conducting the hydrogeophysics field surveys. Finally, we thank Ian Quinn (Skippy) member of the Eyre Peninsula Landscape Board for his generous contribution towards pre−field logistics, engaging engagement with landholders and collection of water samples. We also thank the local farmers/landholders that provided access to their properties to conduct the surveys.

Executive Summary

As part of the National Water Grid project, ‘Ensuring Water Security, Economic Prosperity and Nature−Positive Outcomes for the Small Coastal Township of Elliston, Eyre Peninsula’, Flinders University was engaged to undertake the acquisition, processing, interpretation, and reporting of hydrogeophysical survey data. The project aimed to spatially map the extent of the Quaternary Limestone aquifer and improve understanding of the subsurface geology and hydrogeology around Elliston and Bramfield. Specifically, the hydrogeophysical investigations targeted: 1) the interface and transition zone between seawater and low−salinity groundwater, including its inland extent and depth from the coast; 2) the depth to basement; and 3) potential locations of submarine groundwater discharge around Waterloo Bay.

Hydrogeophysical datasets were collected during field campaigns undertaken in October and November 2024, and January 2026. Transient electromagnetic (TEM) surveys were conducted to characterise subsurface conductivity variations associated with groundwater salinity and geological structure. Surface nuclear magnetic resonance (sNMR) surveys were also undertaken at selected locations along the TEM transects to directly measure aquifer properties, including water content and saturated porosity, and to estimate hydraulic conductivity within the Quaternary Limestone aquifer. The TEM and sNMR datasets were processed and inverted using computer−based inversion modelling software to generate subsurface conductivity sections and profiles of water content and porosity.

Water quality and geophysical logs from the new groundwater monitoring well, 5830−357 (WAD049), constructed along the Birdseye Highway between Elliston and the SA Water town water supply production bores, reaffirmed the hydrogeophysical survey results that the seawater wedge extends up to 3.2 km inland at an elevation between 20 and 40 metres below the Australian Height Datum (mAHD). In combination with a reinterpretation of existing datasets, these findings have led to an updated conceptual understanding of the Quaternary Limestone aquifer and identified potential risks associated with seawater intrusion to the town water supply production bores.

This Final report summarises the key findings from all hydrogeophysical datasets collected during the field investigations around Elliston and Bramfield. Forward modelling was undertaken to assess the sensitivity of the sTEM profiler system to changes in conductivity with depth, supporting confidence in the TEM method for identifying the transition zone between fresh groundwater (low conductivity) and seawater (high conductivity). The modelling demonstrated the detection limits of the interface between low−salinity groundwater and intruding seawater. Across the 4 conceptual models tested, the interface could be identified when the transition zone was diffuse, but not when it became highly diffuse. To reduce ambiguity in future investigations, it may be beneficial to use additional geophysical methods to improve characterisation of more diffuse seawater interfaces and provide greater depth of investigation. For example, larger size TEM systems with bigger transmitter loops could be employed.

The acquisition of hydrogeophysical data around Elliston and Bramfield has provided valuable insights into the likely location and extent of the seawater interface within the coastal aquifer system. These findings improve the conceptual hydrogeological model of the Quaternary Limestone aquifer, which underpins the current groundwater numerical model. The information can be used for water allocation planning purposes to support the provision of informed management decisions for the low−salinity groundwater lens supplying the Elliston and Bramfield communities.

Table of Contents

Acknowledgements iv
Executive Summary v
List of Tables viii
List of Figures viii
1 Background 1
2 Aims 1
2.1 Specific objectives 2
3 Study site 3
3.1 Local geology and hydrogeology 5
4 Hydrogeophysics surveys 7
4.1 Transient electromagnetic surveys to investigate seawater intrusion 7
4.2 Methods used in this study 8
4.3 Data processing 11
5 Hydrogeophysics survey results and analysis 12
5.1 West–East transect line 1 14
5.2 West–East transect line 2 18
5.3 West–East transect line 3 21
5.4 West–East transect line 4 24
5.5 sTEM conductivity–depth slices 28
5.6 Loupe and sTEM data summary 32
5.7 TEM and downhole geophysical logs from 5830–357 (WAD049) 33
5.8 sNMR data summary 37
6 Forward TEM modelling 41
6.1 Forward modelling overview 41
6.2 Forward modelling results 44
6.3 Analysis of forward modelling results 44
7 Coastal groundwater discharge at Waterloo Bay 52
7.1 Surveys 52
7.2 Water levels 52
7.3 Loupe 53
7.4 Electrical conductivity 55
7.5 Radon–222 58

7.6 Physical observations and thermal imagery 60
8 Discussion 62
8.1 Spatial extent of low salinity groundwater within the Quaternary Limestone aquifer . 62
8.2 Location of the interface between seawater and groundwater 62
8.2.1 Forward modelling 63
8.3 Locations of submarine groundwater discharge around Waterloo Bay 64
9 Conclusions 66
9.1 Future recommendations 67
10 References 69
11 Appendix A 72
12 Appendix B 83

List of Tables

Table 1. Summary statistics of the estimated saturated hydraulic conductivity from the sNMR data for sites 2 to 16 and geometric mean across all sites. The saturated thickness of the aquifer is estimated from the depth of the watertable to the depth of resolution of the sNMR for all sites 40
Table 2. TEM forward models for the 4 conceptual models (Very sharp, Sharp, Diffuse, Very diffuse) – Scenario 1 42
Table 3. TEM forward models for the 4 conceptual models (Very sharp, Sharp, Diffuse, Very diffuse) – Scenario 2 43
Table 4. Water quality of groundwater seep at Elliston Jetty, ocean water, and Elliston groundwater pond 60

List of Figures

Figure 1. Salinity trends in groundwater wells constructed in the Quaternary Limestone aquifer near Elliston and Bramfield (modified from DEW, 2022) 3
Figure 2. Location map of all the hydrogeophysics surveys around the township of Elliston and Bramfield 4
Figure 3. Simplified cross section of the Elliston−Bramfield low salinity lens (modified from Evans 2002) 6
Figure 4. Case studies of seawater intrusion investigations around Australia (from Lawrie et al. 2012) 7
Figure 5. Seventeen Eyre Peninsula−based AEM data sets collected mostly for mining exploration. (Figure 21 from Ley−Cooper et al. 2015) 8
Figure 6. Loupe system in action near Elliston, January 2026 9
Figure 7. sTEM profiler in action at Elliston, November 2024 10
Figure 8. sNMR survey being conducted near Birdseye Highway, Elliston, January 2026 10
Figure 9. Location map of selected data sets from the hydrogeophysics surveys around the township of Elliston. White lines are the 4 West−East transects 13
Figure 10. Loupe conductivity–depth section along West−East transect 1. Transparent shading represents the depth of investigation. Grey line is the RMSE. Black crosses on location map represent 1,000 m distances along the line 15
Figure 11. sTEM conductivity–depth section along West−East transect 1. Transparent shading represents the depth of investigation. Grey dots are the RMSE. Black crosses on location map represent 1,000 m distances along the line 16
Figure 12. sNMR profile at Site 3, 491400mE along West−East transect 1 showing water content and estimated hydraulic conductivity (m/d). Depth of resolution is ≈32 m. Estimated depth to water is ≈10 m. The FID (free induction decay) is the NMR signal measured right after excitation, and its T2 (transverse relaxation time) reflects how quickly that signal decays 17
Figure 13. Loupe conductivity–depth section along West−East transect 2. Transparent shading represents the depth of investigation. Grey line is the RMSE. Black crosses on location map represent the 1,000 m distances along the line 19
Figure 14. sTEM conductivity− depth section along West−East transect 2. Transparent shading represents the depth of investigation. Grey dots are the RMSE. Black crosses on location map represent the 1,000 m distances along the line 20

Figure 15. sNMR profile at Site 2, 491300mE along West−East transect 2 showing water content and estimated hydraulic conductivity (m/d) using a conductivity model from the Loupe data adjacent to the site. Depth of resolution is ≈17 m and estimated depth to the water table is ≈2.5 mbgl 21
Figure 16. Loupe conductivity–depth section along West−East transect 3. Transparent shading represents the depth of investigation. Grey line is the RMSE. Black crosses on location map represent the 1,000 m distances along the line 22
Figure 17. sTEM conductivity− depth section along West−East transect 3. Transparent shading represents the depth of investigation. Grey dots are the RMSE. Black crosses on location map represent the 1,000 m distances along the line 23
Figure 18. sNMR profile at Site 14, 491300mE at the western end of West−East transect 3 showing water content and estimated hydraulic conductivity (m/d) using a conductivity model from the Loupe data adjacent to the site. Depth of resolution is ≈28 m and estimated depth to the water table is ≈2 mbgl 24
Figure 19. Loupe conductivity− depth section along West−East transect 4. Transparent shading represents the depth of investigation. Grey line is the RMSE. Black crosses on location map represent the 1,000 m distances along the line 25
Figure 20. sTEM conductivity− depth section along West−East transect 4. Transparent shading represents the depth of investigation. Grey dots are the RMSE. Black crosses on location map represent the 1,000 m distances along the line 26
Figure 21. sNMR at Site 16, located at 491500mE, ≈ 100m north of groundwater monitoring well 5830−357 (WAD049) (SWL 3.27 28/11/25), located on the road verge of Birdseye Highway showing water content and estimated hydraulic conductivity (m/d) using a conductivity model from the Loupe data adjacent to the site. Depth of resolution is ≈28 m and estimated depth to the water table is ≈3 mbgl 27
Figure 22. sTEM conductivity depth−slices at 30, 25, 20, 15, 10, 5 mAHD 29
Figure 23. sTEM conductivity depth−slices at 0, -5, -10, -15, -20, -25 mAHD 30
Figure 24. sTEM conductivity depth−slices at -30, -35, -40, -45, -50, -55 mAHD 31
Figure 25. Map showing the likely extent of seawater intrusion (red hatching) near Elliston, SA 32
Figure 26. Geophysical log of groundwater monitoring well 5830−357 (WAD049), with geological log and formation interpretation added on right 35
Figure 27. Comparison of inverted sTEM measurements adjacent to 5830−357 (WAD049). Station 254 sits immediately adjacent to the well. Station 184 is ≈90 m south of the well and to the west (reflecting conductive conditions related to the seawater wedge), Station 179 is ≈90 m south−east of the well (reflecting conductive conditions related to the transition zone), Station 160 is further upgradient within the toe and station 150 is upgradient of the toe of the wedge. Note that the conductivity scale is linear 36
Figure 28. Comparison of geophysical borehole logs from 5830−357 (WAD049) with adjacent sTEM, Loupe and sNMR data sets 37
Figure 29. sNMR inversions at Site 16 comparing a resistive (top panel) and conductive (bottom panel) earth model 38
Figure 30. Whisker plots showing the water content for bound water (bw), mobile water (mw) and total water (tw) content (porosity) for all the sNMR sites 39
Figure 31. Estimated saturated hydraulic conductivity from the sNMR inversion results for sites 2 to 16 40
Figure 32. Scenario 1: Modelling results of the 4 different conceptual models of the seawater intrusion interface (very sharp, sharp, diffuse, and very diffuse) at 30 m depth. Left

plot in each subfigure shows inverted results in blue and starting model in orange. Horizontal line is the depth of investigation. Right plot in each subfigure shows model fit 46
Figure 33. Scenario 2: Modelling results of the 4 different conceptual models of the seawater intrusion interface (very sharp, sharp, diffuse, and very diffuse) at 30 m depth. Left plot in each subfigure shows inverted results in blue and starting model in orange. Horizontal line is the depth of investigation. Right plot in each subfigure shows model fit 47
Figure 34. Scenario 1: Modelled response at each tested depth of the seawater intrusion interface for the 4 conceptual models. Note that the 100 m target depth forward and inverted modelling results is not presented in Appendix A because at this depth there was minor difference between the conceptual models..... 48
Figure 35. Scenario 2: Modelled response at each tested depth of the seawater intrusion interface for the four conceptual models. Note that the 80,90 and 100 m target depth forward and inverted modelling results is not presented in Appendix A because at these depths there was minor difference between the conceptual models 49
Figure 36. Scenario 1: Forward modelling results of the 4 conceptual models using a top layer conductivity of 200 mS/m and target layer of 3000 mS/m, with seawater interface at 30 m depth 50
Figure 37. Scenario 2: Forward modelling results of the four conceptual models using a top layer conductivity of 200 mS/m and target layer of 750 mS/m, with seawater interface at 30 m depth..... 50
Figure 38. Scenario 2 shows an expanded view of the diffuse conceptual model. The contour lines show where the seawater interface should be based on the forward model with a target depth of 30 m for the seawater 51
Figure 39. Measured water levels in Waterloo Bay at 6−min intervals from a pressure transducer secured to the Elliston Jetty 25−29 November (blue points) with a 12−point average fitted (black line). Bureau of Meteorology tidal predictions for Elliston over the same period (red points) 53
Figure 40. Loupe EM survey at low tide, Waterloo Bay..... 53
Figure 41. Loupe EM conductivity depth−section (North–South), east of jetty, Waterloo Bay, Elliston at low tide, 26 Nov 2024. Note that the conductivity scale range is 20−2,000 mS/m to improve the contrast..... 54
Figure 42. Loupe EM conductivity depth−section (West–East), west of jetty, Waterloo Bay, Elliston at low tide, 26 Nov 2024. Note that the conductivity scale range is 20−2,000 mS/m to improve the contrast..... 54
Figure 43. Loupe EM conductivity depth−section (North–South) survey from highway to beach, Elliston, 27 Nov 2024. Note that the conductivity scale range is 2−2,000 mS/m 55
Figure 44. Loupe EM conductivity depth−section (West–East) survey from beach to highway, Elliston, 27 Nov 2024. Note that the conductivity scale range is 2−2,000 mS/m 55
Figure 45. EC Fieldscout used to identify low salinity hotspots in the intertidal zone to a depth of 0.35 m 56
Figure 46. Using the EC Fieldscout and the Trimble Catalyst GNSS RTK to locate groundwater discharge during low tide, Waterloo Bay..... 57
Figure 47. EC Fieldscout sample locations along Waterloo Bay at low tide 27−29 November 2024 58
Figure 48. Radon−222 and water quality survey to identify potential submarine groundwater discharge within Waterloo Bay 59
Figure 49. Radon−222 survey of the nearshore, Waterloo Bay, 28 November 2024 59

Figure 50. Close up image of a groundwater seep beneath the Elliston jetty 61
Figure 51. Close−up thermal image of a groundwater seep beneath the Elliston jetty 61
Figure 52. Scenario 1: Modelling results of the four different conceptual models of the seawater intrusion interface (very sharp, sharp, diffuse, and very diffuse) at 40 m depth. Left plot in each subfigure shows inverted results in blue and starting model in orange. Horizontal line is the depth of investigation. Right plot in each subfigure shows model fit 73
Figure 53. Scenario 1: Modelling results of the four different conceptual models of the seawater intrusion interface (very sharp, sharp, diffuse, and very diffuse) at 50 m depth. Left plot in each subfigure shows inverted results in blue and starting model in orange. Horizontal line is the depth of investigation. Right plot in each subfigure shows model fit 74
Figure 54. Scenario 1: Modelling results of the four different conceptual models of the seawater intrusion interface (very sharp, sharp, diffuse, and very diffuse) at 60 m depth. Left plot in each subfigure shows inverted results in blue and starting model in orange. Horizontal line is the depth of investigation. Right plot in each subfigure shows model fit. 75
Figure 55. Scenario 1: Modelling results of the four different conceptual models of the seawater intrusion interface (very sharp, sharp, diffuse, and very diffuse) at 70 m depth. Left plot in each subfigure shows inverted results in blue and starting model in orange. Horizontal line is the depth of investigation. Right plot in each subfigure shows model fit 76
Figure 56. Scenario 1: Modelling results of the four different conceptual models of the seawater intrusion interface (very sharp, sharp, diffuse, and very diffuse) at 80 m depth. Left plot in each subfigure shows inverted results in blue and starting model in orange. Horizontal line is the depth of investigation. Right plot in each subfigure shows model fit 77
Figure 57. Scenario 1: Modelling results of the four different conceptual models of the seawater intrusion interface (very sharp, sharp, diffuse, and very diffuse) at 90 m depth. Left plot in each subfigure shows inverted results in blue and starting model in orange. Horizontal line is the depth of investigation. Right plot in each subfigure shows model fit 78
Figure 58. Scenario 2: Modelling results of the four different conceptual models of the seawater intrusion interface (very sharp, sharp, diffuse, and very diffuse) at 40 m depth. Left plot in each subfigure shows inverted results in blue and starting model in orange. Horizontal line is the depth of investigation. Right plot in each subfigure shows model fit 79
Figure 59. Scenario 2: Modelling results of the four different conceptual models of the seawater intrusion interface (very sharp, sharp, diffuse, and very diffuse) at 50 m depth. Left plot in each subfigure shows inverted results in blue and starting model in orange. Horizontal line is the depth of investigation. Right plot in each subfigure shows model fit 80
Figure 60. Scenario 2: Modelling results of the four different conceptual models of the seawater intrusion interface (very sharp, sharp, diffuse, and very diffuse) at 60 m depth. Left plot in each subfigure shows inverted results in blue and starting model in orange. Horizontal line is the depth of investigation. Right plot in each subfigure shows model fit 81
Figure 61. Scenario 2: Modelling results of the four different conceptual models of the seawater intrusion interface (very sharp, sharp, diffuse, and very diffuse) at 70 m depth. Left

plot in each subfigure shows inverted results in blue and starting model in orange. Horizontal line is the depth of investigation. Right plot in each subfigure shows model fit 82

1 Background

Coastal townships in South Australia that are not connected to the regional water supply network are particularly vulnerable to water security issues. In many instances, these townships rely on low salinity groundwater that is stored in shallow aquifers. These aquifers have a finite storage, and groundwater levels have continued to decline due to decreasing rainfall recharge exacerbated by the impacts of climate change and groundwater demand.

The Elliston township on the Eyre Peninsula is sourcing its water supply from the Bramfield low salinity lens with SA Water extracting about 65 to 70 megalitres per year of groundwater since 1974 (DEWNR, 2016). The groundwater resources of this region are under a water allocation plan (WAP), which is currently under review by the Eyre Peninsula Landscape Board with the assistance of the Department for Environment and Water to ensure the long−term sustainability of the groundwater resource to meet competing demands.

It is critical to understand the quantity of groundwater available from these shallow aquifers on the Eyre Peninsula to ensure long−term supply for the community, but the quality of the groundwater, for example salinity, is also important. Many of the aquifer systems along the coast are impacted by seawater intrusion and groundwater extraction can increase the extent and rate of intruding seawater, which can lead to an increase in salinity of the groundwater supply.

Research is needed to assess the long−term sustainability of the Elliston and Bramfield groundwater resource under changing climate conditions, including its capacity to meet competing demands from cultural water needs, water−dependent ecosystems, and non−licensed users. The findings from this research effort will help inform whether a climate−independent water source is required to secure future potable water supply.

2 Aims

As part of the National Water Grid project: ‘Ensuring water security, economic prosperity and nature positive outcomes for the small coastal township of Elliston, Eyre Peninsula’ Flinders University was engaged to deliver data acquisition, processing, interpretation and reporting of hydrogeophysics surveys to spatially map the base and extent of the Quaternary Limestone aquifer and improve understanding of the subsurface geology and hydrogeology around Elliston and Bramfield.

The aims of this project are to spatially map the potential risk to the Elliston and Bramfield communities’ only source of water and improve the hydrogeological conceptual understanding of the different aquifer systems (for example, water quality). This information will be used to improve development of a groundwater numerical model that can be used to explore management options for the low salinity groundwater lens within the Quaternary Limestone aquifer and the potential water quality risks to the main SA Water production bores.

2.1 Specific objectives

The specific objectives of this component of the project were:

1. to investigate the spatial extent of the low salinity groundwater lens within the Quaternary Limestone aquifer around the townships of Elliston and Bramfield
2. to determine the location of the interface between seawater and groundwater and how far and at what depth it extends inland from the coast
3. to identify locations of submarine groundwater discharge around Waterloo Bay.

3 Study site

The Musgrave Prescribed Wells Area (PWA) on the western Eyre Peninsula of South Australia relies primarily on 2 key groundwater aquifers: the Quaternary Bridgewater Formation and the Tertiary Poelpena Formation. Of these, the Bridgewater Formation contains most of the region's low−salinity more productive groundwater resources, which are an important source of town water supply (TWS) for the coastal township of Elliston and the Bramfield community inland. Low salinity shallow groundwater lenses within the area have been spatially mapped from available groundwater water quality data using the 1,500 μS/cm electrical conductivity (EC) isohaline as representative of good quality water. Current groundwater conditions and long−term trends in the Department for Environment and Water (DEW) observation−well network, and SA Water TWS production bores that supply these 2 communities, indicate declining water availability and decreasing water quality, that is, increasing salinity (Figure 1).

Due to the limited groundwater monitoring infrastructure in the region as well as limited well construction details and wells targeting depths greater than a few metres, a suite of hydrogeophysics surveys was designed and conducted around the townships of Elliston and Bramfield in October and November 2024 and January 2026 (Figure 2).

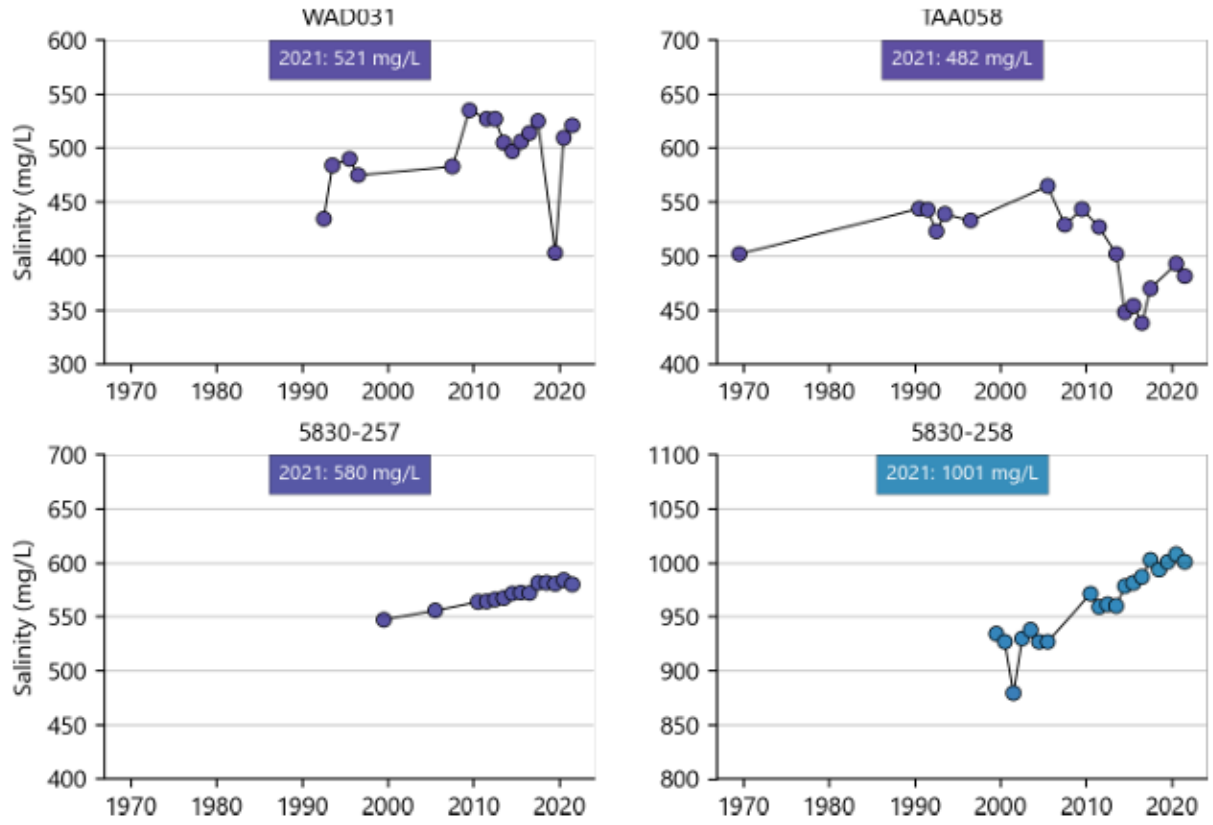


Figure 1. Salinity trends in groundwater wells constructed in the Quaternary Limestone aquifer near Elliston and Bramfield (modified from DEW, 2022)

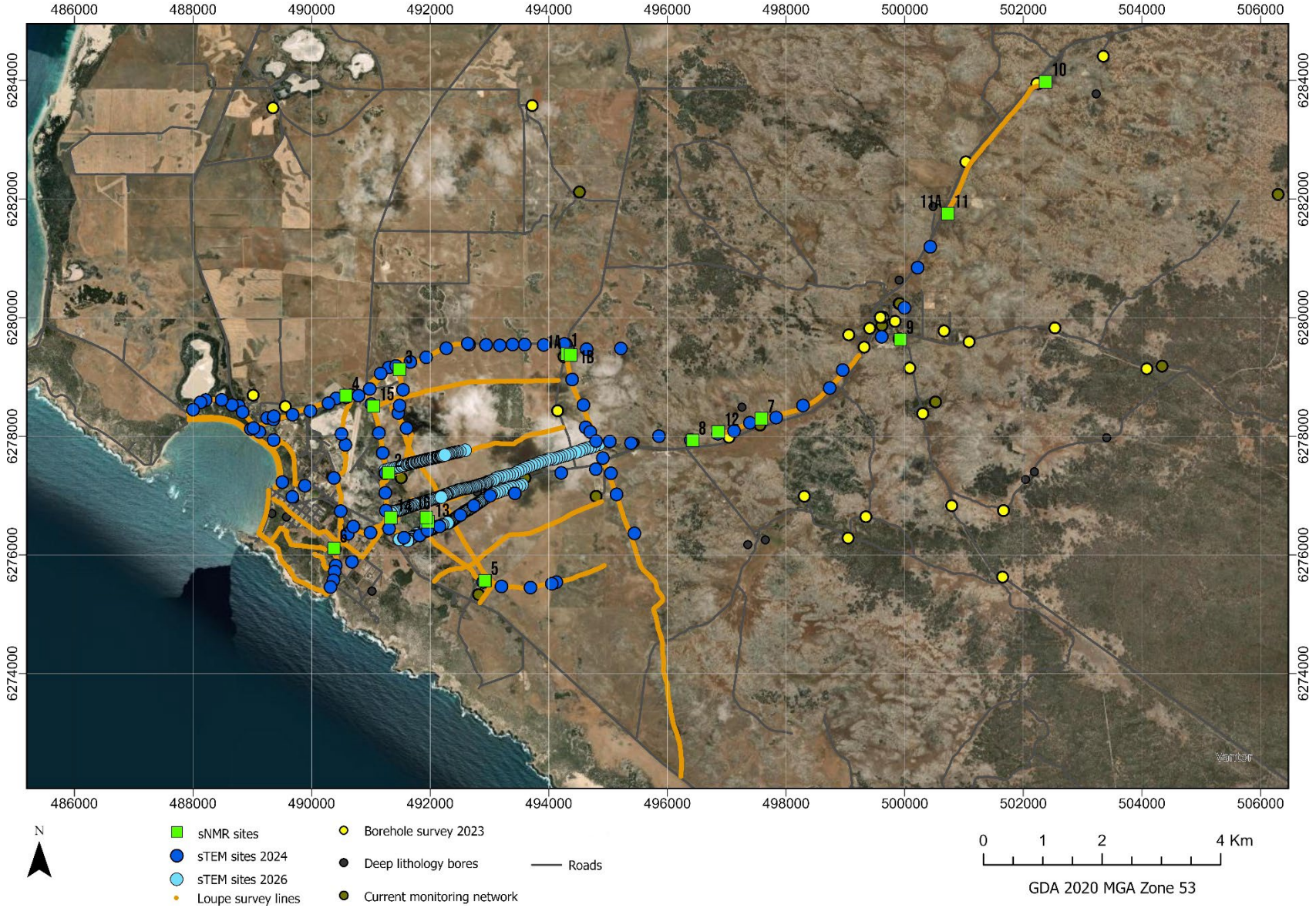


Figure 2. Location map of all the hydrogeophysics surveys around the township of Elliston and Bramfield

3.1 Local geology and hydrogeology

The study area is primarily underlain by the Bridgewater Formation, a Quaternary aeolian limestone (calcarenite) that forms the main unconfined aquifer, commonly referred to as the Quaternary Limestone aquifer (Lanigan, 2025). Extensive dissolution and karst development within the calcarenite indicate significant groundwater interaction and the development of secondary porosity (Twidale and Bourne, 2000). Younger Holocene dune sands of the Semaphore Member occur within the coastal dune systems, while Holocene and Pleistocene playa sediments are present beneath wetlands, surface water features, and some vegetated areas. The Bridgewater Formation in the Elliston–Bramfield region has been classified into 2 units based on some distinct lithological characteristics. The upper section is interpreted to be present across the entirety of the region in varying thickness and is a more gritty, sandy and bioclastic limestone. Whilst at the bottom section, the Bridgewater Formation Clean Limestone is depositionally and petrophysically distinct from the upper section that has less sandy/gritty material and is a harder and denser and more carbonate rich limestone (Lanigan, 2025).

The regional geology also includes older basement rocks exposed locally and offshore, with the Polda Basin extending offshore beneath the study area. Small outcrops of the Archaean Sleaford Complex (gneiss, and felsic to mafic igneous rocks) and the Paleoproterozoic St Peter Suite (both felsic and mafic magmatic rocks) occur near the southern margin of the freshwater lens, while nearby offshore islands expose Proterozoic Calca Granite of the Hiltaba Suite (Reid et al., 2020). Beneath the Bridgewater Formation lies a thin Tertiary clay layer, generally 1 to 5 m thick, interpreted as a discontinuous aquitard that partially confines the underlying Poelpena Formation. The Poelpena Formation consists of unconsolidated fine quartz sands and forms the confined Tertiary Sand aquifer (Stewart et al., 2012). Based on the available geological conceptual model, the Poelpena Formation is likely not to be continuous beneath the Bridgewater Formation, in the south−west towards Elliston. Local erosion and weathering would allow for the Bridgewater Formation to sit unconformably on either weathered Sleaford Complex and St Peter Suite or Jurassic sediments of the Polda Formation (Lanigan, 2025).

Regional hydrogeological studies indicate that groundwater flow within the Bridgewater Formation is strongly controlled by karst development, dune morphology, and the continuity of the Tertiary clay layer (Lanigan, 2025). Variability in the clay aquitard likely influences hydraulic connectivity between the shallow and deeper aquifers and may affect the vulnerability of the freshwater lens to seawater intrusion. Previous studies across the Eyre Peninsula have shown that freshwater lenses within the Bridgewater Formation are sensitive to recharge variability, groundwater extraction, and climatic conditions because of their relatively thin saturated thickness and coastal setting (Davis, et al., 2013; DEW, 2021).

Due to the shallow and weathered nature of the upper Bridgewater Formation, which is characterised by relatively high hydraulic conductivity, seawater intrusion is common along much of the coastline. In areas less affected by seawater intrusion, typically further inland, higher quality groundwater resources occur within the shallow Quaternary Limestone aquifer, including within the Musgrave Prescribed Wells Area (Evans, 2002). A simplified conceptual cross−section of the low−salinity freshwater lens that supplies the Elliston and Bramfield town water supply is presented in Figure 3. Groundwater levels within the shallow unconfined aquifer are primarily climate driven, with recharge strongly dependent on the timing, frequency and intensity of rainfall events. Climate change, together with groundwater extraction, has contributed to declining groundwater levels, reduced aquifer storage, and increasing salinity.

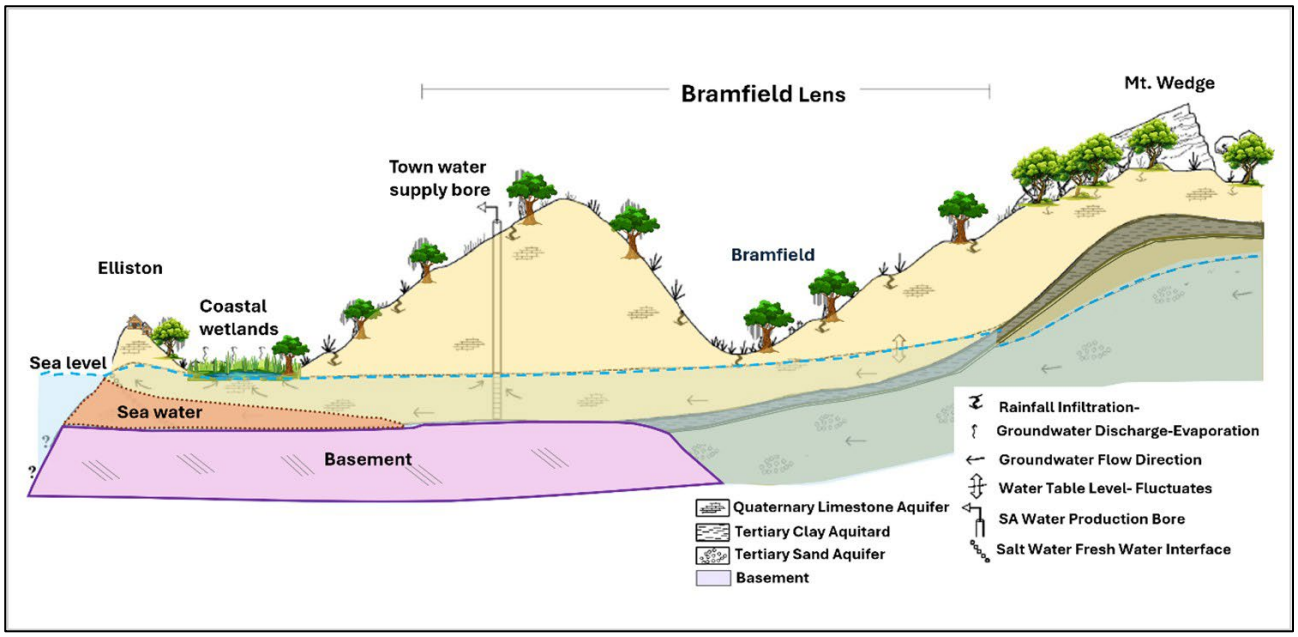


Figure 3. Simplified cross section of the Elliston−Bramfield low salinity lens (modified from Evans 2002)

4 Hydrogeophysics surveys

4.1 Transient electromagnetic surveys to investigate seawater intrusion

TEM investigations have been used across Australia to investigate the impacts of seawater intrusion and have been used to spatially map fresh groundwater in carbonate environments (Figure 4). There have been several airborne electromagnetic (AEM) surveys conducted along South Australia's coastline, including the South−East (Davis, Munday and Ibrahimi, 2025; Davis and Munday, 2025; Gholami et al., 2025) and the Eyre Peninsula including Uley Basin and Coffin Bay (Davis et al., 2013).

As an example of AEM data sets that highlight potential saltwater intrusion along South Australia's coastline, Ley−Cooper et al. (2015) reprocessed AEM data sets from flights across large areas of the Eyre Peninsula, that were originally collected for mineral exploration. Their goal was to reprocess the data sets, highlighting features more pertinent to hydrogeologists. As a result of this work, they identified at least 2 zones that are affected by seawater intrusion (survey areas 1 and 2 on Figure 5). It is worth noting that these surveys were designed to collect data for mining exploration projects, so the need for resolution near to the surface was not of primary importance (as opposed to maximising depth). However, the results appear comparable to other surveys designed specifically for hydrogeological studies.

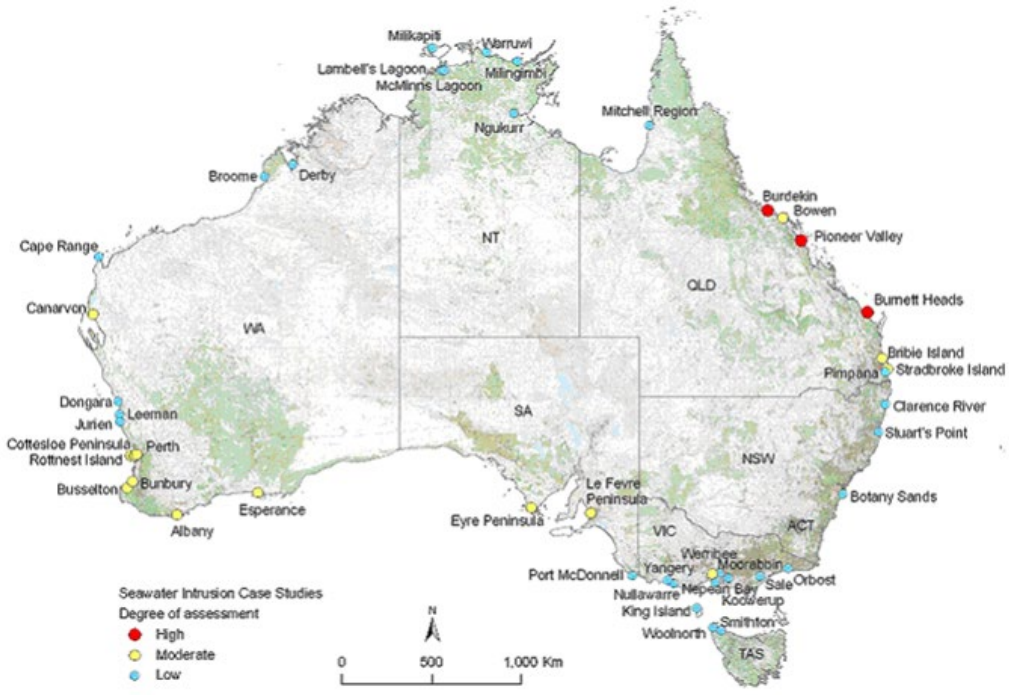


Figure 4. Case studies of seawater intrusion investigations around Australia (from Lawrie et al. 2012)

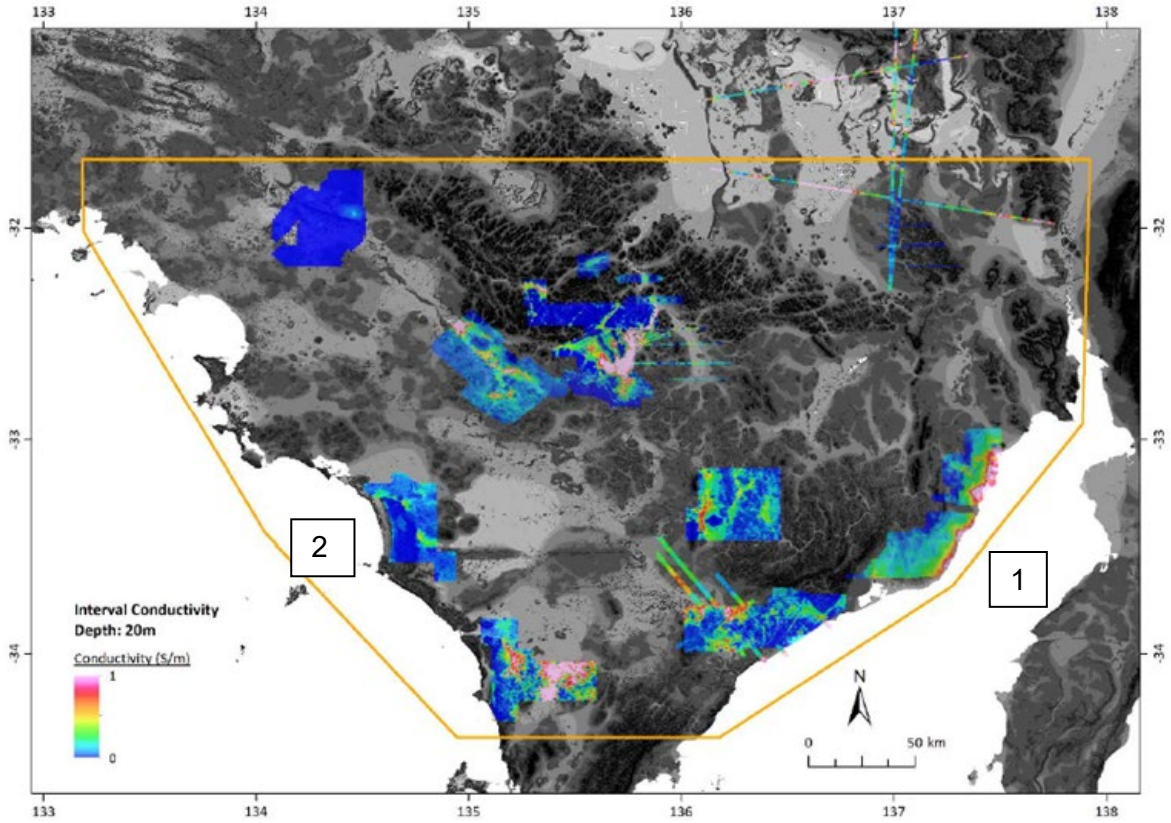


Figure 5. Seventeen Eyre Peninsula–based AEM data sets collected mostly for mining exploration. (Figure 21 from Ley–Cooper et al. 2015)

4.2 Methods used in this study

Hydrogeophysics surveys were undertaken to spatially map the base and extent of the Quaternary Limestone aquifer and to better understand the geology of the area around the townships of Elliston and Bramfield. The surveys aimed to identify: 1) the interface/transition zone between seawater and groundwater and how far and at what depth it extended inland from the coast, 2) the depth to basement, and 3) submarine groundwater discharge into Waterloo Bay.

TEM methods provide information of subsurface conductivity and the data sets in this survey are presented as conductivity in units of millisiemens per meter (mS/m). The measured response in TEM systems is dependent on the distribution of subsurface conductivities, which includes the quality of the water within the pore spaces (for example, salinity), the porosity and the material and mineralogy (for example, sand versus clay). The water quantity and quality within the moisture–filled pore spaces within the matrix of the material can significantly influence the measured response in TEM, particularly where seawater intrusion of freshwater aquifers occurs (Lesmes and Friedman, 2005; McNeil, 1980; Palacky, 1987).

Surveys were completed using a Loupe TEM system (from Loupe Geophysics) and sTEM system (from TEMCompany). The Loupe system (Figure 6) is a backpack–portable, two–person, TEM system that uses a similar configuration to an AEM system to allow data to be collected nearly continuously (Street et al., 2018). The Loupe system has up to 40 to 50 m depth penetration (depending on subsurface properties and site conditions). sTEM and sTEM profiler (Figure 7) is a new TEM system manufactured by TEMCompany that can collect semi–continuous data relatively

quickly with up to 250 m depth penetration for the sTEM and 150 m for the sTEM profiler (depending on subsurface properties and site conditions).

A total of 85−line kilometres of Loupe was surveyed, and 113 sTEM soundings were completed in October and November 2024. Additional work in January 2026 included 20−line kilometres of Loupe, 267 additional sTEM measurements around the inferred location of the seawater toe, and an additional survey transect line between Colton Back Rd, east of the Elliston Aerodrome and Grove Rd (3 to 3.5 km long). This included the TEM station positions accurately georeferenced using a Real−Time Kinematic (RTK) Global Navigation Satellite System (GNSS) with ≈25 m station spacing near the seawater toe and up to 200 m spacings elsewhere.

Surface nuclear magnetic resonance (sNMR) (Figure 8) is a geophysics method that directly measures water content and aquifer saturated porosity and provides an estimate of hydraulic conductivity. sNMR surveys were conducted at 16 sites, generally located along or adjacent to TEM survey transect lines using a Vista Clara GMR Flex system. This provides up to 40 to 50 m depth penetration (depending on subsurface properties and site conditions).



Figure 6. Loupe system in action near Elliston, January 2026

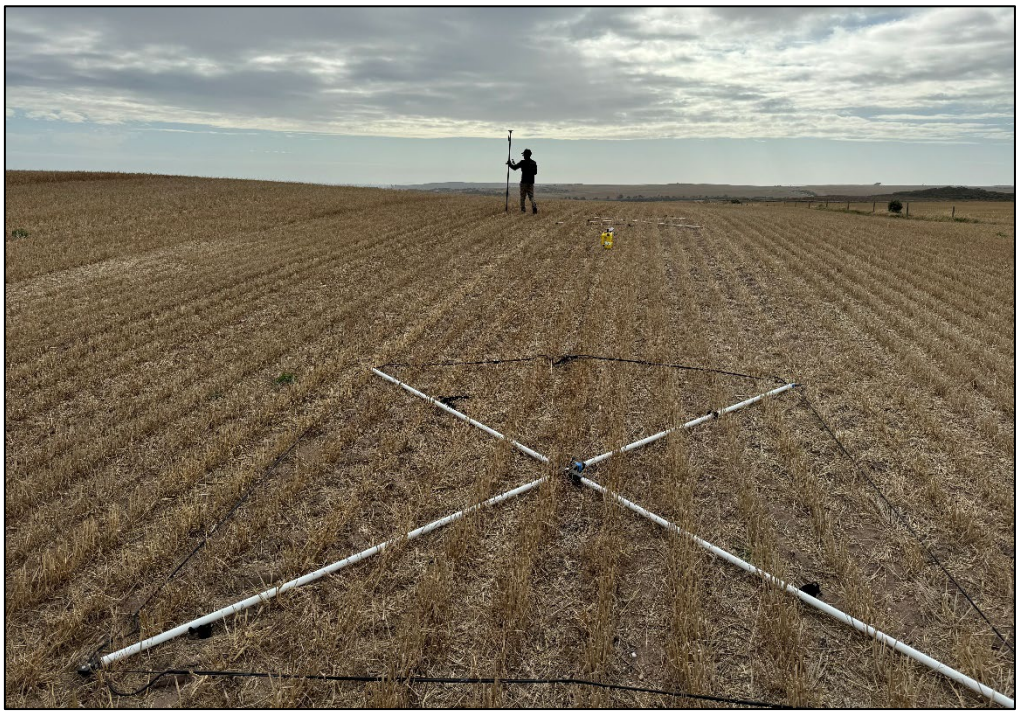


Figure 7. sTEM profiler in action at Elliston, November 2024



Figure 8. sNMR survey being conducted near Birdseye Highway, Elliston, January 2026

4.3 Data processing

TEM and sNMR data sets were processed and inverted using computer modelling inversion software to provide sections of subsurface conductivity, profiles of water content, porosity and estimates of hydraulic conductivity.

The Loupe data were processed by stacking and averaging the raw data and then correcting for system−response, which included the removal of the primary field. The results were converted into a file format similar to the 'standard' Amira TEM file format (Duncan et al., 1998) and the data were inverted using the AarhusInv inversion code in the Aarhus Workbench software (Auken et al., 2015). In this instance, a 35−layer smooth−model configuration was selected, using a laterally constrained inversion (LCI) technique along the survey lines, a reference distance of 1 m, and where the lateral (horizontal) and vertical constraints were set to 1.3 and 2.0, respectively. The lateral depth constraint controls the degree to which layer interface depths (or layer thicknesses) are allowed to vary between neighbouring soundings. Stronger constraints encourage laterally continuous layer geometries, while weaker constraints allow more abrupt changes. Vertical constraints control the allowable variation in model parameters between adjacent layers within an individual sounding. For resistivity (or conductivity), they control the degree of vertical smoothness in the subsurface model, while for layer geometry they help maintain stable and geologically realistic interface depths and layer thicknesses. A lateral (horizontal) constraint of 1.3 is tight and a vertical constraint of 2.0 is moderate. As AarhusInv is a 1D inversion code, the LCI stitches together 1D models along survey transect lines forming a 2D model space. The Root Mean Square Error (RMSE) is also shown on the plots to evaluate how well the geophysical inversion model fits the observed field data.

The sTEM data were also processed and inverted using the AarhusInv inversion code in the Aarhus Workbench software. The low and high moment were filtered, and a 34−layer smooth−model configuration was used to invert the data. A LCI was also used with a reference distance of 25 m, where the lateral and vertical constraints were set to 1.3 and 2.0, respectively.

AarhusInv incorporates depth of investigation (DOI) information estimates as described in Christiansen and Auken (2012). This information is shown in the figures of this report as transparent shading on the conductivity–depth sections. Depth of investigation was up to about 50 m for the Loupe surveys and around 150 m for the sTEM surveys based on the system configuration and subsurface characteristics. Interpretation of the data shown below the DOI should be treated carefully because there is a higher degree of model uncertainty particularly with greater data noise associated with increased depth as well as the resistivity/conductivity of the model layers of the 1D inverted data.

Surface nuclear magnetic resonance (sNMR) datasets were processed and inverted using the Vista Clara GMR Pro inversion software. Because the subsurface conductivity has an influence on the NMR response and the depth of investigation of the sNMR signal, the sNMR data were processed using both the standard resistive earth model and a more realistic conductive earth model based on the TEM survey data collected near the sNMR site.

5 Hydrogeophysics survey results and analysis

Selected data sets from the Loupe, sTEM and sNMR hydrogeophysics surveys that were completed in October and November 2024, and January 2026 are presented for 4 west–east transects that traverse from Elliston inland towards Grove Rd and the SA Water TWS production bores (Figure 9). These data sets were selected because they traverse perpendicular to the coastline and best illustrates the extent of seawater intrusion.

Other hydrogeophysics data sets that were collected during the 3 field trips in October and November 2024, and January 2026 as part of the submarine groundwater investigation are described in other sections of this report and included in Appendix A and in the digital data sets.

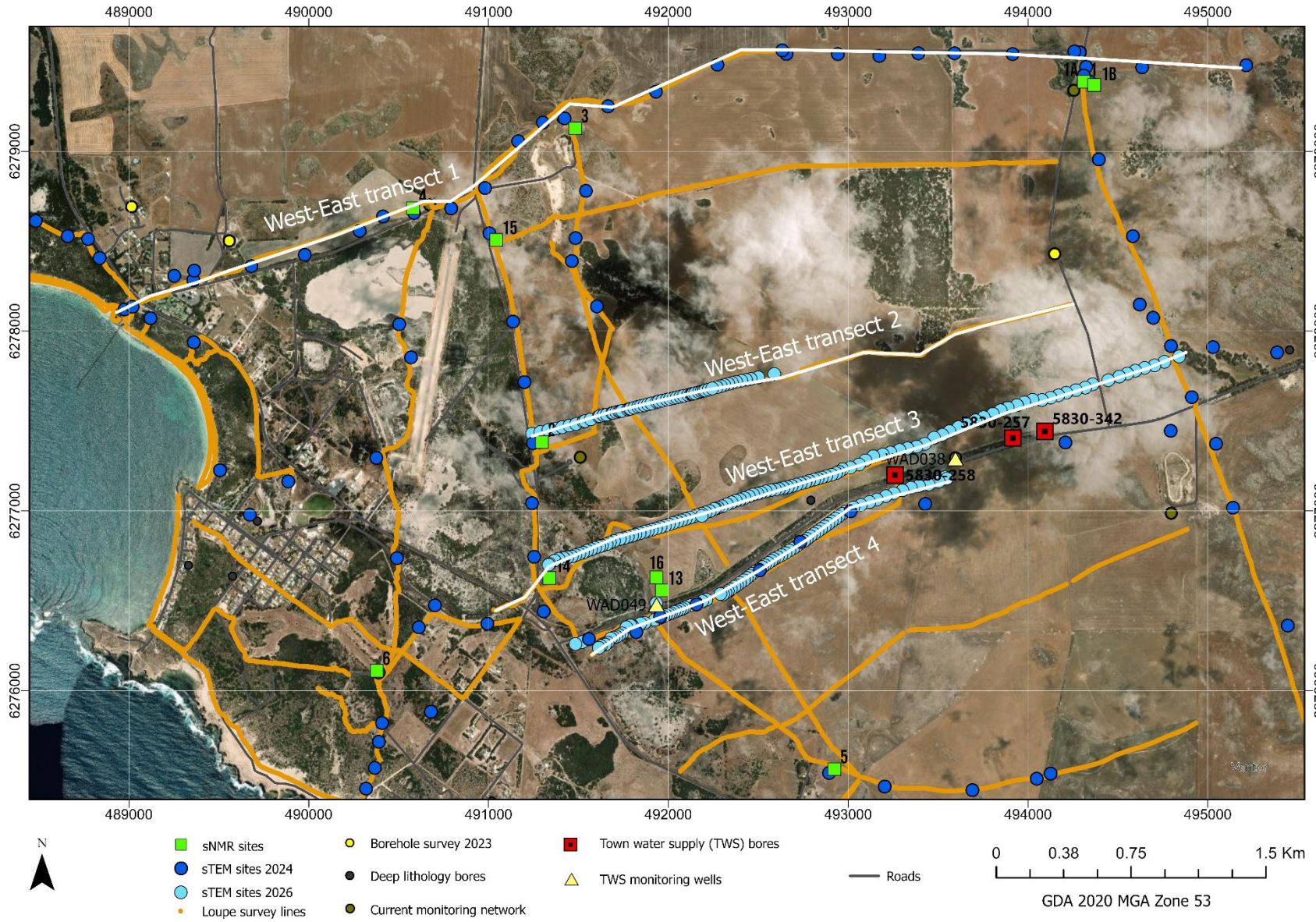


Figure 9. Location map of selected data sets from the hydrogeophysics surveys around the township of Elliston. White lines are the 4 West−East transects

5.1 West−East transect line 1

The West−East transect line 1 is ≈6.2 km long and from the Elliston jetty towards Grove Rd (Figure 9). The Loupe (4.2 km) and sTEM (6.2 km) conductivity–depth sections show that the shallow, lower salinity part of the aquifer (<50 mS/m) extending to about -15 mAHD and appears to be no more than 20 m thick (Figure 10 and Figure 11). Between -15 to -20 mAHD the conductivity increases from that above and at a depth greater than -20 to -25 mAHD, the higher conductivity zone (>500 mS/m) is likely to represent seawater intrusion, where the toe of the seawater wedge extends 3 km inland (≈491700mE). The Loupe survey captures the top of this conductive feature, where the sTEM system's greater depth of investigation shows more information on the extent of the wedge and the subsurface features beneath (Figure 11). Both survey methods provide evidence of seawater intrusion.

At 2.5 km along the transect (≈491500mE) there is a groundwater well (5830−319, ground elevation 12.2 mAHD) that is pumped for agricultural purposes and has a Reduced Standing Water Level (RSWL) of 0.8 mAHD (Standing Water Level (SWL) was 11.45 m below the top of the casing in November 2023). The well is 15 m deep, and the well screen is between 1.3 mAHD to -2.7 mAHD, which is ≈38 m directly above the seawater intrusion toe and may be at risk to seawater upconing due to pumping. The reported groundwater EC for this well is 2,830 μS/cm, which is higher than the median EC (1,088 μS/cm) of the 52 groundwater wells that were surveyed in 2023 around Elliston and Bramfield. The 2 closest groundwater observation wells 5830−71 (WAD032) and 5830−81 (WAD033) had measured EC values of 1,750 μS/cm (12 October 2017) and 2,800 μS/cm (9 August 2024), respectively. However, both wells are very shallow (<3 m depth) and were hand dug, large diameter (>0.7m) wells that are equipped with a windmill, so they are less reliable compared to a properly constructed groundwater well with casing. The RSWL of 5830−71 (WAD032) and 5830−81 (WAD033) is 3.0 mAHD and 5.68 mAHD, respectively, and only a few metres below ground elevation. Hence surface evaporation and the large diameter open well completion is likely to contribute to the high salinity values reported.

The West−East transect line 1 traverses to the north of Lake Hamp, which is one of the low−lying wetlands (elevation below mean sea level) adjacent to the Elliston Aerodrome. The low salinity lens (subsurface conductivity <50 mS/m) appears to continue all the way towards the coast along this transect; however, other Loupe surveys that traversed parallel to the airstrip and the Colton Back Road showed that there was high subsurface conductivity at the near surface suggesting evapoconcentration of groundwater discharge in these low−lying areas. This implies that the regional groundwater flow direction from the upgradient areas near Bramfield may converge towards these low−lying wetlands and discharge because of surface elevations below mean sea level or possibly continue further and discharge at Waterloo Bay and along the coast.

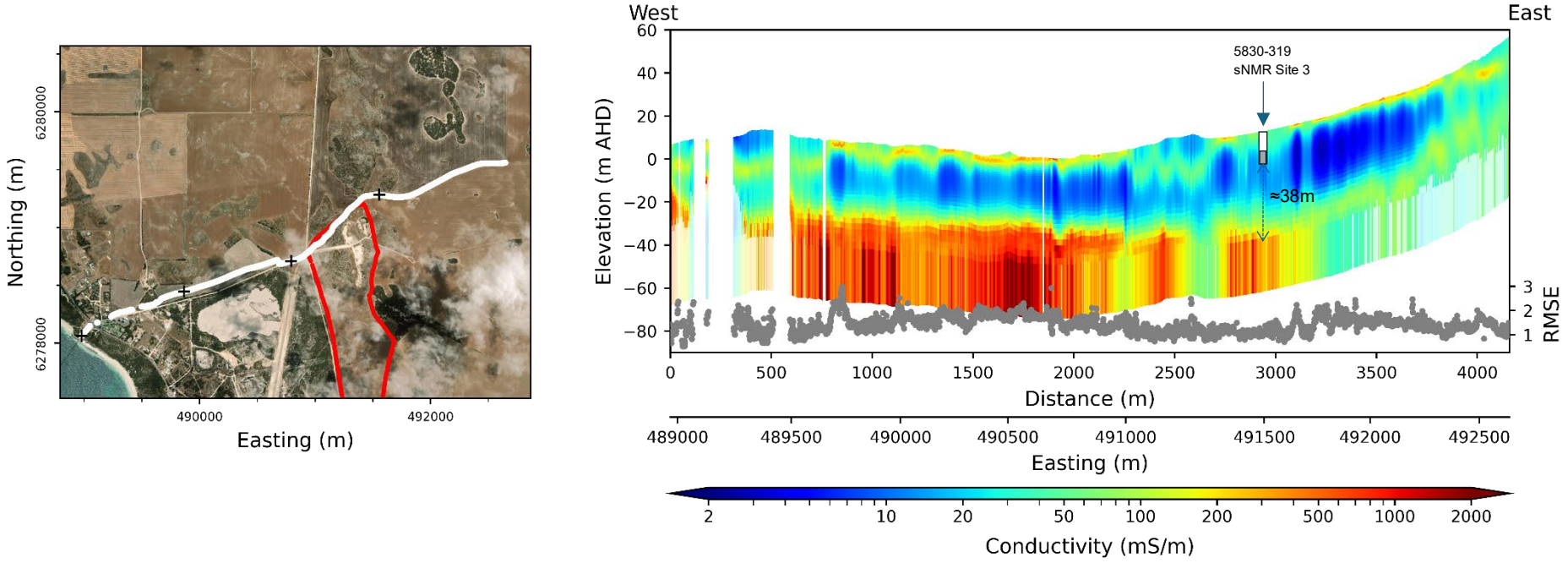


Figure 10. Loupe conductivity–depth section along West−East transect 1. Transparent shading represents the depth of investigation. Grey line is the RMSE. Black crosses on location map represent 1,000 m distances along the line

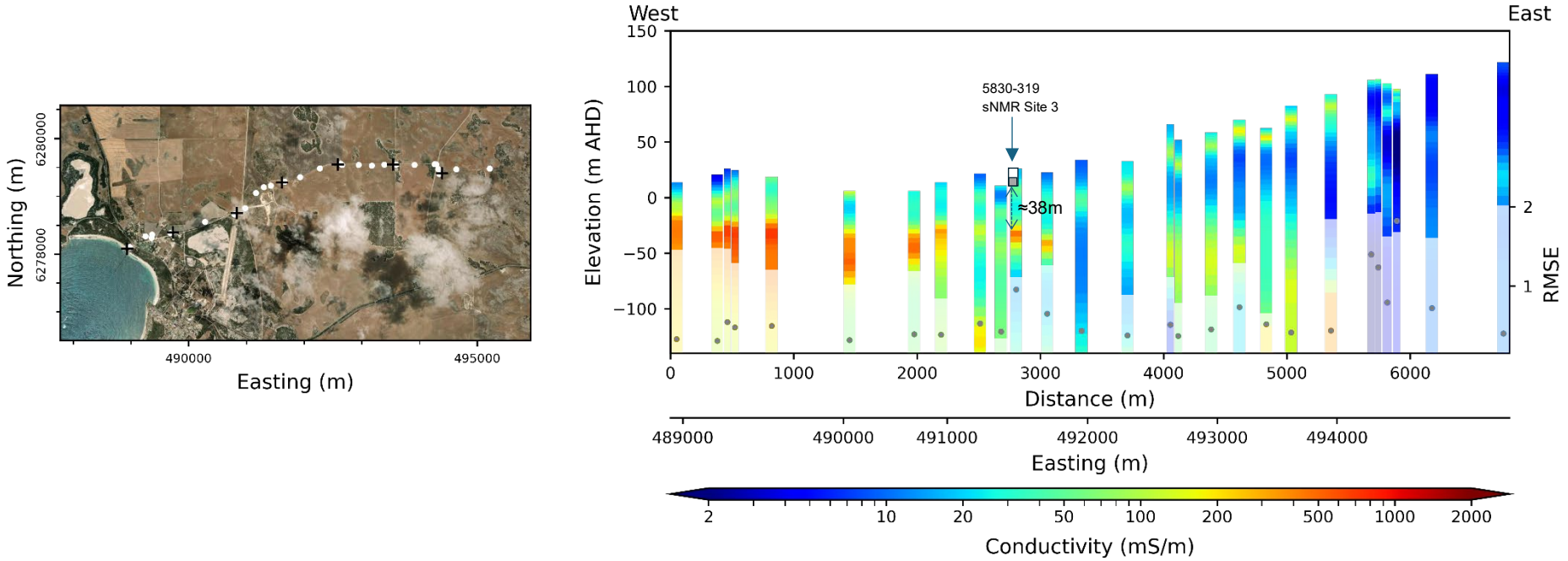


Figure 11. sTEM conductivity–depth section along West−East transect 1. Transparent shading represents the depth of investigation. Grey dots are the RMSE. Black crosses on location map represent 1,000 m distances along the line

The sNMR profile at Site 3 (491400mE along West−East transect 1) shows that the specific yield (free draining water measured by sNMR: T2 > 33ms) is up to 13% and the total porosity is ≈17% at 23 m depth. The estimated hydraulic conductivity ranges from 6 to 10 m/day for the higher porosity zones of the Bridgewater Formation aquifer (Figure 12). The estimated depth to the water table is about 10 m (2 mAHD). The resolution depth limit of the sNMR (indicated with the orange line at 32 m) is at the depth interface of the transition zone and the more conductive feature as shown by the TEM data. The conductivity model from the TEM data adjacent to the sNMR site was used to constrain the NMR signal in the inversion.

The closest groundwater observation well (WAD037) with gamma and geological logs is located at the eastern most end of West−East transect line 1 on the road verge of Grove Rd. It is at an elevation of ≈90 mAHD, approximately 80 m higher in elevation than Site 3 and the well. At WAD037, the top of the Bridgewater Formation is nearly 72 m thick, and the Bridgewater Clean Limestone is mapped between 72 m (17 mAHD) and 108 m (-19 mAHD) depth. The correlation between the geology and the gamma results suggest that the gamma is a good proxy for the near−surface geology. Where it is present, the location of the upper, less consolidated part of the Bridgewater Formation correlates well with relatively high gamma values. The more consolidated part of the Bridgewater (Clean Limestone) correlates well with a zone of lower gamma values, and again, where present, there is good correlation with a second zone of higher gamma values and the logged location of the Poelpena Formation.

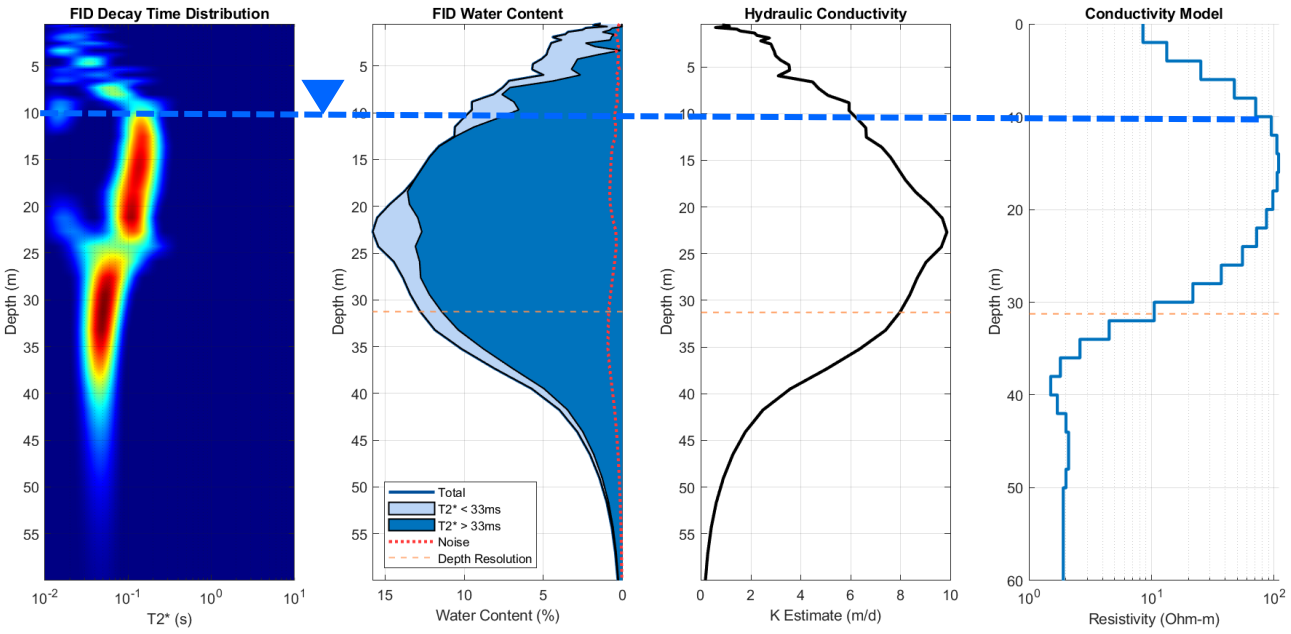


Figure 12. sNMR profile at Site 3, 491400mE along West−East transect 1 showing water content and estimated hydraulic conductivity (m/d). Depth of resolution is ≈32 m. Estimated depth to water is ≈10 m. The FID (free induction decay) is the NMR signal measured right after excitation, and its T2 (transverse relaxation time) reflects how quickly that signal decays

5.2 West−East transect line 2

West−East transect line 2 is ≈1.6 km long and extends from the Coulter Back Rd to the east of the Elliston Aerodrome towards Grove Rd (Figure 9). Loupe and sTEM conductivity–depth sections show that the shallow, lower salinity aquifer (<50 mS/m) extending to about -25 mAHD and appears to be no more than 20 to 25 m thick (Figure 13 and Figure 14). At a depth greater than -25 mAHD, the higher conductivity zone (>500 mS/m) is likely to represent seawater intrusion, where the toe of the seawater wedge extends 2.5 km inland from the coast (≈491900mE). The sTEM section shows that at the western end of the transect at Coulter Back Rd, the seawater wedge is up to 50 m thick (-25 mAHD to -75 mAHD). There is a sharp transition between the lower conductive feature in the near surface, representative of the low salinity groundwater of the lens, and the underlying more conductive feature representing seawater intrusion.

At an elevation of -75 mAHD and below, the subsurface conductivity decreases again beneath the seawater wedge. This transition in conductivity may be due to the underlying basement rock of the Sleaford Complex or St Peters Suite (Reid et al., 2020). The Tertiary sands of the Poelpena Formation, which consists of poorly sorted, fine to coarse grained quartz, silt and clay (Flint, 1992) is absent in this part of the basin and is only present further inland (Lanigan, 2025). This suggests that the seawater is intruding within the lower parts of the Bridgewater Formation and across the top of the basement rock; however, drilling would need to confirm if this is the case.

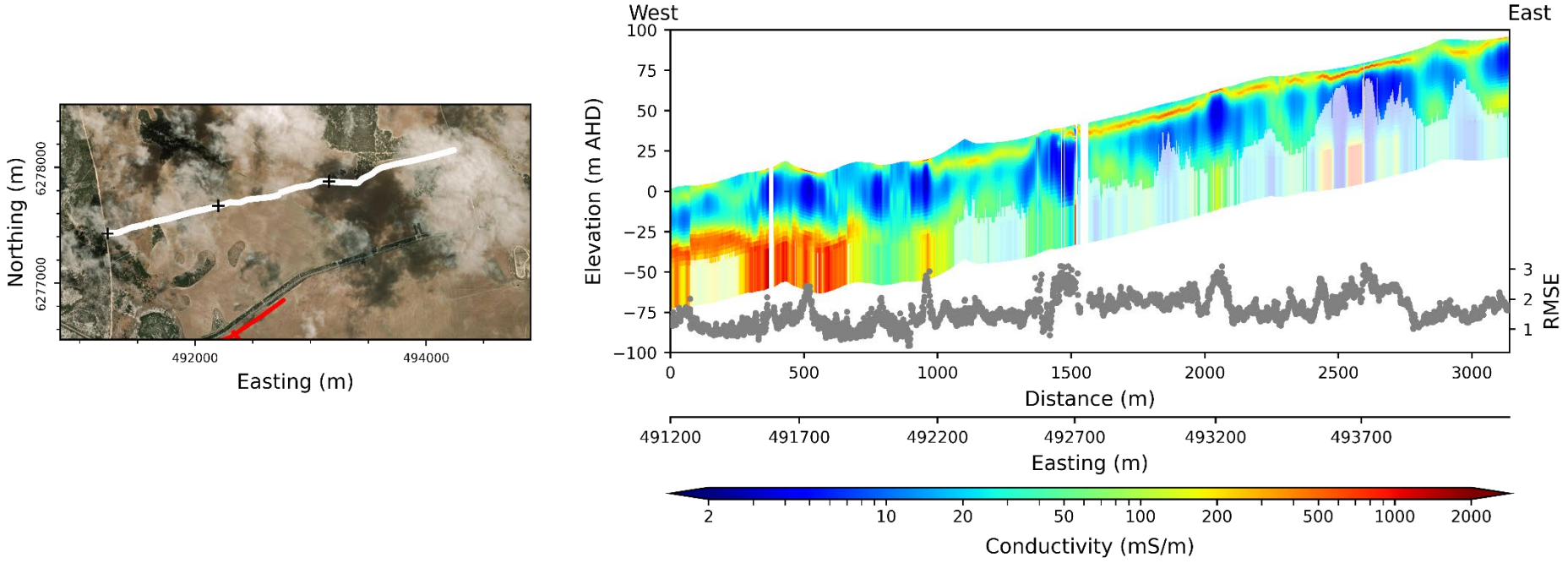


Figure 13. Loupe conductivity–depth section along West−East transect 2. Transparent shading represents the depth of investigation. Grey line is the RMSE. Black crosses on location map represent the 1,000 m distances along the line

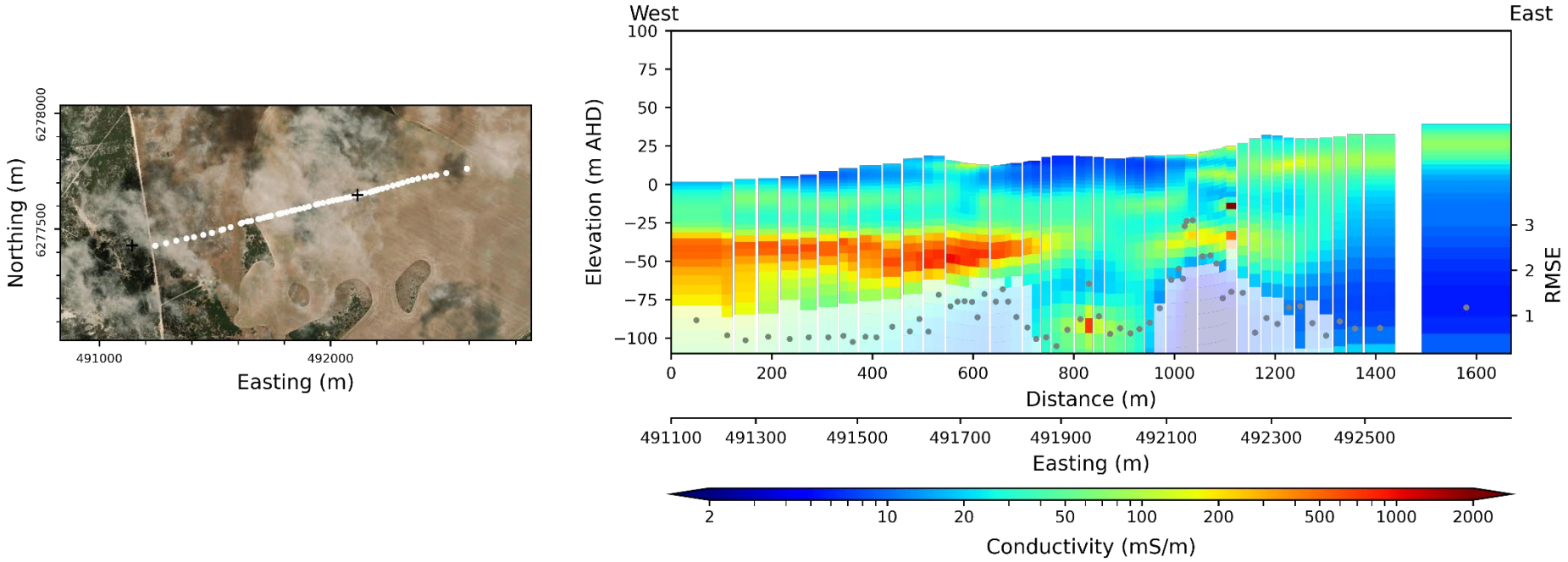


Figure 14. sTEM conductivity− depth section along West−East transect 2. Transparent shading represents the depth of investigation. Grey dots are the RMSE. Black crosses on location map represent the 1,000 m distances along the line

The sNMR profile at Site 2 (491300mE along the West−East transect line 2) shows that the specific yield (free draining water measured by sNMR, T2 > 33ms) is up to 35% at about 7 m depth (Figure 15). The estimated saturated hydraulic conductivity is up to 21 m/day. The sNMR resolution depth limit (indicated by the orange line at 17 m) is strongly influenced by the high subsurface conductivity conditions at this site and therefore reporting on the data below this depth needs to be considered with a degree of caution. The estimated depth to the watertable is about 2.5 mbgl.

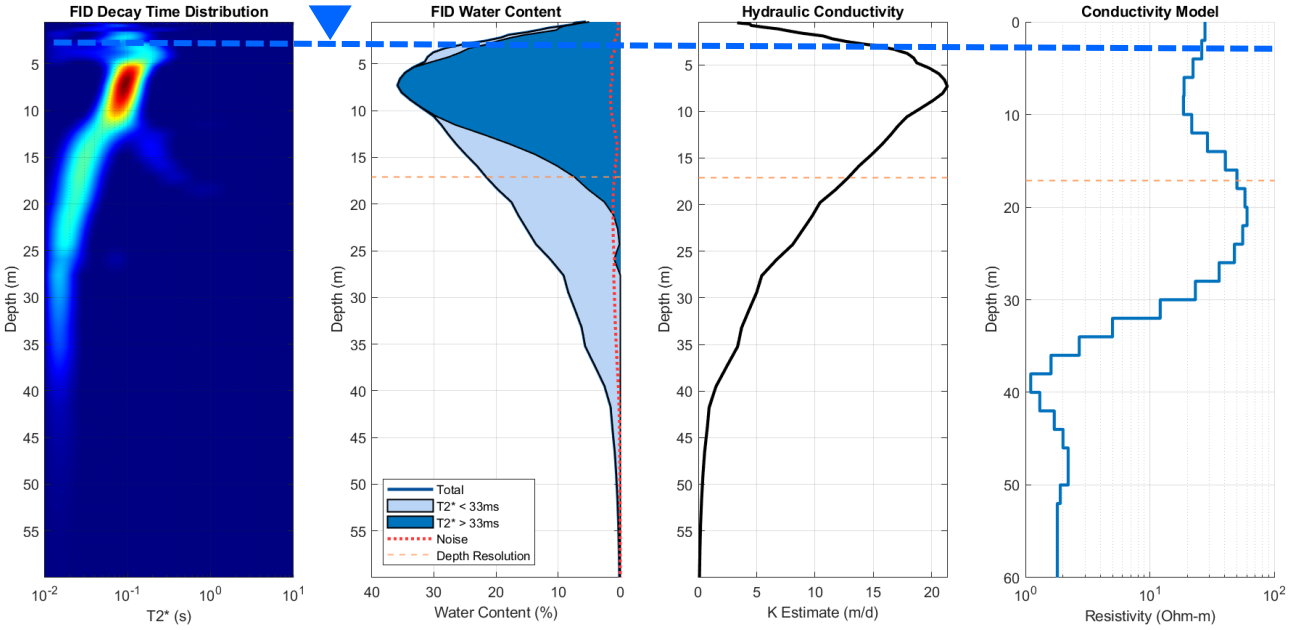


Figure 15. sNMR profile at Site 2, 491300mE along West−East transect 2 showing water content and estimated hydraulic conductivity (m/d) using a conductivity model from the Loupe data adjacent to the site. Depth of resolution is ≈17 m and estimated depth to the water table is ≈2.5 mbgl

5.3 West−East transect line 3

West−East transect line 3 is ≈4 km long and traverses from the Coulton Back Rd parallel to the Birdseye Highway on the northern side of the SA Water TWS production bores and over Grove Rd (Figure 9). The Loupe and sTEM conductivity–depth section captures the same high conductive feature at -26 mAHD as the other transect lines (Figure 16 and Figure 17). The westernmost end shows that the seawater wedge extends approximately 3.2 km inland from the coast (≈492300mE) on the conductivity–depth sections. The seawater toe is about 950 m away from SA Water production bore TWS 2A (5830−258), which is screened from -13 to - 22 mAHD.

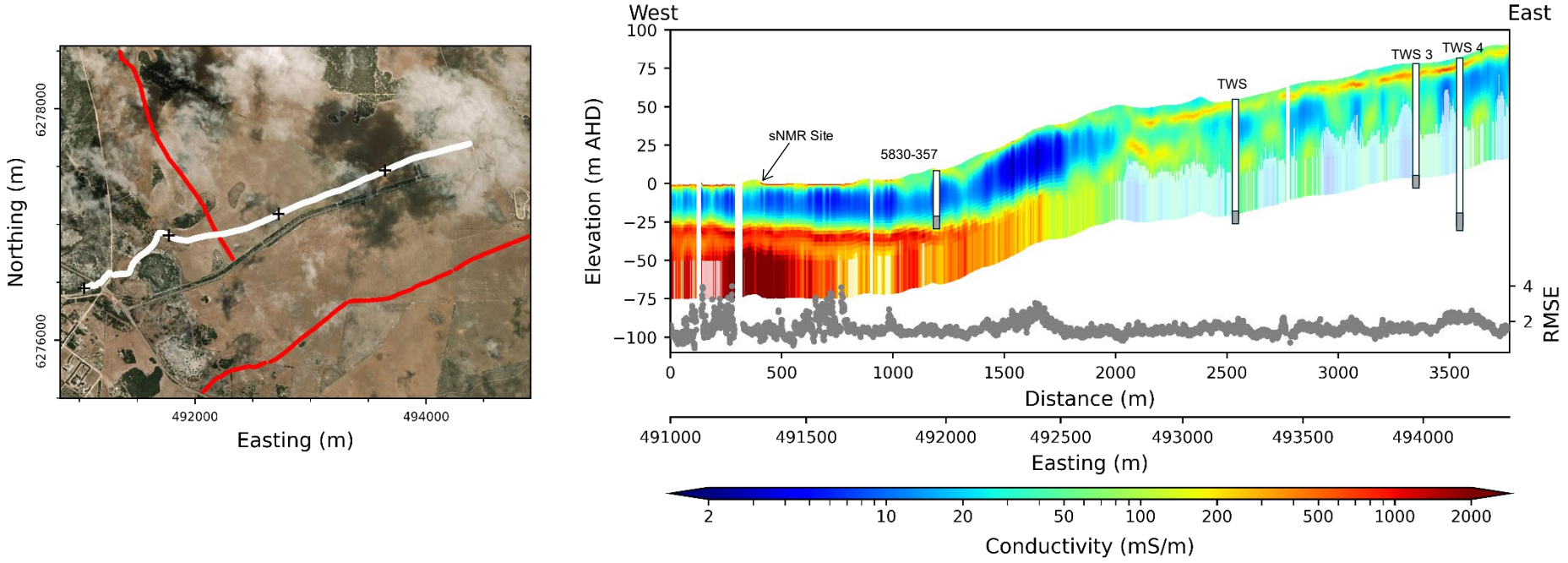


Figure 16. Loupe conductivity–depth section along West−East transect 3. Transparent shading represents the depth of investigation. Grey line is the RMSE. Black crosses on location map represent the 1,000 m distances along the line

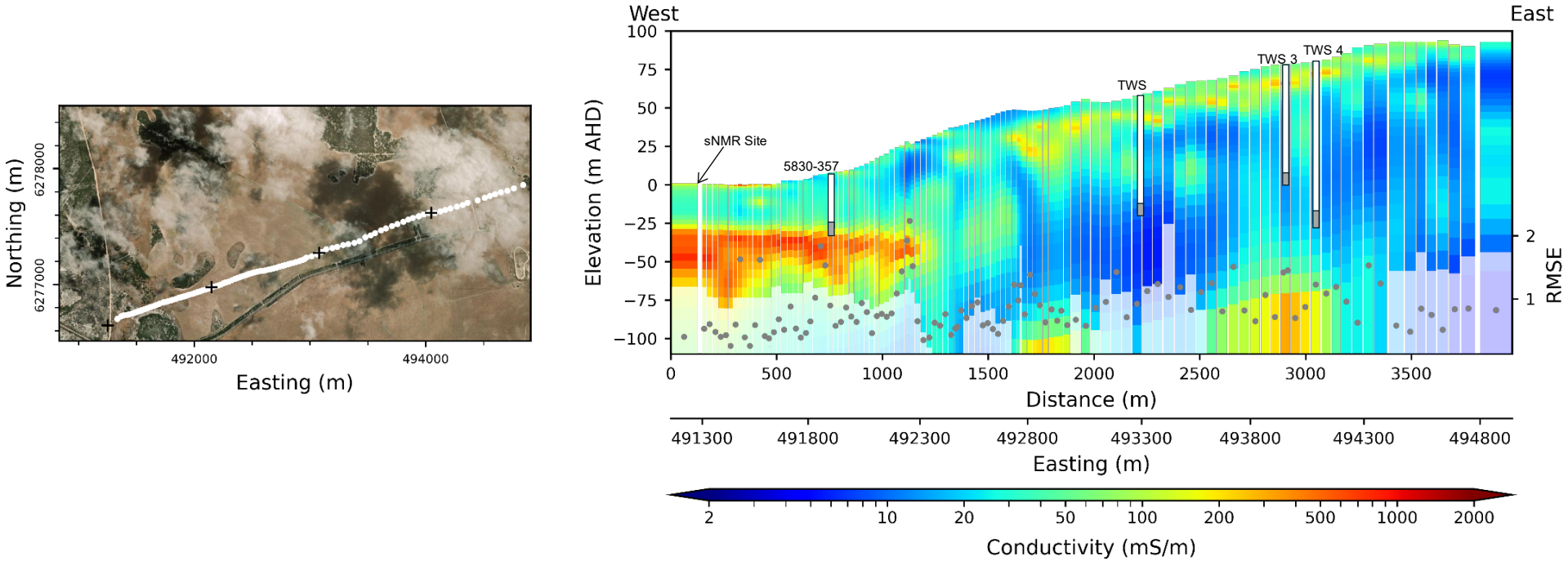


Figure 17. sTEM conductivity− depth section along West−East transect 3. Transparent shading represents the depth of investigation. Grey dots are the RMSE. Black crosses on location map represent the 1,000 m distances along the line

The sNMR profile at Site 14 (491300mE along West−East transect 3) shows that the specific yield (free draining water measured by sNMR: T2 > 33ms) is up to 32% at a depth of 5 m. The estimated depth to the watertable is ≈2 mbgl. The resolution depth limit of the sNMR (indicated with the orange line at 28 m) is at the transition zone above the more conductive feature in the TEM sections.

Based on the sNMR data, the estimated average hydraulic conductivity is about 12 m/day in the shallow part of the aquifer (Figure 18).

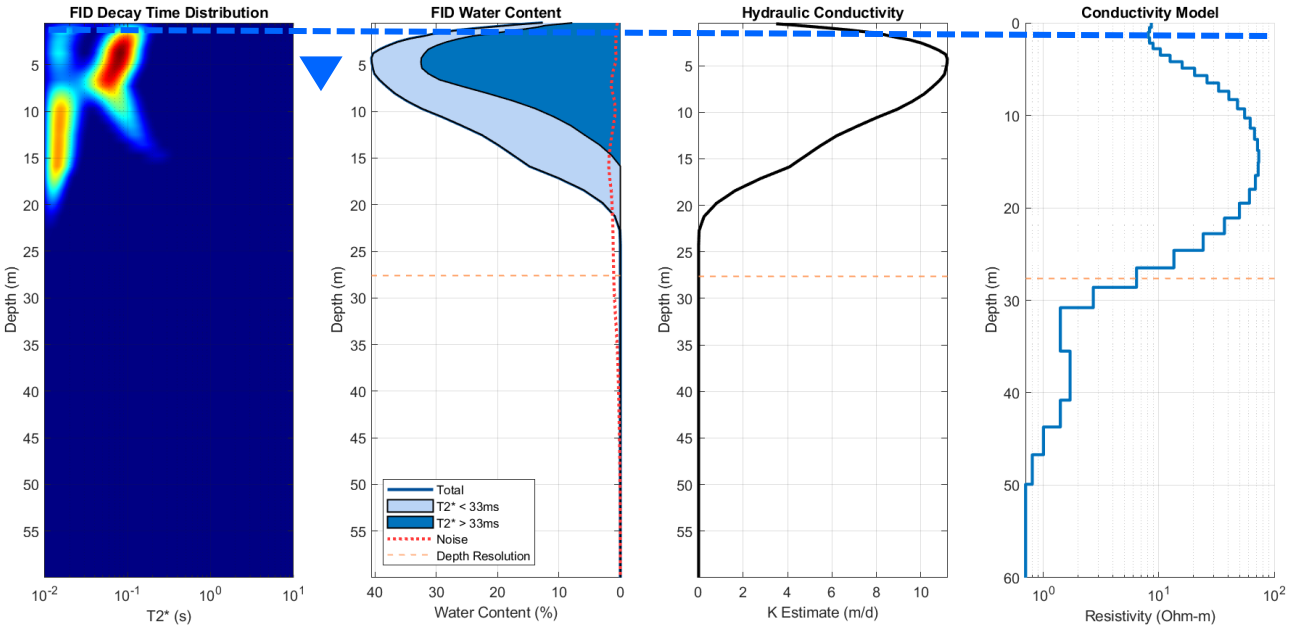


Figure 18. sNMR profile at Site 14, 491300mE at the western end of West−East transect 3 showing water content and estimated hydraulic conductivity (m/d) using a conductivity model from the Loupe data adjacent to the site. Depth of resolution is ≈28 m and estimated depth to the water table is ≈2 mbgl

5.4 West−East transect line 4

West−East transect line 4 is ≈2.6 km long and traverses from the Flinders Highway inland towards Bramfield parallel to the Birdseye Highway and on its southern side (Figure 9). The Loupe and sTEM conductivity–depth−section captures the same high conductive feature at around -25 mAHD (Figure 19 and Figure 20). The westernmost end of the West−East transect line 4 shows that the seawater wedge extends from the coast approximately 2.95 km inland (≈492550mE) on the conductivity–depth sections. The seawater toe is about 900 m away from SA Water production bore TWS 2A (5830−258), which has its screen between -13 to -22 mAHD. Between 750 and 1,000 m along the sTEM transect there is a higher RMSE with the measurements and therefore some of the data from below -40 mAHD is of lower quality and masks the high conductivity feature at this location.

At 0.5 km along the transect (≈491900mE) on the northern side of the Birdseye highway the new groundwater monitoring well 5830−357 (WAD049) has a RSWL of 1.87 mAHD (SWL = 3.27 m, November 2025). The well is 33 m deep, and the well screen is between 30 m to 33 m and specifically completed in the seawater interface for groundwater monitoring purposes. The reported groundwater EC for this well is 32,700 µS/cm, which is higher than the median EC (1,088 µS/cm) of the 52 wells that were surveyed in 2023. The closest groundwater well is 5830−258, which is one of the SA TWS production bores and is 1.5 km further inland with an EC of 1,811 µS/cm (3 November 2025).

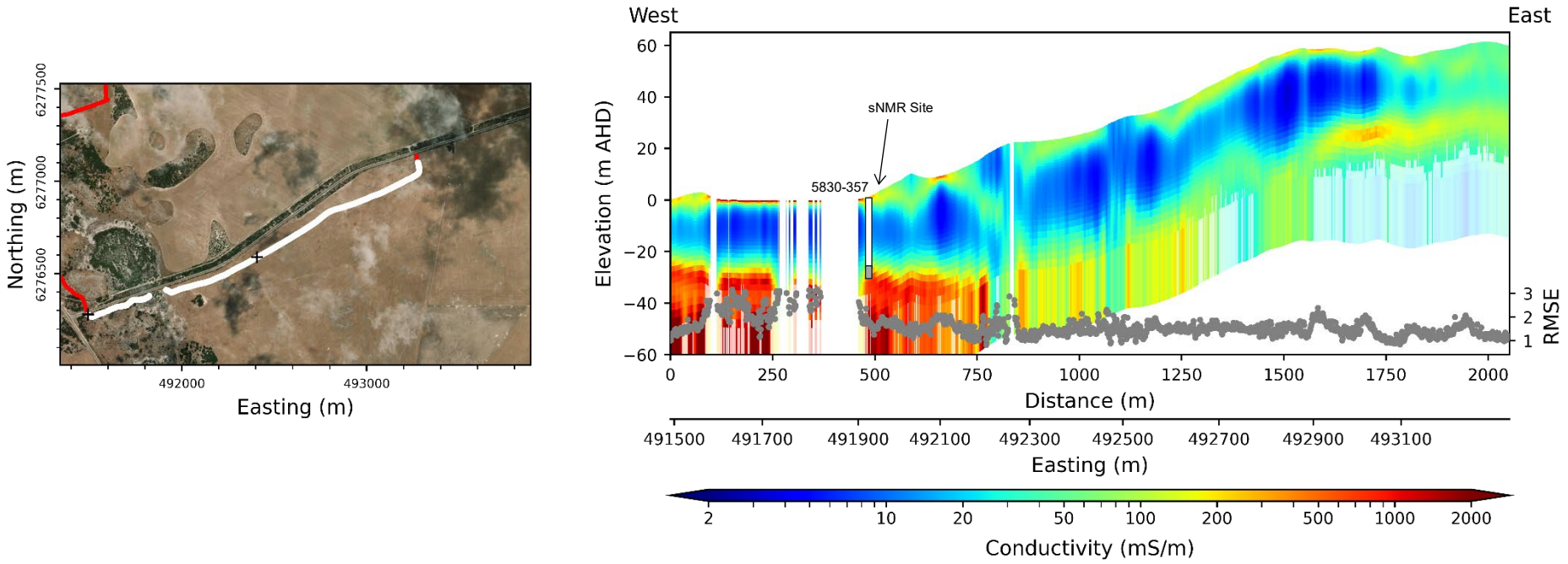


Figure 19. Loupe conductivity− depth section along West−East transect 4. Transparent shading represents the depth of investigation. Grey line is the RMSE. Black crosses on location map represent the 1,000 m distances along the line

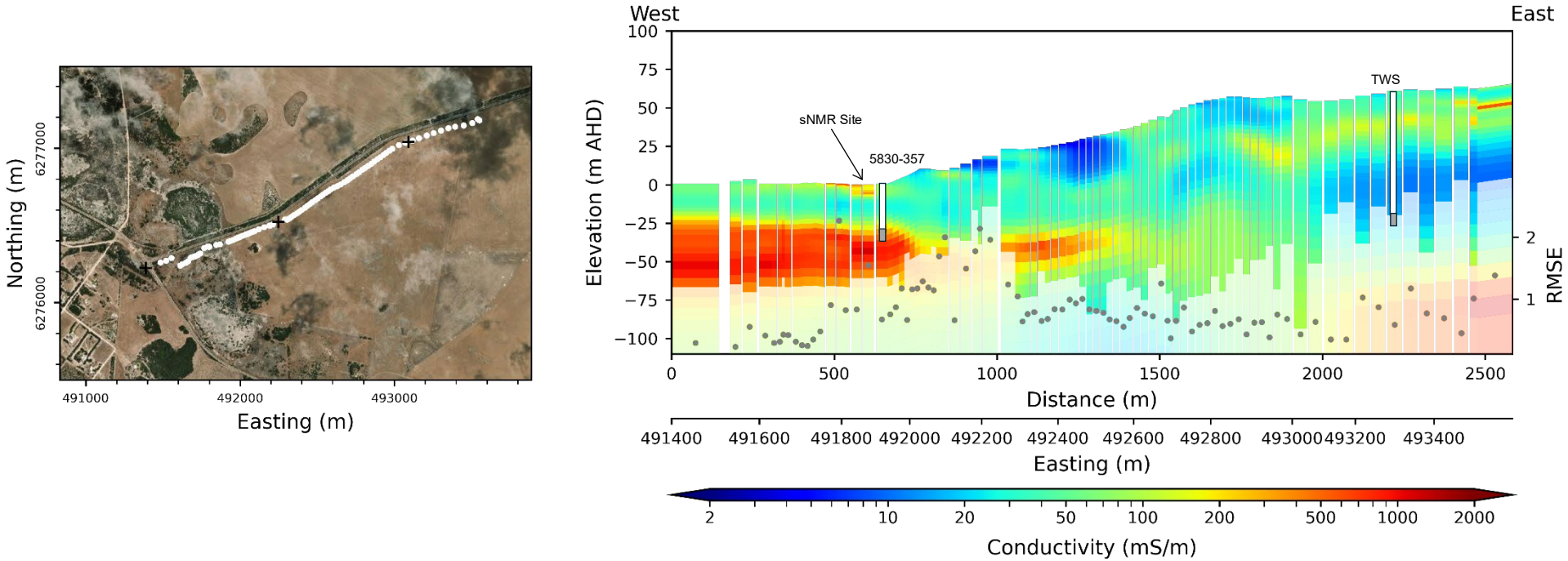


Figure 20. sTEM conductivity− depth section along West−East transect 4. Transparent shading represents the depth of investigation. Grey dots are the RMSE. Black crosses on location map represent the 1,000 m distances along the line

The sNMR water content profile at Site 16 is located ≈100m to the north of groundwater well 5830−357 (WAD049) and in between West−East transect 2 and West−East transect 3 (491950mE) (Figure 9). The specific yield (free draining water measured by sNMR: T2* > 33ms) is up to 35% at 8 m depth and then decreases to 12% at 20 m depth. Between 15 m and the depth of resolution at 28 m, the more tightly bound water or finer porosity material (sNMR: T2* < 33ms) increases. At 20 m depth it is close to 30% water content.

At the new groundwater monitoring well 5830−357 (WAD049) the Bridgewater Formation extends from 0 to 49 m. Between 17.7 m and 49 m it was logged as the Bridgewater Clean Limestone, based on the lower gamma and hard to very hard limestone drilling chip samples. This appears to correspond with the sNMR water content profile. The water content of the Clean Limestone is associated with smaller pore sizes compared to the upper weathered Bridgewater Formation limestone, which has larger pore sizes.

Based on the sNMR model inversion, the estimated hydraulic conductivity is up to 56 m/day (Figure 21). This was the highest value reported across all sites.

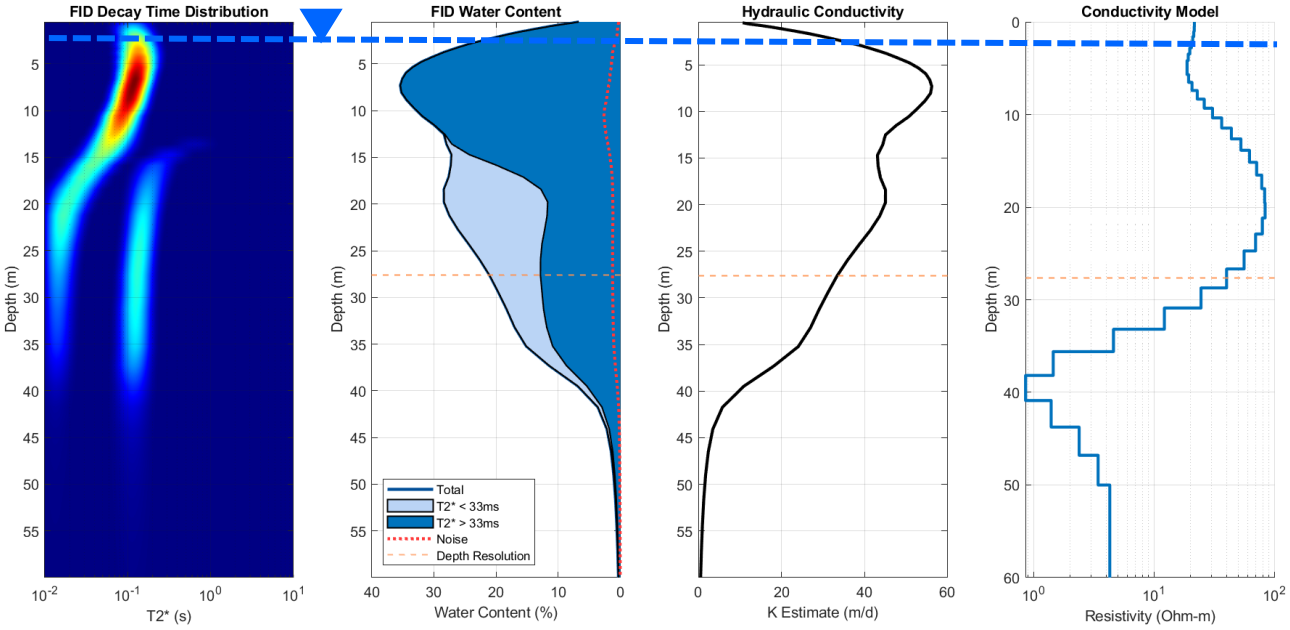


Figure 21. sNMR at Site 16, located at 491500mE, ≈ 100m north of groundwater monitoring well 5830−357 (WAD049) (SWL 3.27 28/11/25), located on the road verge of Birdseye Highway showing water content and estimated hydraulic conductivity (m/d) using a conductivity model from the Loupe data adjacent to the site. Depth of resolution is ≈28 m and estimated depth to the water table is ≈3 mbgl

5.5 sTEM conductivity–depth slices

Conductivity–depth slices (elevation, mAHD) from the sTEM surveys (West−East transect 2, 3 and 4) surveyed in January 2026 are shown in Figure 22, Figure 23 and Figure 24. These slices were created by collating the results from the laterally constrained inversion model outputs at a selected depth interval (or depth slice). In processing these data sets, the inversion results were produced in discrete depth intervals, that is, the inversion routine set the resistivity (the inverse of conductivity, Ohm's Law), as well as the thickness of each layer. The thickness of each layer increases with depth, reflecting the inherent loss of resolution as the EM signal progresses into the ground. Depth slices of the inverted TEM data sets were prepared for this report at 5 m depth intervals.

The 4 survey transect lines clearly show the extent of seawater intrusion in the area east of the Elliston township, to about 3.2 km inland from the coast. The depth to the top of the more conductive zone (seawater) is at an elevation of -20 to -40 mAHD (Figure 23 and Figure 24). The depth slices along each transect line demonstrate how the intruding seawater extent varies within the landscape. This is likely to be influenced by the surrounding topography and varying thickness and deposition of the Bridgewater Formation overlying an undulating surface of the basement rocks. Towards the western end of the survey transects near the Colton Back Road and the Elliston Aerodrome the shallow subsurface conductivity increases, which is likely to be associated with the low−lying wetlands, lakes and salt scalds, for example, Lake Hamp and Myrtle Swamp, that have an elevation below mean sea level and therefore behave as a groundwater discharge feature.

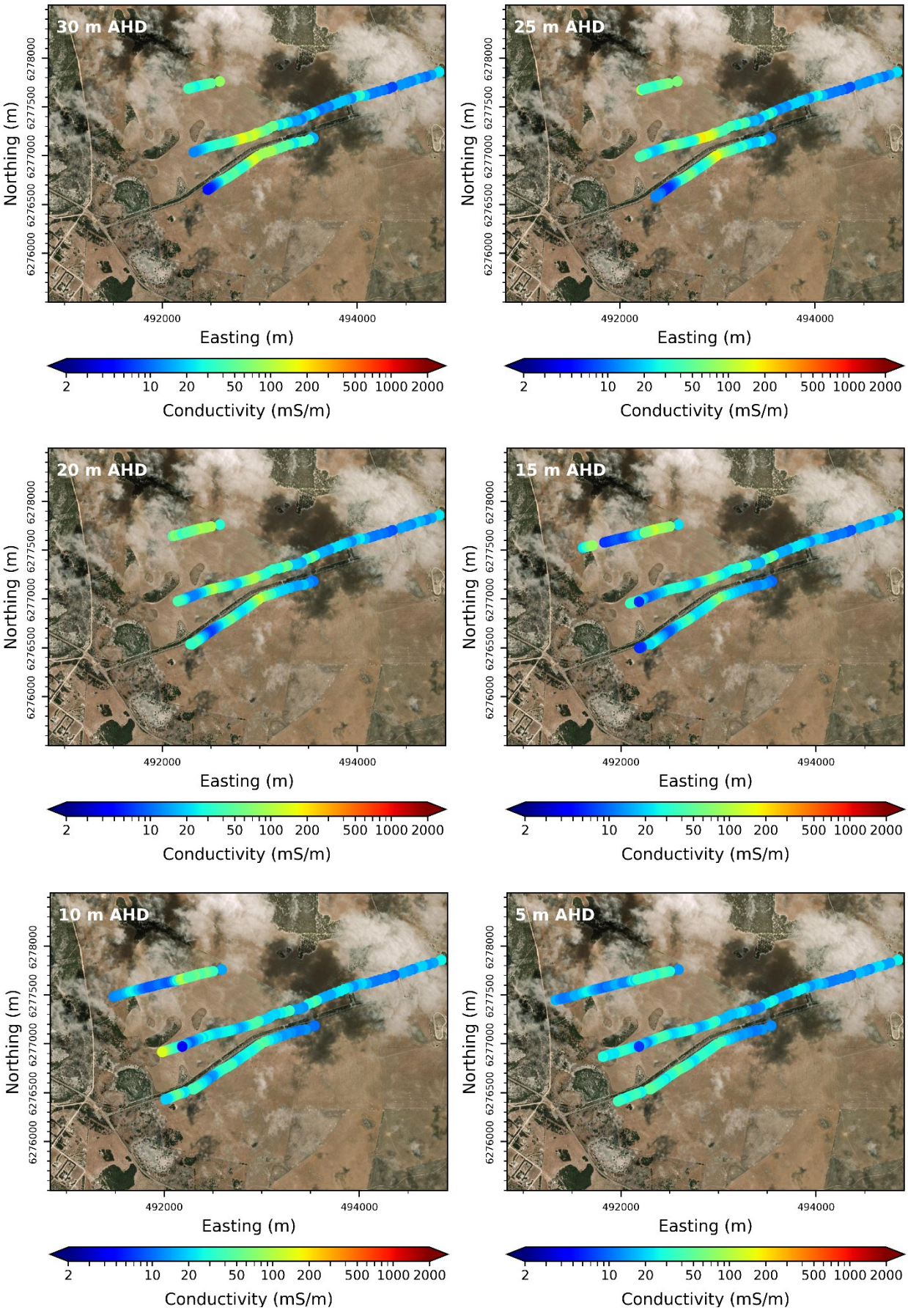


Figure 22. sTEM conductivity depth−slices at 30, 25, 20, 15, 10, 5 mAHD

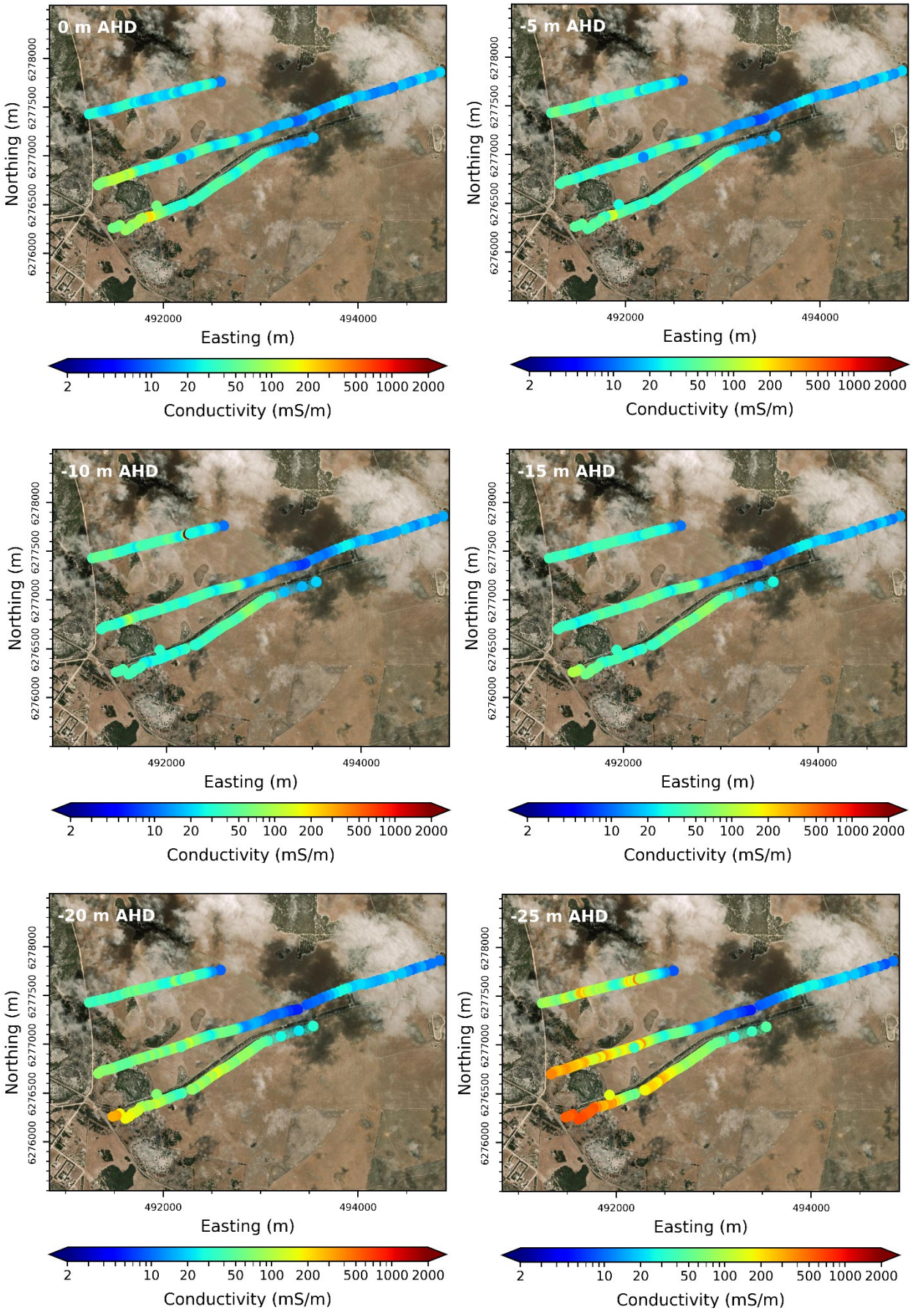


Figure 23. sTEM conductivity depth−slices at 0, -5, -10, -15, -20, -25 mAHD

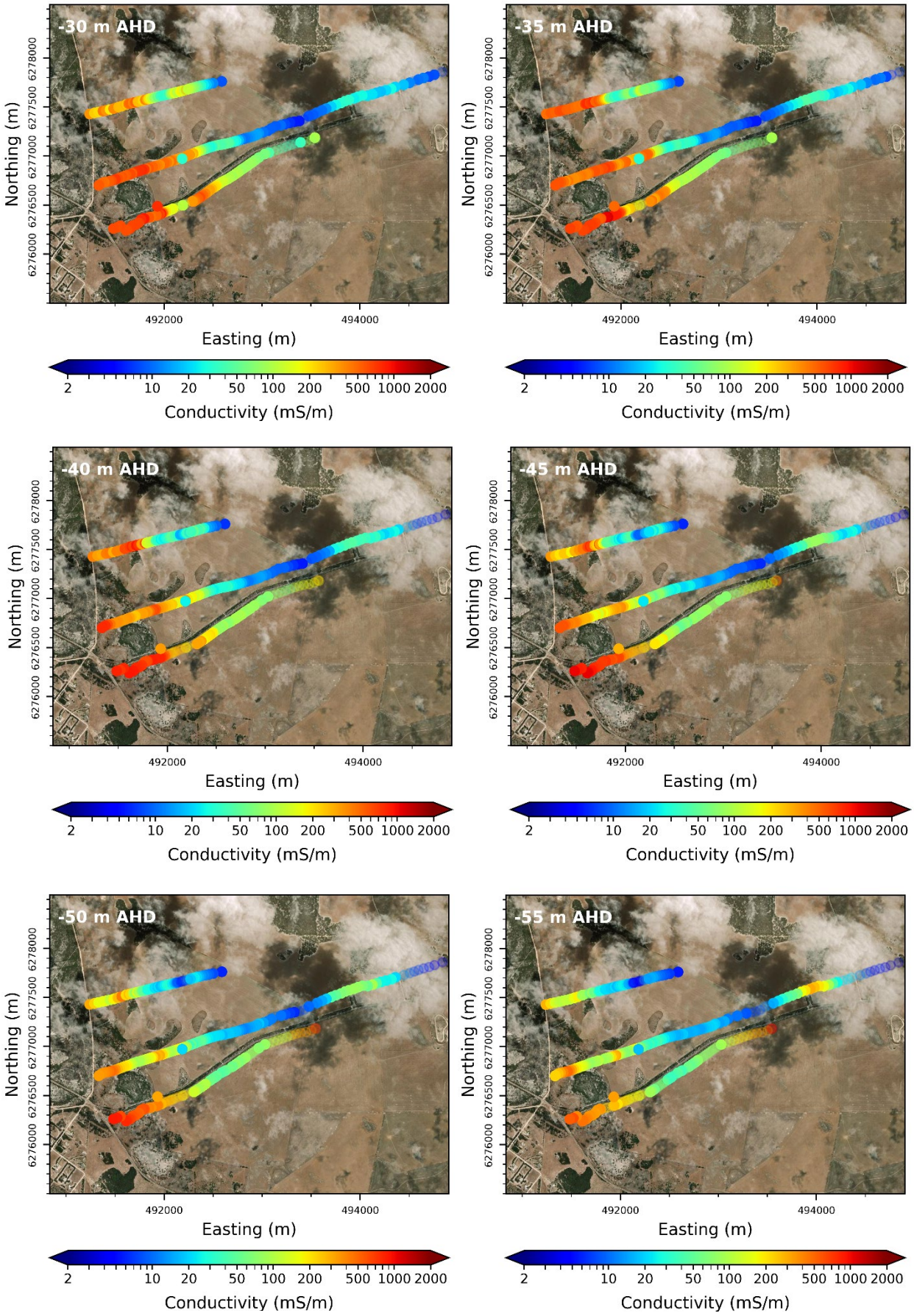


Figure 24. sTEM conductivity depth−slices at -30, -35, -40, -45, -50, -55 mAHD

5.6 Loupe and sTEM data summary

The extent of seawater intrusion in the area around Elliston, SA is up to about 3.2 km inland from the coast (Figure 25). This map is based on examining all the Loupe and sTEM conductivity–depth sections and identifying the location of the toe of the seawater intrusion wedge, which is approximately at an elevation of -40 mAHD. Approximate locations of contact between seawater and fresh groundwater are indicated with a thick solid red line. The inferred seawater extent inland across the coastal region is indicated with thick dashed red lines based on the locations of the TEM survey transect lines. These data sets provide a snapshot in time as to where the interface is and follow up surveys in combination with a solute transport model would be necessary to assess the rate of seawater intrusion under various climatic and groundwater extraction scenarios.

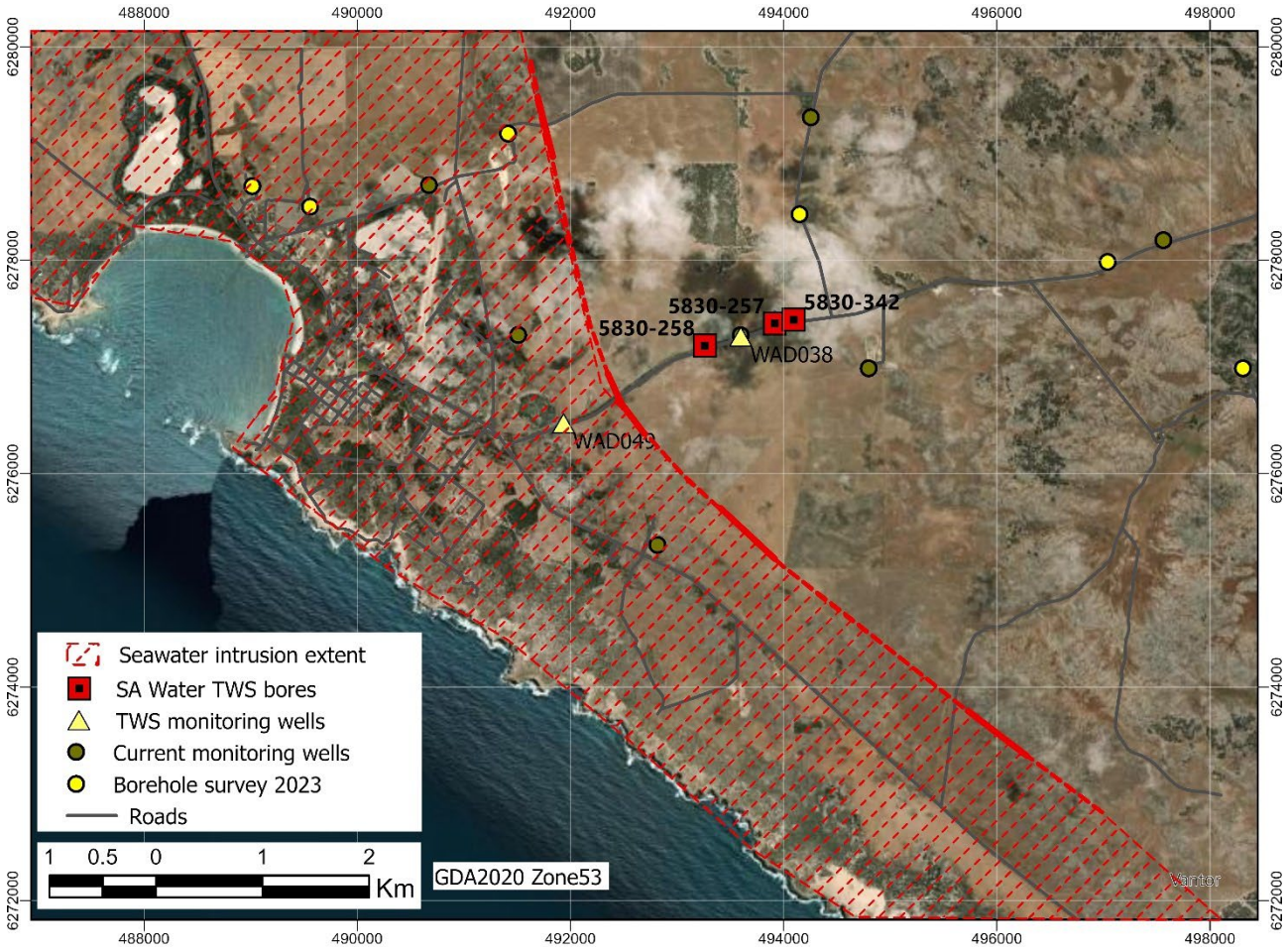


Figure 25. Map showing the likely extent of seawater intrusion (red hatching) near Elliston, SA

5.7 TEM and downhole geophysical logs from 5830−357 (WAD049)

Following the hydrogeophysics surveys that were completed in November 2024 and the successful identification of the seawater wedge, a drilling program was undertaken by DEW in May 2025. The objectives of this program were to drill and construct a groundwater monitoring well within the wedge and towards the seawater intrusion toe along the road easement of the Birdseye Highway towards the SA Water TWS bores. The geophysical data collected from this groundwater monitoring well (5830−357 (WAD049)) is shown in Figure 26, along with a simplified geological and lithological interpretation of the drillhole log. Unfortunately, the drillhole contained a significant amount of fill after drillhole circulation and cleaning, and therefore the geophysical logs only go down to ≈47.7 m depth, when the hole was drilled to 56.5 m depth. The interpretation of the St Peter Suite basement material encountered at the bottom of the drillhole was based on the hard drilling and the pale grey abundant quartz overgrowths, angular grains and abundant fine black specks in the drilling cuttings that were recovered. As with the previous analysis of well logs from the Elliston and Bramfield area by DEW in 2025, lithological interpretation is based both on geological and drillers logs, as well as gamma ray data.

In general, we have interpreted that where the gamma ray data is relatively elevated and more irregular, the formation is likely to be the more porous and weathered Bridgewater Formation, and where the gamma levels tend to be lower and slightly less variable, we are logging in the Bridgewater Clean Limestone. We note here that strictly speaking both are in the Bridgewater Formation. For the purposes of this report, we are dividing the Bridgewater into 2 units – the weathered upper unit (Bridgewater Formation) and the bottom fresh limestone (Bridgewater Clean Limestone). We have interpreted the contact between the 2 units to occur at approximately 40 m depth at 5830−357 (WAD049) based on the gamma data. However, the hydrostratigraphic log interprets it from 17.7 m depth based on the lower gamma. There is a notable gamma increase between 32 and 40 m depth, which suggests that there is some inherent heterogeneity across the formation, making an absolute definition difficult.

It was originally assumed that the contact between the fresher groundwater and the underlying saltwater intrusion would be more obvious than it is in the inductive logs. Interestingly, based on the ground TEM data collected in this area, the variability seen in the EM inductive log is unexpected. We have interpreted the contact between the low salinity groundwater and the seawater to be located at ≈29 m depth (-25 mAHD). This is supported by the fluid water conductivity log, which puts the contact at ≈33 m depth (but is not as reliable because these logs are dependent on the location of the well screen and may also be impacted by the drillhole having recently been drilled). Similarly, the EC of the water samples collected during drilling suggests that the contact is located between 32.6 m and 38.6 m depth, again, these depths (and associated conductivities) are relatively imprecise as they will be affected by fluid mixing during drilling. Taken together, all these lines of evidence from the drillhole logs point to a transition between the low salinity groundwater and seawater at less than 35 m depth.

Loupe and sTEM data sets along West−East transect 3 and transect 4 show that the new groundwater monitoring well 5830−357 (WAD049) is well placed in the approximate toe of the wedge. Examination of the sTEM soundings to the east and west of 5830−357 (WAD049) clearly show the transition from: the lower salinity groundwater ahead of the toe (station 150); within the toe (station 160); the transition zone (station 179); the seawater wedge (Site 254 located at 5830−357 (WAD049); and Site 184) (Figure 27). The inset map in Figure 27 shows the locations of the measurement sites adjacent to the bore.

Comparing the borehole EM induction log from 5830−357 (WAD049) and the sTEM, Loupe and sNMR data sets from the adjacent area shows similar trends in the bulk conductivity from the low salinity groundwater across the transition zone and into the seawater wedge (Figure 28). While the Loupe and sTEM are not capturing as much variation in the top 30 m as the borehole EM does, the Loupe appears to be trying to show a small conductor in the top 5 to 10 m, as is well defined in the borehole EM. The Loupe and sTEM are not resolving any of the finer features visible in the borehole EM from 13 to 27 m depth, which is most likely related to the geometry and instrument set up and the spatial resolution that can be achieved (that is, the sTEM and Loupe systems have different size transmitter and receiver coils and spacing so their spatial footprint of the subsurface is much larger than the borehole EM tool). The Loupe, sTEM and the borehole EM data all show a transition to the relatively conductive feature (the seawater intrusion) starting at about 29 m depth and continuing to depth.

The adjacent sNMR at Site 16 shows steadily increasing water content from the surface to its depth or resolution at ≈28 m depth. The depth to the watertable at this site is ≈2.7 m, which is similar to the measured SWL of 3.27 m at WAD049 ≈200 m to the south.

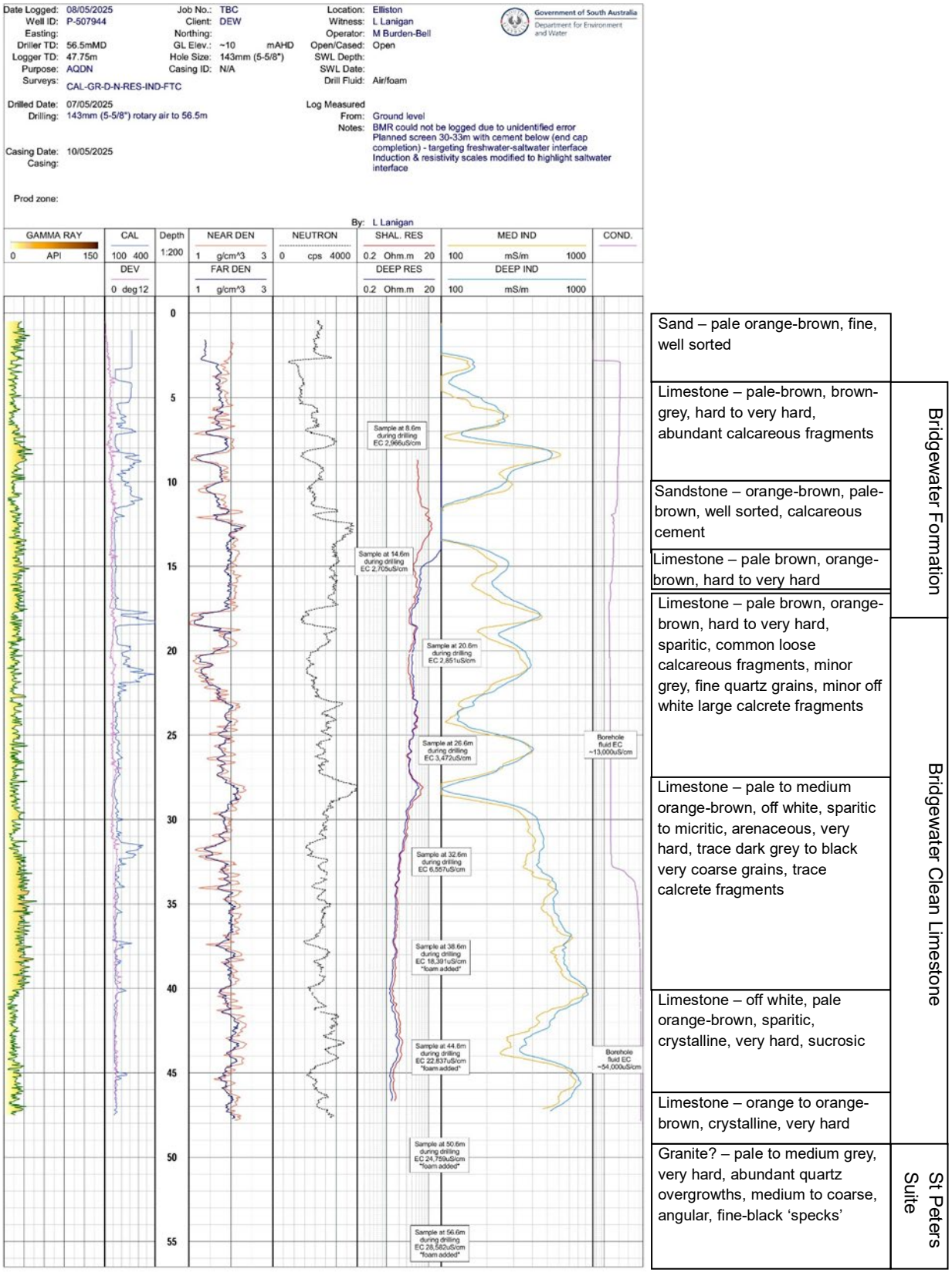


Figure 26. Geophysical log of groundwater monitoring well 5830−357 (WAD049), with geological log and formation interpretation added on right

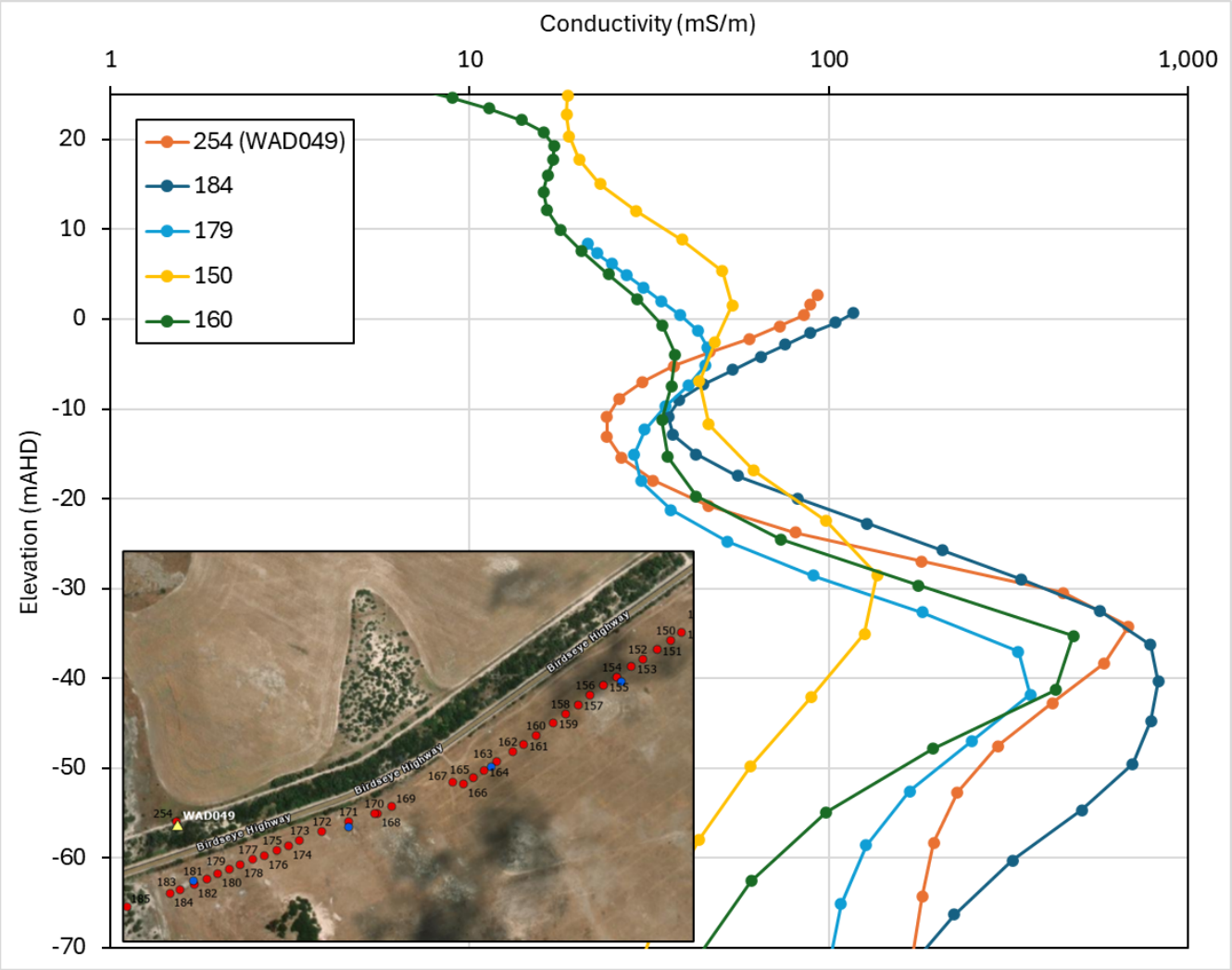


Figure 27. Comparison of inverted sTEM measurements adjacent to 5830−357 (WAD049). Station 254 sits immediately adjacent to the well. Station 184 is ≈90 m south of the well and to the west (reflecting conductive conditions related to the seawater wedge), Station 179 is ≈90 m south−east of the well (reflecting conductive conditions related to the transition zone), Station 160 is further upgradient within the toe and station 150 is upgradient of the toe of the wedge. Note that the conductivity scale is linear

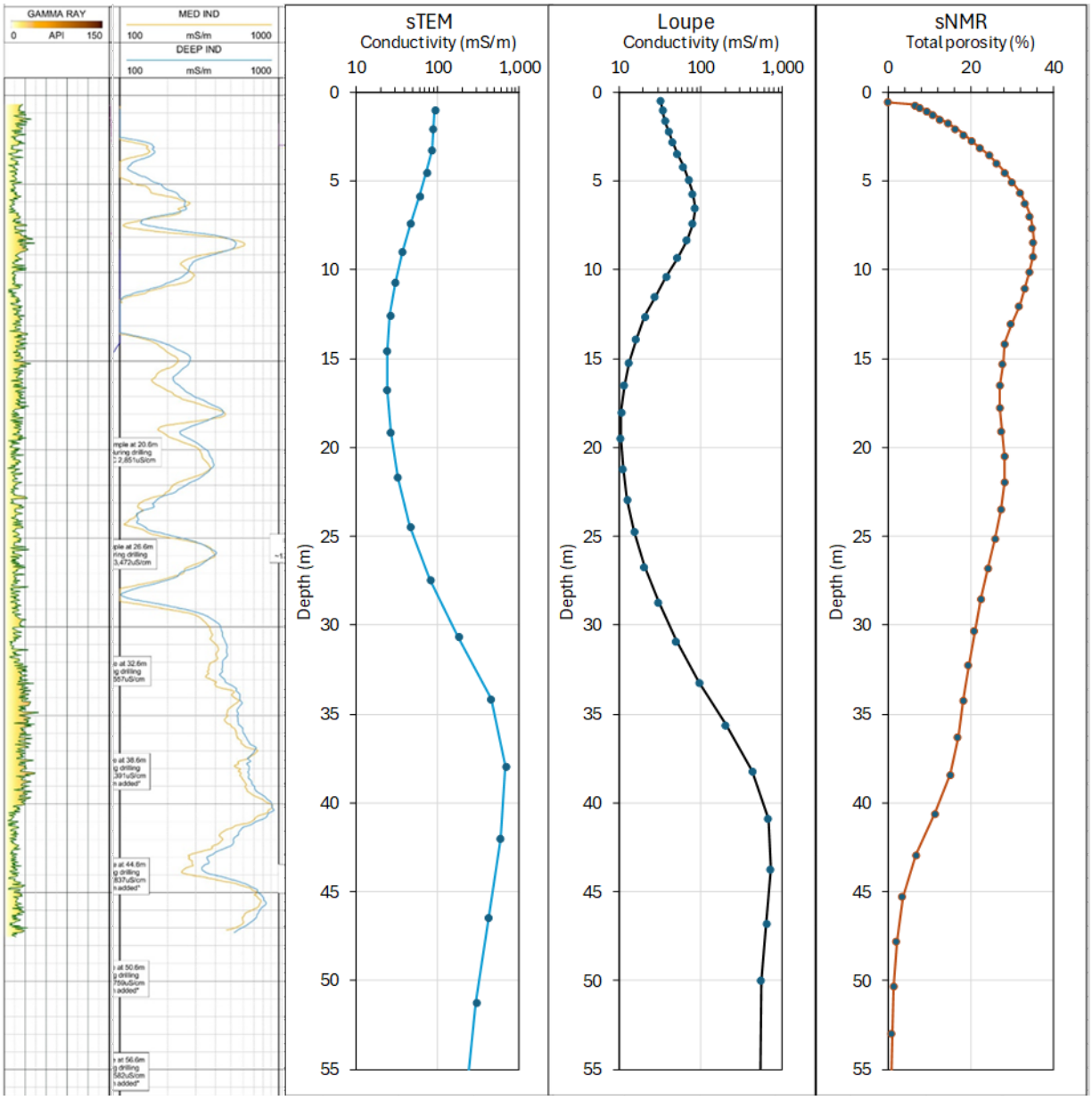


Figure 28. Comparison of geophysical borehole logs from 5830−357 (WAD049) with adjacent sTEM, Loupe and sNMR data sets

5.8 sNMR data summary

Sixteen surface NMR surveys were completed across the Elliston/Bramfield area; these sites were co−located with the Loupe and sTEM survey lines (Figure 2). The data from 14 of the 16 sites were deemed valid. Unfortunately, the depth to the watertable at Site 1 (>70 m below ground) was beyond the depth of investigation of the GMR Flex system and therefore there were no useable data. The data set from Site 8 were extremely noisy making the inverted results unusable. This may be attributed to cultural (electrical) noise and interference from overhead powerlines and electricity transformers adjacent to the site.

Normally (and often as a first pass) a resistive earth model is used in the inversion process (for example, see top panel, Figure 29). This provides a depth resolution to about 35 m depth for Site 16, which is ≈100 m to the north of groundwater monitoring well, 5830−357 (WAD049). A more robust inversion incorporated the subsurface conductivity structure model outputs based on the Loupe TEM

data set to improve the sNMR model inversion results. Including information on the subsurface conductivity changed the depth resolution of the sNMR inversion to about 27 m for Site 16 (see the bottom panel, Figure 29).

The subsurface conductivity has an influence on the NMR response and the depth of investigation of the sNMR signal. In this instance, the depth resolution is 27 m for the conductive earth model compared to 35 m for the resistive earth model. There are also some subtle changes to the percentage of free draining water with the results showing slightly lower values for the conductive model (up to 35% at 7.5 m depth) compared to 38% at 20 m for the resistive model.

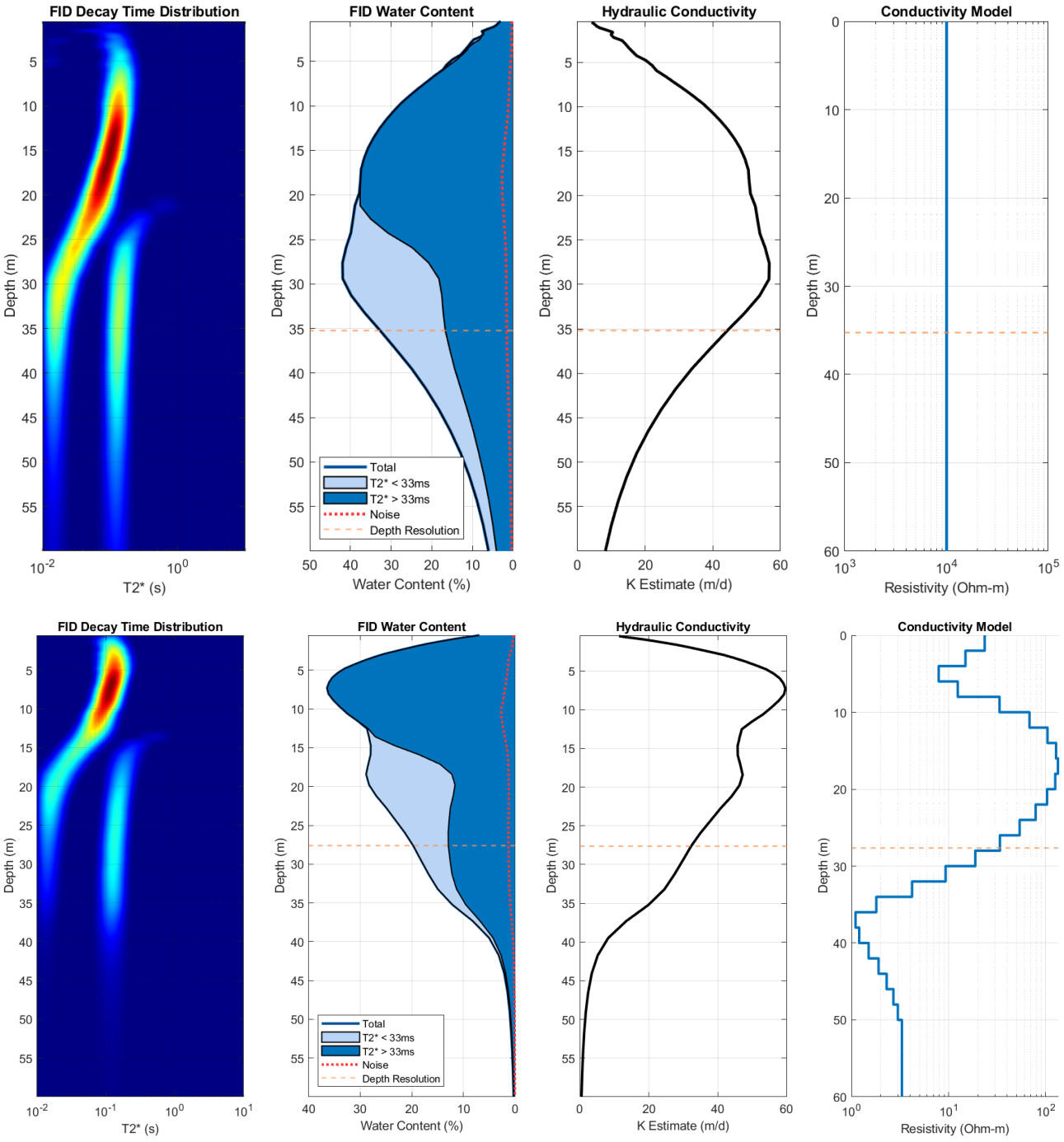


Figure 29. sNMR inversions at Site 16 comparing a resistive (top panel) and conductive (bottom panel) earth model

Based on the 14 successful sNMR soundings, whisker plots show the range in water content for bound water (bw), mobile water (mw – free draining water measured by sNMR: T2 > 33ms) and the total water content (tw− porosity) (Figure 30). For all sites over the entire profile: the median bound water is 2.2% (Lower quartile (LQ) = 0.9%; upper quartile (UQ) = 4.4%); the median mobile water is 5.3% (LQ = 2.7%; UQ = 7.8%); and the median total water content is 14.1% (LQ = 8.4%; UQ = 16.2%). The total porosity of the shallow Quaternary Limestone aquifer is relatively high; based on the distribution of the site locations there is significant spatial heterogeneity but there is also heterogeneity with depth; the latter is related to the variable lithology of the Bridgewater Formation (Lanigan, 2025).

Specific yield estimates from previous studies across the Eyre Peninsula have been summarised by Stewart et al., (2012). Their report for the Musgrave PWA reported specific yield estimates from 0.006 to 0.045 (0.06% to 4.5%), which are towards the low end of the estimates based on the sNMR.

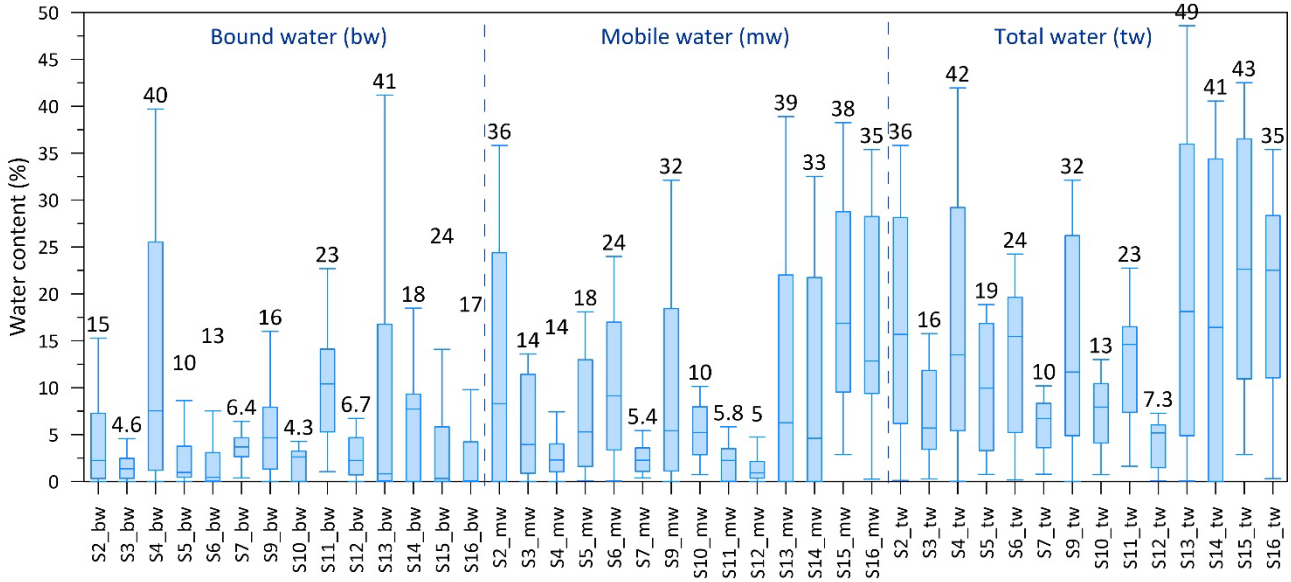


Figure 30. Whisker plots showing the water content for bound water (bw), mobile water (mw) and total water (tw) content (porosity) for all the sNMR sites

The whisker plots in Figure 31 show that the geometric mean estimated hydraulic conductivity for the 14 sites is 3.5 m/day (LQ= 1.0 m/day; UQ= 10.3 m/day) for the saturated portion of the aquifer, which was determined as the zone between the watertable depth and the depth of resolution of the sNMR inversion model (Table 1). The final sNMR site, no. 16, which is located ≈ 100 m north of the new groundwater monitoring well 5830−357 (WAD049), had the highest estimated hydraulic conductivity values (LQ= 19.6 m/day to UQ= 42.9 m/day).

Stewart et al., (2012) summarised available data from previous hydrogeological studies for the Musgrave PWA and reported that the geometric mean transmissivity value (n=6) is 1,505 m^2/d, which would translate to hydraulic conductivity estimates of 50 to 150 m/day for a 10 to 30 m thick aquifer. The four downhole NMR surveys completed in 2025 on groundwater monitoring wells TAA060, TAA059, WAD030 and WAD040 for the saturated Bridgewater Formation gave median hydraulic conductivity estimates (based on the sum of echoes) of between 28 and 749 m/day (Lanigan, 2025). The sNMR estimates of hydraulic conductivity are towards the low end of this range in values;

however, the instrument is averaging over a much larger spatial footprint compared to the zone of measurement for the downhole NMR tool.

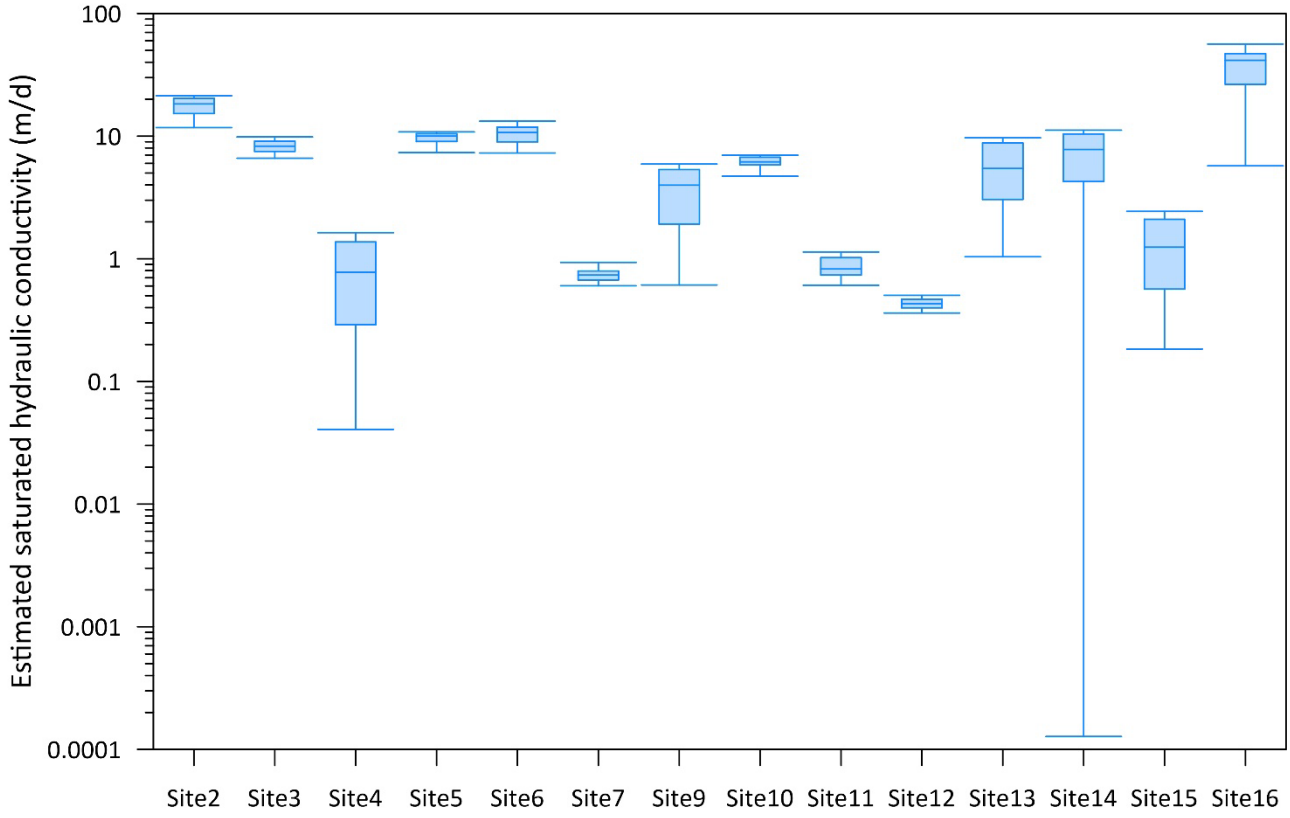


Figure 31. Estimated saturated hydraulic conductivity from the sNMR inversion results for sites 2 to 16

Table 1. Summary statistics of the estimated saturated hydraulic conductivity from the sNMR data for sites 2 to 16 and geometric mean across all sites. The saturated thickness of the aquifer is estimated from the depth of the watertable to the depth of resolution of the sNMR for all sites

	Estimated saturated hydraulic conductivity														
	S2	**S3**	**S4**	**S5**	**S6**	**S7**	**S9**	**S10**	**S11**	**S12**	**S13**	**S14**	**S15**	**S16**	**Geometric mean across all sites**
Geometric mean	17.3	8.2	1.3	9.1	10.8	0.7	2.4	6.1	0.8	0.4	4.6	8.0	1.5	27.9	3.5
Median	18.3	8.3	1.4	9.8	11.3	0.7	3.5	6.2	0.8	0.4	4.7	9.1	1.8	30.8	5.4
Lower Quartile	15.5	7.6	1.2	8.5	9.3	0.7	1.3	5.8	0.7	0.4	3.7	6.5	1.1	19.6	1.0
Upper Quartile	20.2	9.1	1.6	10.4	12.6	0.8	4.9	6.7	0.8	0.5	6.2	10.9	2.3	42.9	10.3

6 Forward TEM modelling

Geophysical forward modelling is a process that has the potential to provide the end−user with information about the sensitivity of a chosen geophysical technique to the intended geological and hydrogeological targets. It provides a geological scenario or data set where the conductivity structure of the subsurface is modified to change with depth, reflecting geological conditions.

6.1 Forward modelling overview

Forward TEM modelling was completed to test the sensitivity of the sTEM profiler TEM system to changes in conductivity with depth, using the data processing and inversion modelling approach (for example, sensitivity to a sharp versus diffuse seawater interface). This was undertaken to assess the applicability of the sTEM system to measuring the thickness of the transition zone and depth to the seawater wedge.

In this section we describe the forward modelling that was done to evaluate the sTEM profiler for 2 geological scenarios where seawater is intruding into the aquifer. Different target depths of the seawater interface were considered (30, 40, 50, 60, 70, 80, 90 and 100 metres) as well as 4 different conceptual models describing the interface as very sharp, sharp, diffuse, and very diffuse. The forward model explicitly describes the conductivity of model layers.

TEM forward modelling was performed using the AarhusInv program (Auken et al., 2015), the 1D forward modelling engine that underlies Aarhus Workbench SPIA geophysical inversion software. All the parameters used for inversion, that characterise the sTEM system, that is, waveform, time windows, and system geometry were used in the forward modelling shown here, to mimic the sTEM profiler system response and sensitivities as closely as possible. The forward model calculates a data set that is like what the geophysical system would observe in the field and thereby predicts system behaviour. These forward modelled data sets are inverted and treated in exactly the same way as the raw data collected from the sTEM system, and the model results compared with the original geological scenario. This allows us to examine whether the geophysical system that is being used can effectively image the geological scenario of interest.

Two modelling scenarios were explored where each forward model contained a total of 6 layers with different geological structure, conductivities and thicknesses. Scenario 1 was based on information and suggestions shared by Kent Inverarity from DEW (Table 2). In modelling performed for Scenario 2 all the original conductivities used in Scenario 1 were multiplied by ¼ (Table 3). This was to reflect the sTEM and Loupe data sets that were collected in the Elliston area, which appeared to show slightly less conductive values than those used in Scenario 1.

For each scenario, a total of 40 models were evaluated with different target depths to the seawater intrusion interface, while varying the thickness of the interface and transition zone between low salinity groundwater above and seawater below. The 4 conceptual models and different depths to the seawater interface and variation in conductivity and thickness of the layers above the interface provided a range of plausible models to investigate with the forward modelling using the sTEM profiler system. These were set to model Very sharp, Sharp, Diffuse or Very diffuse transition zones. For example, in Scenario 1 the top layer (1) is always set to 200 mS/m and the layers below (2, 3, 4 and 5) vary in conductivity until layer 6, which represents seawater with a conductivity of 3,000 mS/m. All the models tested are summarised in Table 2 and Table 3 and selected results are presented in this Chapter with additional figures shown in Appendix A for other target depths of the interface.

Table 2. TEM forward models for the 4 conceptual models (Very sharp, Sharp, Diffuse, Very diffuse) – Scenario 1

Conceptual models	Layer 1 Conductivity (Thickness)	Layer 2 Conductivity (Thickness)	Layer 3 Conductivity Thickness	Layer 4 Conductivity (Thickness)	Layer 5 Conductivity (Thickness)	Layer 6 Conductivity
Seawater interface at 30 m						
Very sharp	200 mS/m (10 m)	200 mS/m (5 m)	200 mS/m (5 m)	200 mS/m (5 m)	200 mS/m (5 m)	3,000 mS/m
Sharp	200 mS/m (10 m)	200 mS/m (5 m)	200 mS/m (5 m)	200 mS/m (5 m)	200 mS/m (5 m)	3,000 mS/m
Diffuse	200 mS/m (5 m)	400 mS/m (5 m)	800 mS/m (5 m)	1,200 mS/m (5 m)	1,800 mS/m (5 m)	3,000 mS/m
Very diffuse	200 mS/m (10 m)	800 mS/m (5 m)	1,500 mS/m (5 m)	2,000 mS/m (5 m)	2,500 mS/m (5 m)	3,000 mS/m
Seawater interface at 40 m						
Very sharp	200 mS/m (10 m)	200 mS/m (10 m)	200 mS/m (10 m)	200 mS/m (5 m)	200 mS/m (5 m)	3,000 mS/m
Sharp	200 mS/m (10 m)	200 mS/m (10 m)	200 mS/m (10 m)	400 mS/m (5 m)	1,000 mS/m (5 m)	3,000 mS/m
Diffuse	200 mS/m (10 m)	400 mS/m (10 m)	800 mS/m (10 m)	1,200 mS/m (5 m)	1,800 mS/m (5 m)	3,000 mS/m
Very diffuse	200 mS/m (10 m)	800 mS/m (10 m)	1,500 mS/m (10 m)	2,000 mS/m (5 m)	2,500 mS/m (5 m)	3,000 mS/m
Seawater interface at 50 m						
Very sharp	200 mS/m (10 m)	200 mS/m (10 m)	200 mS/m (10 m)	200 mS/m (10 m)	200 mS/m (10 m)	3,000 mS/m
Sharp	200 mS/m (10 m)	200 mS/m (10 m)	200 mS/m (10 m)	400 mS/m (10 m)	1,000 mS/m (10 m)	3,000 mS/m
Diffuse	200 mS/m (10 m)	400 mS/m (10 m)	800 mS/m (10 m)	1,200 mS/m (10 m)	1,800 mS/m (10 m)	3,000 mS/m
Very diffuse	200 mS/m (10 m)	800 mS/m (10 m)	1,500 mS/m (10 m)	2,000 mS/m (10 m)	2,500 mS/m (10 m)	3,000 mS/m
Seawater interface at 60 m						
Very sharp	200 mS/m (20 m)	200 mS/m (10 m)	200 mS/m (10 m)	200 mS/m (10 m)	200 mS/m (10 m)	3,000 mS/m
Sharp	200 mS/m (20 m)	200 mS/m (10 m)	200 mS/m (10 m)	400 mS/m (10 m)	1,000 mS/m (10 m)	3,000 mS/m
Diffuse	200 mS/m (20 m)	400 mS/m (10 m)	800 mS/m (10 m)	1,200 mS/m (10 m)	1,800 mS/m (10 m)	3,000 mS/m
Very diffuse	200 mS/m (20 m)	800 mS/m (10 m)	1,500 mS/m (10 m)	2,000 mS/m (10 m)	2,500 mS/m (10 m)	3,000 mS/m
Seawater interface at 70 m						
Very sharp	200 mS/m (30 m)	200 mS/m (10 m)	200 mS/m (10 m)	200 mS/m (10 m)	200 mS/m (10 m)	3,000 mS/m
Sharp	200 mS/m (30 m)	200 mS/m (10 m)	200 mS/m (10 m)	400 mS/m (10 m)	1,000 mS/m (10 m)	3,000 mS/m
Diffuse	200 mS/m (30 m)	400 mS/m (10 m)	800 mS/m (10 m)	1,200 mS/m (10 m)	1,800 mS/m (10 m)	3,000 mS/m
Very diffuse	200 mS/m (30 m)	800 mS/m (10 m)	1,500 mS/m (10 m)	2,000 mS/m (10 m)	2,500 mS/m (10 m)	3,000 mS/m
Seawater interface at 80 m						
Very sharp	200 mS/m (40 m)	200 mS/m (10 m)	200 mS/m (10 m)	200 mS/m (10 m)	200 mS/m (10 m)	3,000 mS/m
Sharp	200 mS/m (40 m)	200 mS/m (10 m)	200 mS/m (10 m)	400 mS/m (10 m)	1,000 mS/m (10 m)	3,000 mS/m
Diffuse	200 mS/m (40 m)	400 mS/m (10 m)	800 mS/m (10 m)	1,200 mS/m (10 m)	1,800 mS/m (10 m)	3,000 mS/m
Very diffuse	200 mS/m (40 m)	800 mS/m (10 m)	1,500 mS/m (10 m)	2,000 mS/m (10 m)	2,500 mS/m (10 m)	3,000 mS/m
Seawater interface at 90 m						
Very sharp	200 mS/m (50 m)	200 mS/m (10 m)	200 mS/m (10 m)	200 mS/m (10 m)	200 mS/m (10 m)	3,000 mS/m
Sharp	200 mS/m (50 m)	200 mS/m (10 m)	200 mS/m (10 m)	400 mS/m (10 m)	1,000 mS/m (10 m)	3,000 mS/m
Diffuse	200 mS/m (50 m)	400 mS/m (10 m)	800 mS/m (10 m)	1,200 mS/m (10 m)	1,800 mS/m (10 m)	3,000 mS/m
Very diffuse	200 mS/m (50 m)	800 mS/m (10 m)	1,500 mS/m (10 m)	2,000 mS/m (10 m)	2,500 mS/m (10 m)	3,000 mS/m
Seawater interface at 100 m						
Very sharp	200 mS/m (60 m)	200 mS/m (10 m)	200 mS/m (10 m)	200 mS/m (10 m)	200 mS/m (10 m)	3,000 mS/m
Sharp	200 mS/m (60 m)	200 mS/m (10 m)	200 mS/m (10 m)	400 mS/m (10 m)	1,000 mS/m (10 m)	3,000 mS/m
Diffuse	200 mS/m (60 m)	400 mS/m (10 m)	800 mS/m (10 m)	1,200 mS/m (10 m)	1,800 mS/m (10 m)	3,000 mS/m
Very diffuse	200 mS/m (60 m)	800 mS/m (10 m)	1,500 mS/m (10 m)	2,000 mS/m (10 m)	2,500 mS/m (10 m)	3,000 mS/m

Table 3. TEM forward models for the 4 conceptual models (Very sharp, Sharp, Diffuse, Very diffuse) – Scenario 2

Conceptual models	Layer 1 Conductivity (Thickness)	Layer 2 Conductivity (Thickness)	Layer 3 Conductivity Thickness	Layer 4 Conductivity (Thickness)	Layer 5 Conductivity (Thickness)	Layer 6 Conductivity
Seawater interface at 30 m						
Very sharp	50 mS/m (10 m)	50 mS/m (5 m)	50 mS/m (5 m)	50 mS/m (5 m)	50 mS/m (5 m)	750 mS/m
Sharp	50 mS/m (10 m)	50 mS/m (5 m)	50 mS/m (5 m)	100 mS/m (5 m)	250 mS/m (5 m)	750 mS/m
Diffuse	50 mS/m (10 m)	100 mS/m (5 m)	200 mS/m (5 m)	300 mS/m (5 m)	450 mS/m (5 m)	750 mS/m
Very diffuse	50 mS/m (10 m)	200 mS/m (5 m)	375 mS/m (5 m)	500 mS/m (5 m)	625 mS/m (5 m)	750 mS/m
Seawater interface at 40 m						
Very sharp	50 mS/m (10 m)	50 mS/m (10 m)	50 mS/m (10 m)	50 mS/m (5 m)	50 mS/m (5 m)	750 mS/m
Sharp	50 mS/m (10 m)	50 mS/m (10 m)	50 mS/m (10 m)	100 mS/m (5 m)	250 mS/m (5 m)	750 mS/m
Diffuse	50 mS/m (10 m)	100 mS/m (10 m)	200 mS/m (10 m)	300 mS/m (5 m)	450 mS/m (5 m)	750 mS/m
Very diffuse	50 mS/m (10 m)	200 mS/m (10 m)	375 mS/m (10 m)	500 mS/m (5 m)	625 mS/m (5 m)	750 mS/m
Seawater interface at 50 m						
Very sharp	50 mS/m (10 m)	50 mS/m (10 m)	50 mS/m (10 m)	50 mS/m (10 m)	50 mS/m (10 m)	750 mS/m
Sharp	50 mS/m (10 m)	50 mS/m (10 m)	50 mS/m (10 m)	100 mS/m (10 m)	250 mS/m (10 m)	750 mS/m
Diffuse	50 mS/m (10 m)	100 mS/m (10 m)	200 mS/m (10 m)	300 mS/m (10 m)	450 mS/m (10 m)	750 mS/m
Very diffuse	50 mS/m (10 m)	200 mS/m (10 m)	375 mS/m (10 m)	500 mS/m (10 m)	625 mS/m (10 m)	750 mS/m
Seawater interface at 60 m						
Very sharp	50 mS/m (20 m)	50 mS/m (10 m)	50 mS/m (10 m)	50 mS/m (10 m)	50 mS/m (10 m)	750 mS/m
Sharp	50 mS/m (20 m)	50 mS/m (10 m)	50 mS/m (10 m)	100 mS/m (10 m)	250 mS/m (10 m)	750 mS/m
Diffuse	50 mS/m (20 m)	100 mS/m (10 m)	200 mS/m (10 m)	300 mS/m (10 m)	450 mS/m (10 m)	750 mS/m
Very diffuse	50 mS/m (20 m)	200 mS/m (10 m)	375 mS/m (10 m)	500 mS/m (10 m)	625 mS/m (10 m)	750 mS/m
Seawater interface at 70 m						
Very sharp	50 mS/m (30 m)	50 mS/m (10 m)	50 mS/m (10 m)	50 mS/m (10 m)	50 mS/m (10 m)	750 mS/m
Sharp	50 mS/m (30 m)	50 mS/m (10 m)	50 mS/m (10 m)	100 mS/m (10 m)	250 mS/m (10 m)	750 mS/m
Diffuse	50 mS/m (30 m)	100 mS/m (10 m)	200 mS/m (10 m)	300 mS/m (10 m)	450 mS/m (10 m)	750 mS/m
Very diffuse	50 mS/m (30 m)	200 mS/m (10 m)	375 mS/m (10 m)	500 mS/m (10 m)	625 mS/m (10 m)	750 mS/m
Seawater interface at 80 m						
Very sharp	50 mS/m (40 m)	50 mS/m (10 m)	50 mS/m (10 m)	50 mS/m (10 m)	50 mS/m (10 m)	750 mS/m
Sharp	50 mS/m (40 m)	50 mS/m (10 m)	50 mS/m (10 m)	100 mS/m (10 m)	250 mS/m (10 m)	750 mS/m
Diffuse	50 mS/m (40 m)	100 mS/m (10 m)	200 mS/m (10 m)	300 mS/m (10 m)	450 mS/m (10 m)	750 mS/m
Very diffuse	50 mS/m (40 m)	200 mS/m (10 m)	375 mS/m (10 m)	500 mS/m (10 m)	625 mS/m (10 m)	750 mS/m
Seawater interface at 90 m						
Very sharp	50 mS/m (10 m)	50 mS/m (10 m)	50 mS/m (10 m)	50 mS/m (10 m)	50 mS/m (10 m)	750 mS/m
Sharp	50 mS/m (10 m)	50 mS/m (10 m)	100 mS/m (10 m)	250 mS/m (10 m)	50 mS/m (10 m)	750 mS/m
Diffuse	100 mS/m (10 m)	200 mS/m (10 m)	300 mS/m (10 m)	450 mS/m (10 m)	100 mS/m (10 m)	750 mS/m
Very diffuse	200 mS/m (10 m)	375 mS/m (10 m)	500 mS/m (10 m)	625 mS/m (10 m)	200 mS/m (10 m)	750 mS/m
Seawater interface at 100 m						
Very sharp	50 mS/m (60 m)	50 mS/m (10 m)	50 mS/m (10 m)	50 mS/m (10 m)	50 mS/m (10 m)	750 mS/m
Sharp	50 mS/m (60 m)	50 mS/m (10 m)	50 mS/m (10 m)	100 mS/m (10 m)	250 mS/m (10 m)	750 mS/m
Diffuse	50 mS/m (60 m)	100 mS/m (10 m)	200 mS/m (10 m)	300 mS/m (10 m)	450 mS/m (10 m)	750 mS/m
Very diffuse	50 mS/m (60 m)	200 mS/m (10 m)	375 mS/m (10 m)	500 mS/m (10 m)	625 mS/m (10 m)	750 mS/m

6.2 Forward modelling results

The forward modelling results are plotted in 2 different ways to highlight various characteristics of the data sets. First, the results are displayed as individual soundings, allowing comparison between the forward model and the inverted results of the forward modelling. The inverted results are also presented as conductivity–depth sections with stations 50 m apart along the horizontal axis. All the conductivity–depth sections shown in this, and previous milestone reports as part of the project, use a similar conductivity scale.

The 4 conceptual models (Very sharp, Sharp, Diffuse and Very diffuse) for Scenario 1 are shown as subfigures in Figure 32 (30 m deep to target of the seawater interface). The figures showing the other forward model results for 40 m, 50 m, 60 m, 70 m, 80 m, and 90 m depth to the interface are in Appendix A. The plot on the left in each subfigure shows the model tested (refer to Table 2 and

Table 3) in blue, and the forward modelled results in orange. The horizontal axis is a conductivity (log scale) in mS/m and the vertical axis is depth from the ground surface in metres. The plot on the right in each subfigure compares the forward model (Input mag) fit to the inversion model (Out mag) fit. The horizontal axis shows time (seconds) and the y−axis the signal magnitude (volts/Amp metres squared = V/Am^2), which is very similar to what is recorded on the receiver in the field. Note that for Scenario 1, results are shown with target seawater interface depths ranging from 30 m to 90 m. For Scenario 2, results are only shown for 30 m to 70 m depth.

Comparison plots of the modelled response (signal magnitude vs time) for the 4 conceptual models and the different target depths of the seawater interface (30 m, 40 m, 50 m, 60 m, 70 m, 80 m, 90 m and 100 m) are shown in Figure 34 (Scenario 1) and Figure 35 (Scenario 2). This is intended to provide the reader with a method of visualising the differences between the 4 conceptual models and how the response changes based on the thickness and conductivity of the transition zone above the more conductive seawater and what can be discerned from this.

Forward modelling results of the 4 conceptual models, where the target depth of the seawater interface is at 30 m depth, are shown as conductivity depth−sections in Figure 36 (Scenario 1) and Figure 37 (Scenario 2). Scenario 1 uses a top layer conductivity of 200 mS/m and target layer of 3000 mS/m whereas Scenario 2 has a top layer conductivity of 200 mS/m and target layer of 750 mS/m.

6.3 Analysis of forward modelling results

Key findings from the forward modelling include:

- Examination of the individual soundings for Scenario 1 suggest that the sTEM profiler cannot clearly identify the intruding seawater (layer 6) at depths greater than 60 to 70 m (Figure 32 and Appendix A). This is consistent with the data sounding curves shown in Figure 34.
- Similar findings were observed for Scenario 2, except that it may be possible to resolve the seawater interface to a depth of 70 m (Figure 35).
- The fit between the modelled and inverted data for both the Very sharp and Sharp interfaces (especially in Scenario 2) appear to be characterised by model inversion artefacts in the results that vary across the conductivity value in the top part of the model. It seems unlikely that these artefacts would change the interpretation in that area significantly.

- It is worth reiterating that in each subfigure the contact with the target layer (3,000 mS/m for Scenario 1 and 750 mS/m for Scenario 2) occurs at 30 m depth.
- Examining the results for both scenarios for when the seawater interface is at a depth of 30 m, it is easy to conclude that the transition zone is getting shallower, when in fact, the transition zone is becoming more diffuse (Figure 36 and Figure 37).
- The more diffuse transition zone can result in the depth of the seawater interface being misinterpreted at a shallower depth. This is more pronounced with the Very diffuse conceptual model.
- The coloured conductivity depth−section for Scenario 2 that includes the contour lines shows that the conductivity gradually increases to a maximum at about 30 m depth (Figure 38). Note that the contour labels are logarithmic and the 2.8519 shown corresponds to $10^{2.8519}$ and is equivalent to 711 mS/m (the target layer is 750 mS/m).
- The choice of colour extent and range in colours that are used for the conductivity scale can hide subtle features, which makes it a challenge in identifying and mapping the spatial extent of the transition zone between the low salinity groundwater and seawater. Adjusting the scale can improve visualisation of specific features; however, no single scale effectively reveals both the full conductivity range and finer gradients within the mixing zone.

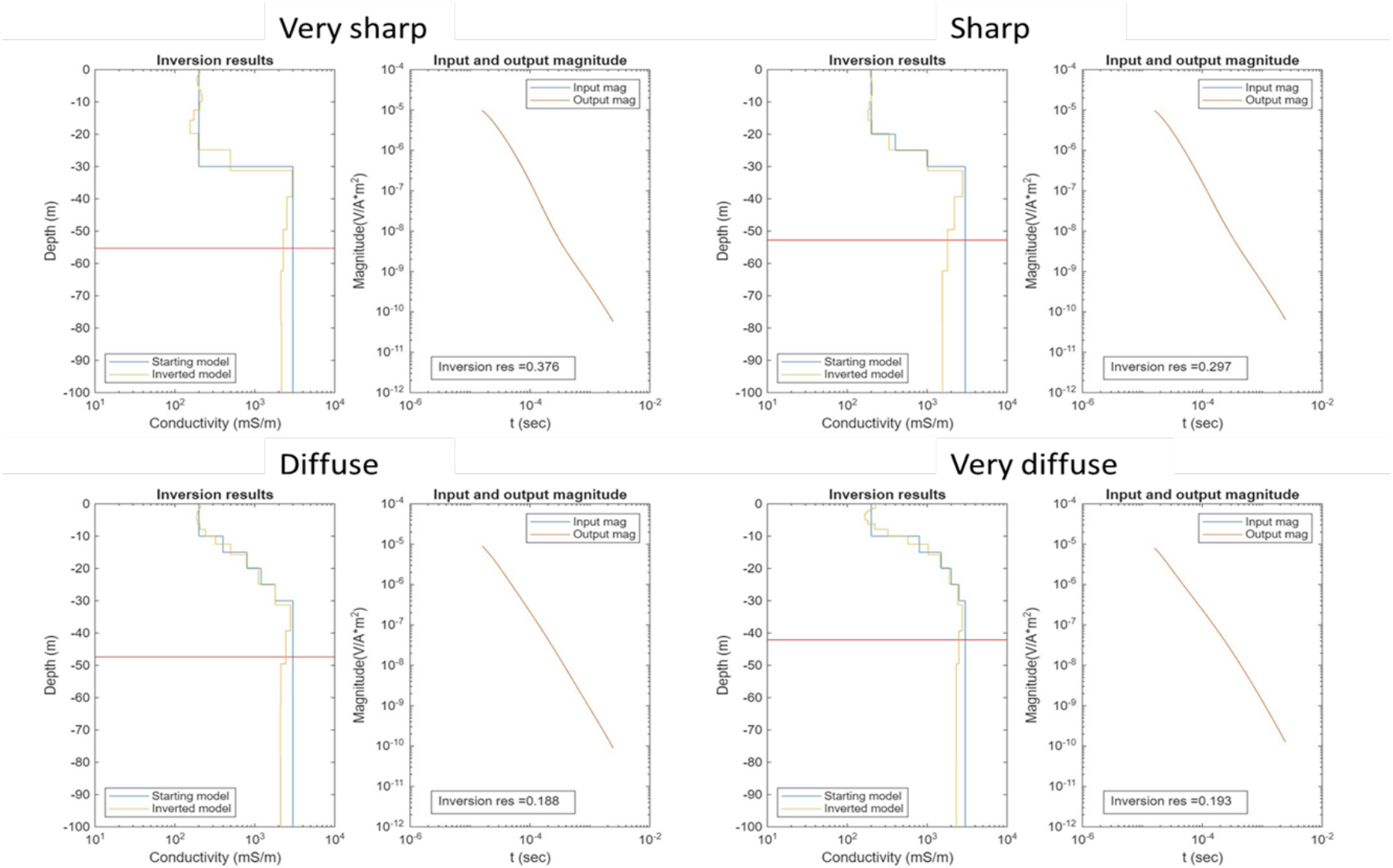


Figure 32. Scenario 1: Modelling results of the 4 different conceptual models of the seawater intrusion interface (very sharp, sharp, diffuse, and very diffuse) at 30 m depth. Left plot in each subfigure shows inverted results in blue and starting model in orange. Horizontal line is the depth of investigation. Right plot in each subfigure shows model fit

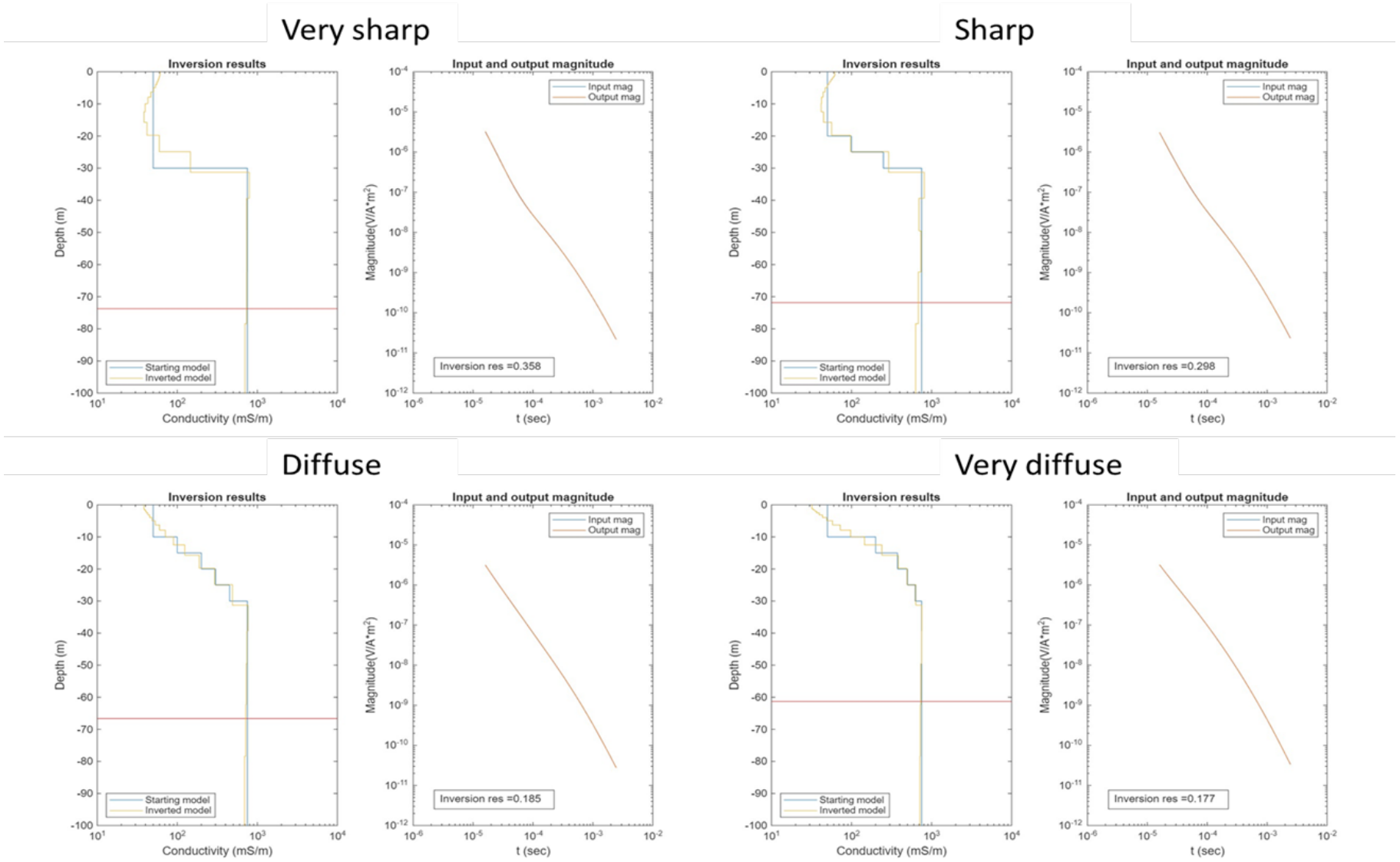


Figure 33. Scenario 2: Modelling results of the 4 different conceptual models of the seawater intrusion interface (very sharp, sharp, diffuse, and very diffuse) at 30 m depth. Left plot in each subfigure shows inverted results in blue and starting model in orange. Horizontal line is the depth of investigation. Right plot in each subfigure shows model fit

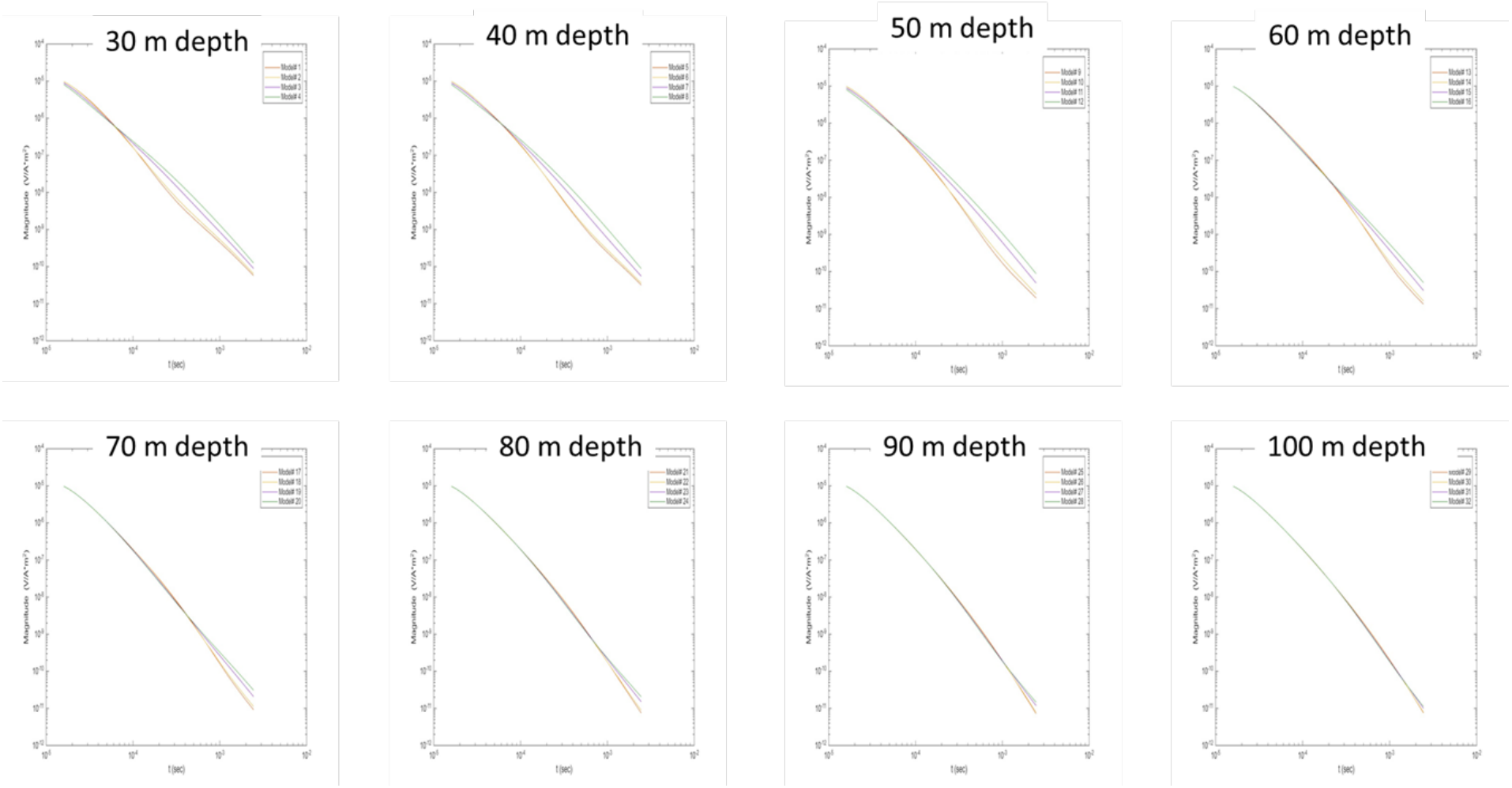


Figure 34. Scenario 1: Modelled response at each tested depth of the seawater intrusion interface for the 4 conceptual models. Note that the 100 m target depth forward and inverted modelling results is not presented in Appendix A because at this depth there was minor difference between the conceptual models

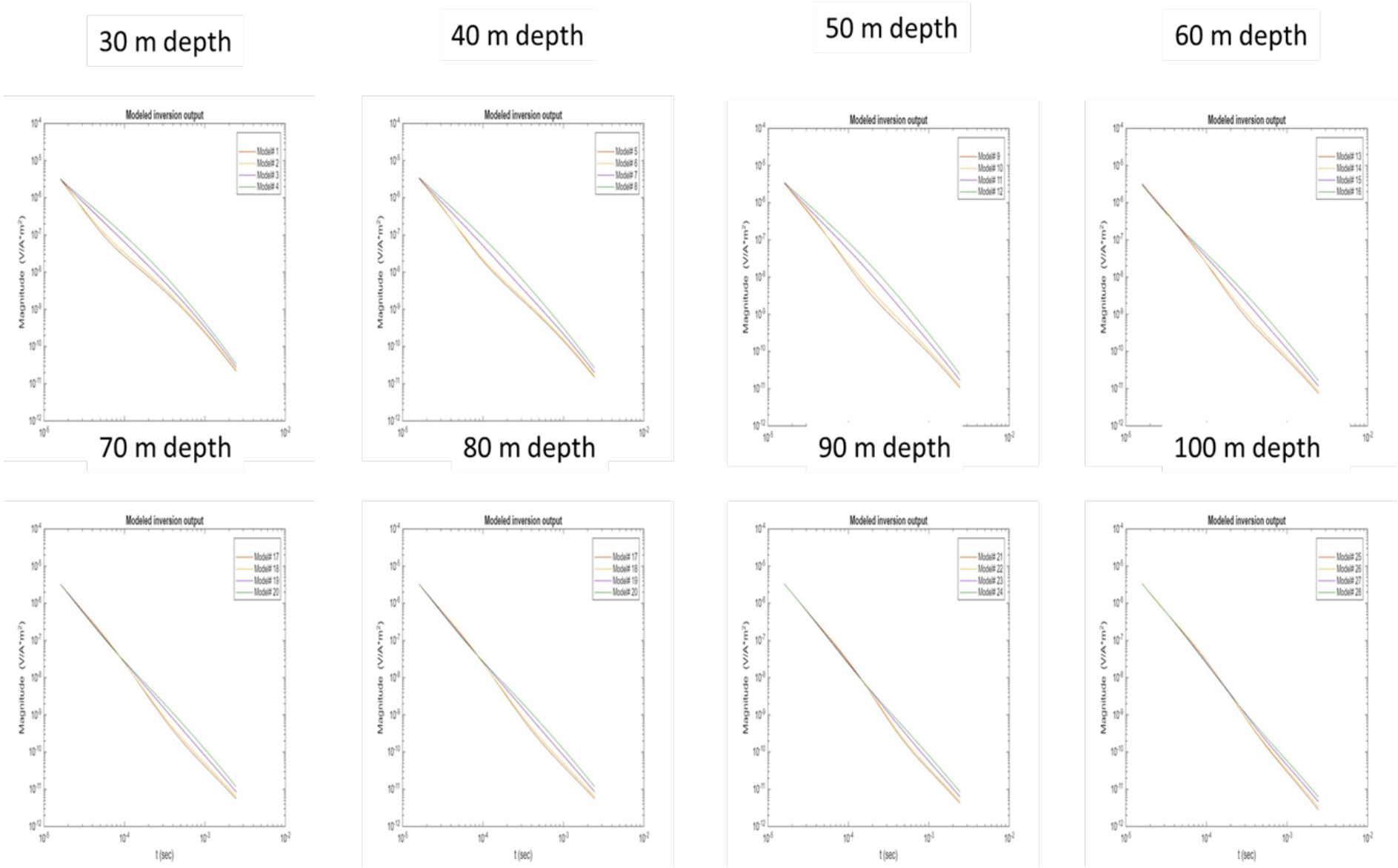


Figure 35. Scenario 2: Modelled response at each tested depth of the seawater intrusion interface for the four conceptual models. Note that the 80,90 and 100 m target depth forward and inverted modelling results is not presented in Appendix A because at these depths there was minor difference between the conceptual models

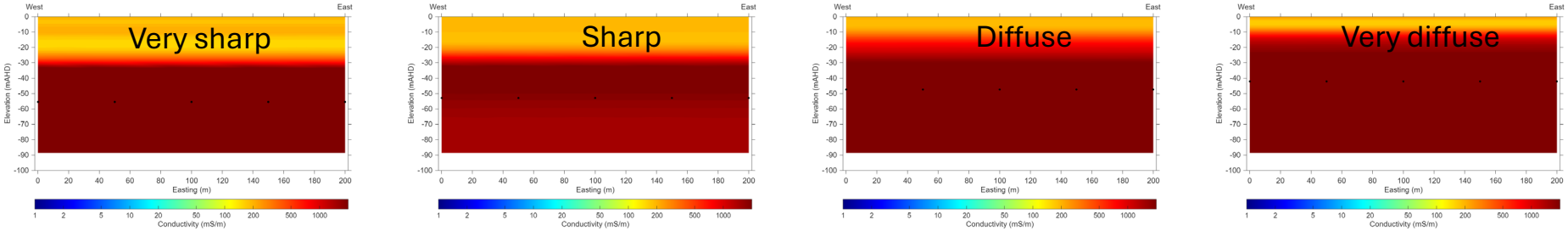


Figure 36. Scenario 1: Forward modelling results of the 4 conceptual models using a top layer conductivity of 200 mS/m and target layer of 3000 mS/m, with seawater interface at 30 m depth

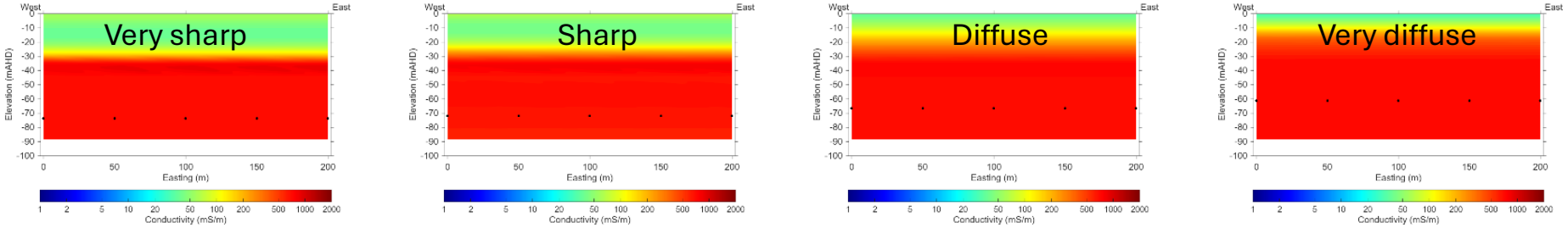


Figure 37. Scenario 2: Forward modelling results of the four conceptual models using a top layer conductivity of 200 mS/m and target layer of 750 mS/m, with seawater interface at 30 m depth

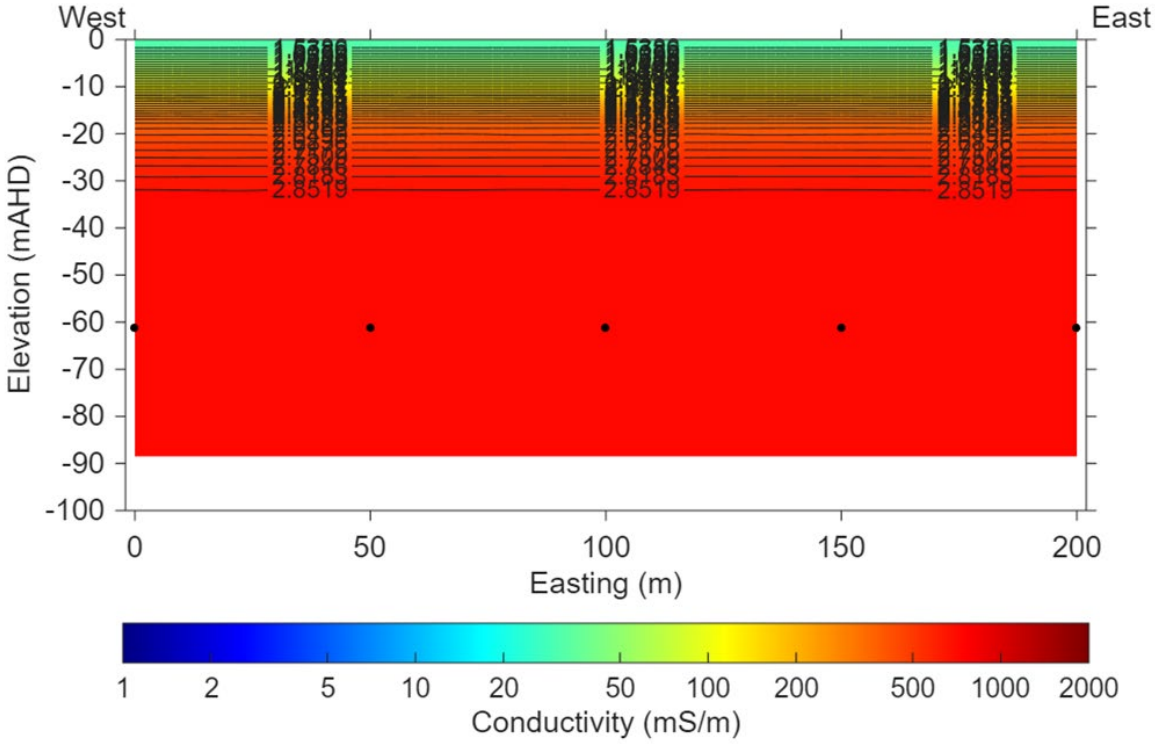


Figure 38. Scenario 2 shows an expanded view of the diffuse conceptual model. The contour lines show where the seawater interface should be based on the forward model with a target depth of 30 m for the seawater

7 Coastal groundwater discharge at Waterloo Bay

7.1 Surveys

A suite of surveys and hydrological assessments were conducted along the beach and within Waterloo Bay, at Elliston in November 2024 to assess groundwater discharge at the coast. This included:

- spatial mapping the near surface beach interface using an EC probe
- Loupe surveys along the beach at low tide
- a water level elevation survey between the ocean and nearby groundwater wells
- a Radon−222 survey
- thermal imaging
- discussions with residents to understand spatial patterns in discharge beyond the sampling period.

7.2 Water levels

A high−resolution in−situ Level TROLL 700 pressure transducer was attached to the Elliston Bay jetty (Eastings: 488834, Northings: 6277861, Elevation: 3.182 mAHD) between 25 and 29 November 2024 and its elevation surveyed using a Trimble RTK GNSS Catalyst DA2 receiver. Water levels were recorded every 6 minutes and a 12−sample running average was used to smooth the wave noise. Measurements were reported as metres above mAHD and compared to the predicted low and high tidal data from the Bureau of Meteorology for Elliston over the same period (Figure 39). The Bureau of Meteorology predicted tides were generally higher than the actual water levels measured during the sampling period, but the overall trend was similar.

For comparison, the RSWL at groundwater observation well 5830−71 (WAD032) in the Quaternary Limestone, located approximately 300 m inland from the Elliston jetty, was 0.89 mAHD, approximately one month prior on 22 October 2024 (downloaded from WaterConnect May 2026). Since 2020, RSWL measurements at 5830−71 (WAD032) (which appears to be the closest monitoring well to the coast) have ranged from 0.63 to 1.05 mAHD (first measured in 1963, but regularly only since 2015). Based on this information, the hydraulic gradient between the observation well and the ocean is exceedingly small and close to 0 m/m during high tide conditions. The reported groundwater EC at this observation well shows that the water is relatively fresh (<1,800 mS/cm).

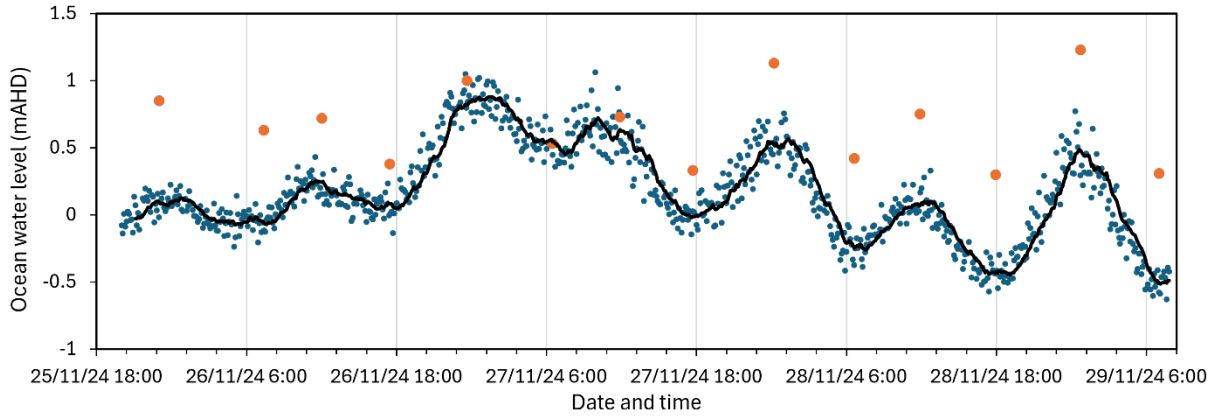


Figure 39. Measured water levels in Waterloo Bay at 6−min intervals from a pressure transducer secured to the Elliston Jetty 25−29 November (blue points) with a 12−point average fitted (black line). Bureau of Meteorology tidal predictions for Elliston over the same period (red points)

7.3 Loupe

Loupe surveys were conducted along the beach at Waterloo Bay, at 2 hours either side of the low tide on 26 and 27 November 2024 to determine if there were low salinity subsurface features that may be associated with submarine groundwater discharge to the bay (Figure 40).



Figure 40. Loupe EM survey at low tide, Waterloo Bay

The processed Loupe data are shown as conductivity depth−sections in Figure 41 to Figure 44. At the intertidal zone (≈-0.5 mAHD), the beach is mostly conductive along the entire beach of Waterloo Bay, where the surveys were undertaken (Figure 41 and Figure 42). There are small zones at a depth of ≈-10 mAHD, where the subsurface is less than 100 mS/m (for example at 100 m east of the jetty). The rocky limestone outcrop protrudes into the bay in this area and small groundwater seeps were observed at the intertidal zone during low tide but were inundated by the high tide. This also corresponds with the shallow geology of the region, as mapped in the DEW Bramfield Groundwater Model report (Figure 2.5; Lanigan, 2025). The North−South section (Figure 43) and the West−East section (Figure 44) that are orientated from the coast towards the highway shows a more conductive

feature (>500 mS/m) intruding inland, which is likely to be seawater. This supports the other Loupe and sTEM survey results further and the existing conceptual model (DEW, 2026). The lower subsurface conductivity features above the intruding seawater are likely to represent the sand dunes between the beach face and the highway. These sand dunes may also act as a local perched aquifer system and potential source of low salinity groundwater discharge at the coast, which is a separate aquifer system to the regional shallow Quaternary Limestone aquifer.

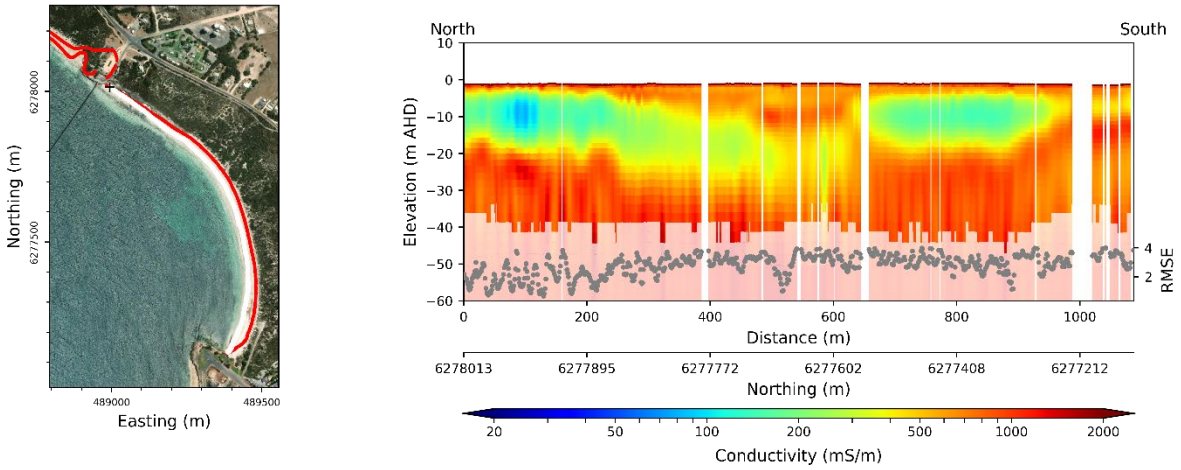


Figure 41. Loupe EM conductivity depth−section (North–South), east of jetty, Waterloo Bay, Elliston at low tide, 26 Nov 2024. Note that the conductivity scale range is 20−2,000 mS/m to improve the contrast

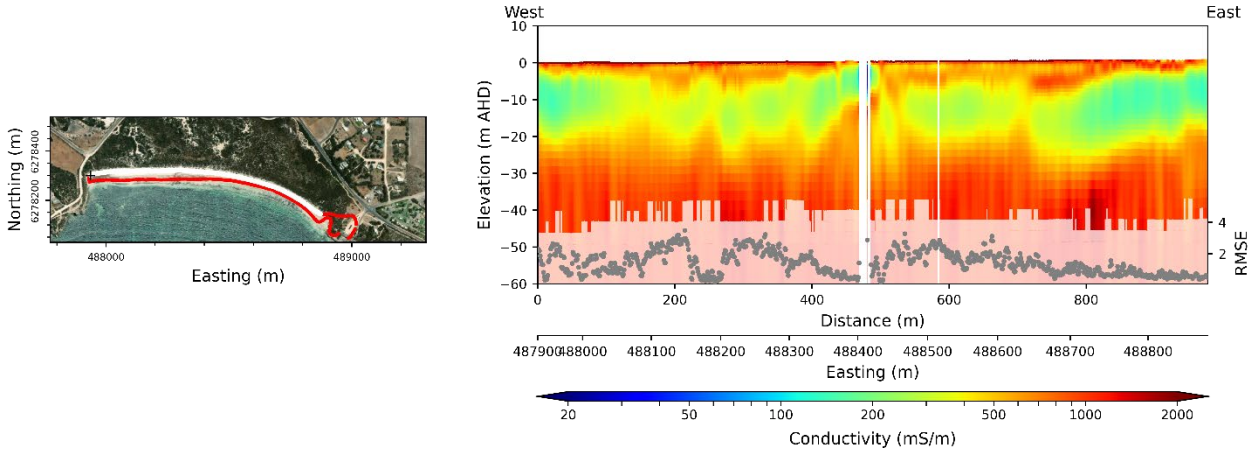


Figure 42. Loupe EM conductivity depth−section (West–East), west of jetty, Waterloo Bay, Elliston at low tide, 26 Nov 2024. Note that the conductivity scale range is 20−2,000 mS/m to improve the contrast

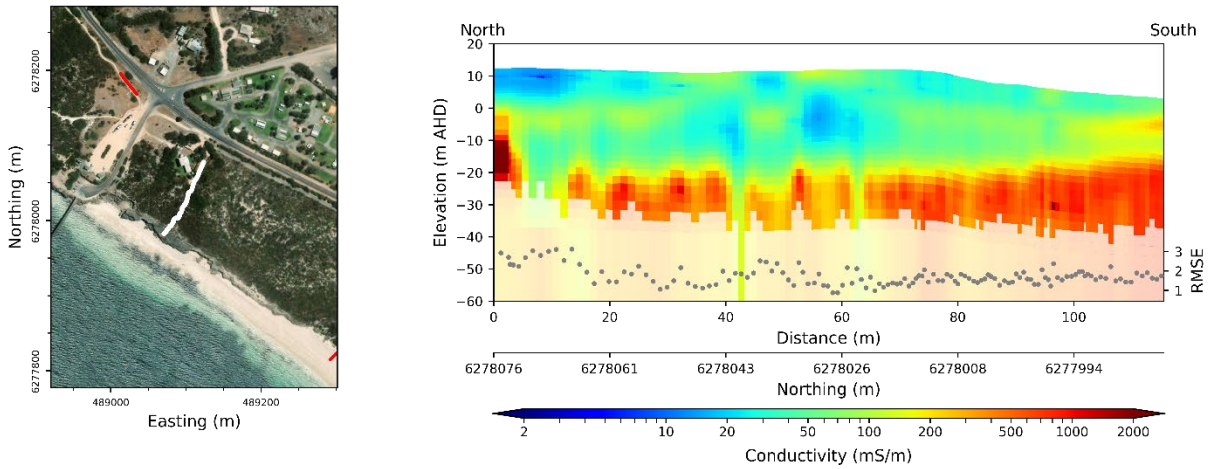


Figure 43. Loupe EM conductivity depth−section (North–South) survey from highway to beach, Elliston, 27 Nov 2024. Note that the conductivity scale range is 2−2,000 mS/m

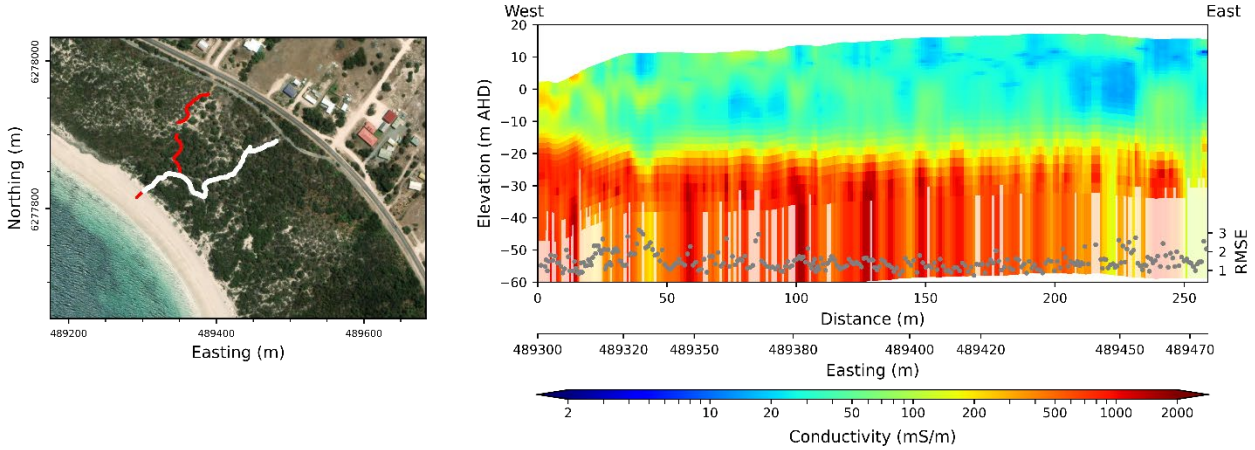


Figure 44. Loupe EM conductivity depth−section (West–East) survey from beach to highway, Elliston, 27 Nov 2024. Note that the conductivity scale range is 2−2,000 mS/m

7.4 Electrical conductivity

An EC Fieldscout instrument was used to measure the saturated sediment EC along the beach at 2 hours either side of low tide around Waterloo Bay every ≈100 m, on 26 and 27 November 2024. The probe was inserted into the beach to the full probe depth of 0.35 m (Figure 45 and Figure 46). The probe must be in saturated sediment to give an accurate reading, which is not the case at low tide; therefore, the reported values are intended to give a qualitative estimate of fresh versus saline and do not directly correspond to fluid salinity. Sampling was conducted within the intertidal zone where fresh groundwater would be expected to lower the salinity if coastal groundwater discharge is occurring. When the probe was set into the sand saturated with seawater (just below low tide), the reported value was between 17 mS/cm (equivalent to 17,000 µS/cm) and the NaN. The NaN represents values greater than the 20 mS/cm, which is the maximum reported value for the probe); values around 17 mS/cm were assumed to indicate a lack of freshwater contribution or entirely seawater composition.



Figure 45. EC Fieldscout used to identify low salinity hotspots in the intertidal zone to a depth of 0.35 m

Most of the sample locations around Waterloo Bay returned values around 17 mS/cm, indicating a lack of freshwater discharge. At the northern end of the bay (the blue line on Figure 47), samples were collected at a consistent frequency, similar to the rest of the bay, but GPS locations could not be recorded. All the measurements in this area had values of approximately 17 mS/cm.

Consistently low values (indicating freshwater discharge) were recorded at 2 locations: directly under the Elliston jetty, and at the far south−east corner of Waterloo Bay (Figure 47). This is consistent with the observations by local residents. Under the jetty, the area of discharge was confined to the rock outcrop directly under the jetty (Figure 46). It was not possible to measure the outflow as it appeared to be coming directly out of the rock with only ≈0.1 m of sand above the exposed rock. At the south−east corner of the bay the situation was similar; there was only about a 3 m rocky stretch where outflow could be measured, although low fluxes may also be discharging from the rock that juts out south of this area that is below the low tide mark.

Intermediate values of salinity were measured at the east end of the bay. These observations may indicate low levels of groundwater discharge, or localised outflows following a rainfall event at the site during the field sampling. Investigating and sampling these locations for the stable isotopes of water and major ion chemistry at other times of the year, for example after winter, could provide insight into the recharge and discharge processes of the low salinity lens and the variation in discharge in response to annual rainfall/recharge. Environmental age−dating tracers, such as tritium would confirm if the groundwater discharge at the seeps was recent or old groundwater and whether it is coming from a local perched aquifer beneath the sand dunes or from the regional groundwater flow system within the Quaternary Limestone aquifer.



Figure 46. Using the EC Fieldscout and the Trimble Catalyst GNSS RTK to locate groundwater discharge during low tide, Waterloo Bay

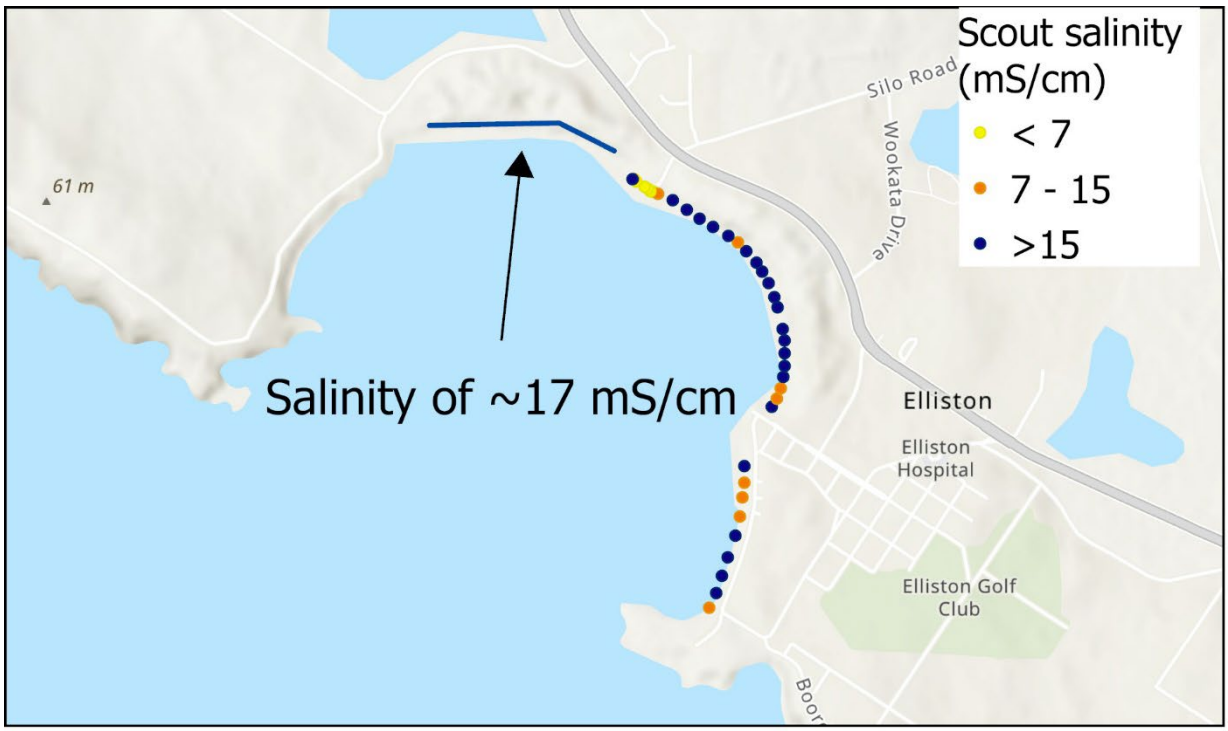


Figure 47. EC Fieldscout sample locations along Waterloo Bay at low tide 27−29 November 2024

7.5 Radon−222

The radon−222 survey tracked the nearshore of Waterloo Bay to try and identify potential submarine groundwater discharge locations. The Rad7 was deployed on a sit−on kayak, and the survey was conducted 1 to1.5 hours either side of the low tide on 28 November 2024 (Figure 48 and Figure 49). The measured radon−222 concentrations ranged from 0 to 0.07 becquerels per litre (Bq/L) and the measurement uncertainty was between 0.07 to 0.18 Bq/L. Therefore, the reported values were close to the precision of the instrument. There are some trends in the data with higher radon−222 concentrations in the intertidal zone compared to within the bay, which is likely to be associated with the wave disturbance and stirring up the beach sediment in the nearshore environment.

All these radon−222 values measured across the bay are approximately 2 orders of magnitude lower than radon−222 measurements collected in groundwater samples at nearby groundwater dependent ecosystem sites in karst limestone areas across the Eyre Peninsula (Banks and Shanafield, 2023). This suggests that radon may not be a sufficiently sensitive tracer to investigate groundwater discharge in this environment if the source concentrations are already relatively low.

Based on this radon−222 survey that was conducted in November, there is little evidence of submarine groundwater discharge into Waterloo Bay. Surveys at other times of the year or at extremely low tides would confirm if this were the case.



Figure 48. Radon−222 and water quality survey to identify potential submarine groundwater discharge within Waterloo Bay



Figure 49. Radon−222 survey of the nearshore, Waterloo Bay, 28 November 2024

7.6 Physical observations and thermal imagery

Small discrete point sources of groundwater discharge were observed directly beneath the Elliston Jetty at 0700 on Friday 29 November 2024 during low tide (0.31 mAHD). This area of the beach was the only location where there was unambiguous evidence of groundwater discharge to Waterloo Bay at the time of the survey. The sand boil beneath the jetty was discharging directly alongside the rock outcrop at the beach (fissure in the rock) and had a diameter of 2 to3 cm (Figure 50). Close−up thermal images using a DJI Mavic Enterprise thermal drone showed that the groundwater discharging had a temperature of ≈18 degrees, while the surrounding seawater was 14.5 degrees (noting that the thermal sensor measures the surface temperature reflected back to the sensor and can be slightly different to the fluid temperature) (Figure 51).

Water samples of the discharging groundwater were collected for stable isotope analysis and for major ions and were sent to CSIRO which were focusing on the environmental tracer sampling component of the project (Taylor et al., 2026).

The measured physical parameters are listed in Table 4 and compared to the ocean water at the jetty as well as the small groundwater pond adjacent to the Elliston airfield that is used for irrigation. Due to the discrete fracture that the groundwater was discharging from within the intertidal zone and the incoming tide it was challenging to collect a discrete and representative sample from the seep/sand boil. This is evident by the measured EC of the sample that is slightly less than half the measured EC of seawater within Waterloo Bay.

Table 4. Water quality of groundwater seep at Elliston Jetty, ocean water, and Elliston groundwater pond

Sample	Easting	Northing	Elevation (mAHD)	Date	Specific electrical conductivity (µS/cm)	Temp. (°C)	pH	Dissolved oxygen (mg/L)	Redox (mV)
Elliston jetty groundwater seep	488943	6278029	-0.379	29/11/24 07:30 am	22,600	19.6	7.5	5.2	-62
Ocean	488834	6277861	0	29/11/24 07:35 am	57,535	17.7	8.0	6.9	12
Elliston groundwater pond	490271	6277019	4	29/11/24 11:26 am	5,850	21.4	7.8	7.7	103



Figure 50. Close up image of a groundwater seep beneath the Elliston jetty

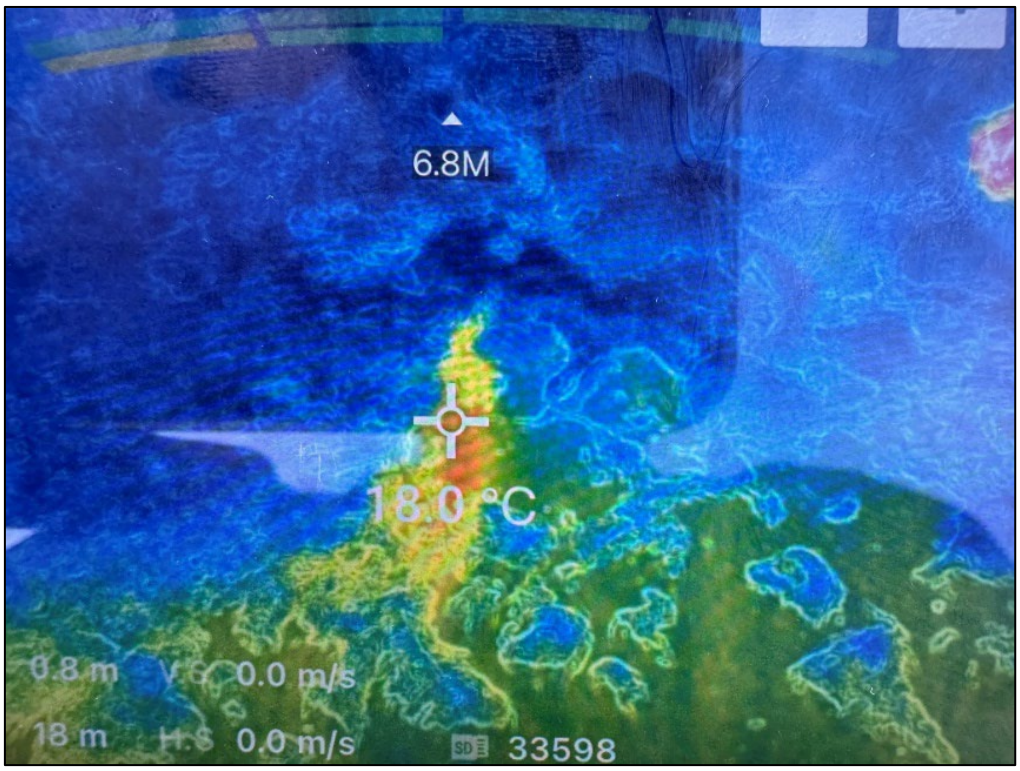


Figure 51. Close−up thermal image of a groundwater seep beneath the Elliston jetty

8 Discussion

8.1 Spatial extent of low salinity groundwater within the Quaternary Limestone aquifer

The Loupe system provides an elevated level of vertical resolution of subsurface conductivity (up to ≈50 m) and because of the higher sampling frequency there is significantly more data captured along the Loupe survey lines compared to the sTEM. The latter has a larger transmitter and can investigate greater depths (up to ≈150 m). The low salinity groundwater lens appears to be around 15 m to 35 m thick, based on subsurface conductivity values less than 50 mS/m across the Elliston−Bramfield region.

The sNMR profiles show that the aquifer properties of the Quaternary Limestone aquifer are spatially variable across this coastal landscape and that there is vertical heterogeneity, which is reflective of the lithology of the Bridgewater Formation (Lanigan, 2025). Estimated hydraulic conductivity values based on the sNMR seem plausible when compared to a limited number of downhole NMR measurements (Lanigan, 2025) as well as the values reported in a summary report by Stewart et al., (2012) and the Bramfield groundwater numerical modelling report (DEW, 2026). Further testing, that is, collection and comparison of downhole NMR, sNMR and aquifer hydraulic tests would be warranted to better understand using the non−invasive hydrogeophysical techniques to estimate hydraulic conductivities and physical properties of the Bridgewater Formation and Poelpena aquifers of interest. In turn, this can lead to improved numerical flow and solute transport models. The sNMR profiles indicate that the Bridgewater Clean Limestone is characterised by relatively small pore sizes, whereas the overlying weathered unit of the Bridgewater Formation exhibits a broader distribution of larger pore sizes. These variations in lithology and pore size distribution are likely to influence groundwater flow behaviour and consequently, how rapidly seawater may intrude inland.

8.2 Location of the interface between seawater and groundwater

Results from the TEM surveys provided valuable insights into the spatial extent, spatial variability, and depth of the interface between lower salinity groundwater (<50 mS/m) and seawater (>500 mS/m) within the Bridgewater Formation aquifer. The additional Loupe and TEM surveys that were completed in January 2026 helped to characterise the transition zone between the toe of the seawater wedge and the low salinity groundwater. Along each of the 4 West−East survey transect lines the toe of the seawater wedge extended up to 3.2 km inland at an elevation between -20 to -40 mAHD. The seawater toe is about 900 m away from SA Water production bore TWS 2A (5830−258), which has its screen between -13 to - 22 mAHD. The observed increases in EC over the last 25 to30 years (see Figure 1) in the SA Water production bores along the Birdseye Highway are likely to be a result of the seawater intruding towards the base of the Bridgewater Formation aquifer. Other studies have shown that for coastal aquifer settings the reduction in groundwater discharge towards the coast due to groundwater extraction and declining rainfall recharge is a primary driver for seawater intrusion (Costall et al., 2020; Ferguson and Gleeson, 2012; Ivkovic et al., 2013; Morgan and Werner 2015).

The downhole EM induction log and measured fluid EC at the time of drilling the new groundwater monitoring well 5830−357 (WAD049) provided confidence in the TEM surveys in identifying and locating the interface between the low salinity groundwater and seawater intrusion. According to the geological log at 5830−357 (WAD049), the base of the Bridgewater Formation is at 49 m depth overlaying what appeared to be the St Peter Suite (granite), which is considered basement to the much younger overlying formations.

The nature of the basement topography, the bedding plane angle and variation in depth to the basement rock is likely to be a contributing factor to the extent and rate of seawater intrusion within the Bridgewater Formation, which lies unconformably on top. The sTEM datasets show that the subsurface conductivity decreases beneath the wedge, which suggests that this is the top of the basement and that seawater intrusion may be tracking along this geological boundary, which is on a slight incline heading inland.

Additional drilling between 5830−357 (WAD049) and the TWS production bores would be able to help verify if this is the case. Already groundwater salinity data from TWS bores indicates a rising trend (see Figure 1). While still within drinking water guidelines (EC= 1,600 μS/cm; TDS= 1,000 mg/L), this trend suggests that the influence of saline water diffusion and dispersion within the aquifer may be more significant than previously assumed.

8.2.1 Forward modelling

Forward modelling is an often−underutilised tool that is used to understand the limits of a given geophysics system, in this case the sTEM profiler. It also helps assess how effective the data processing and inversion routines are that are used to generate representations of the conductivity structure of the subsurface.

Several scenarios were evaluated to determine the character of the transition (interface) between the low salinity groundwater and the seawater wedge and how the forward modelling results could be used to determine whether the transition is likely to be sharp versus diffuse, and what this implies for potential salinity impacts ahead of the toe. Assuming that our interpretation of the depth of the contact is correct from the electromagnetic induction log 5830−357 (WAD049), it appears that the vertical transition occurs over a depth of ≈3 m.

Examination of the forward modelling results presented in (Figure 33 and Figure 38) suggests that the transition is likely to be Very sharp to sharp (that is, occurring abruptly at the interpreted depth, to occurring over a depth interval of 10 m), but is tending toward Very sharp. Assuming that there is a sharp vertical transition zone across the Elliston−Bramfield region, suggests that the degree of hydrodynamic dispersion is low and that there is reasonable groundwater flow within the aquifer. The horizontal or lateral aquifer dispersivity is likely to be an order of magnitude higher than the vertical dispersivity and therefore the lateral extent of the transition or mixing zone would stretch potentially hundreds of meters, depending on local flow conditions and the aquifer properties of the Bridgewater Formation.

To examine this further would require a variable−density solute transport model to explore and help interpret the transition zone ahead of the seawater wedge toe and the TWS production bores further inland. Also, the transition zone is dynamic and likely to oscillate seasonally with recharge variability and the impacts of groundwater pumping and therefore a transient variable−density solute transport model would provide greater insights.

8.3 Locations of submarine groundwater discharge around Waterloo Bay

Continuous geophysical surveys, supported by intertidal salinity measurements and thermal camera observations, identified discrete zones of lower−salinity groundwater discharging at the coast around Waterloo Bay. The most significant discharge was located directly beneath the jetty, where groundwater emerged at several discrete points. Additional discharge appears to occur at the margins of the Bay and at the topographic break where Beach Terrace meets the Esplanade on the eastern side; however, no visual confirmation of these locations was obtained. All discharge locations correspond with localised structural features in the surface geology (DEW, 2026 – Bramfield Groundwater Model Report, Figure 2.3).

The source of groundwater discharging near the jetty remains uncertain, primarily due to the absence of suitably constructed observation wells at sufficient depth in the vicinity. The nearest groundwater observation well 5830−71 (WAD032) is located 300 m inland, is only a few metres deep and was hand−dug for windmill installation. Its shallow depth and limited historical water level record make it unsuitable for interpreting aquifer responses to recharge or pumping.

Water level data from wells further inland indicate a very low hydraulic gradient across the shallow Quaternary Limestone aquifer from the coast toward the TWS production bores. This almost−flat gradient means that even modest changes such as reduced recharge or increased groundwater pumping, could meaningfully affect both coastal discharge and discharge to low−lying wetlands inland, such as Lake Hamp and Myrtle Swamp. Water level data prior to 2015 is sparse, but significant declines had already occurred in the northern aquifer beyond Bramfield by that time, suggesting similar declines likely occurred in the coastal zone as well.

The available evidence, including hydrogeophysics surveys and environmental tracer sampling (Taylor et al., 2026), suggests that coastal discharge near the jetty likely reflects a combination of two sources: 1) localised recharge, event−driven flow through coastal dunes following rainfall events; and 2) regional discharge from the shallow Quaternary Limestone aquifer system, potentially supplemented by deeper Tertiary aquifer contributions.

Anecdotal observations from a local resident that jetty freshwater flows occur following rainfall support the first mechanism. However, the similar hydraulic conditions across the aquifer make it difficult to definitively separate these contributions at this stage.

These findings are based on a single survey period conducted under antecedent dry conditions, and temporal variability in both recharge and discharge is likely to be significant. Radon sampling within the Bay did not identify substantial submarine groundwater discharge beyond the tidal zone, suggesting that coastal discharge is not a major component of the regional water balance. Higher rates of groundwater discharge in the Elliston region are more likely associated with the low−lying wetlands surrounding the township, where the watertable is shallow and evapotranspiration losses are elevated.

To refine the conceptual model and better constrain the contributions to coastal discharge, the following are recommended:1) installation of new observation wells between the coast and the TWS bores, constructed to adequate depth within the Quaternary Limestone, 2) time−series water level and salinity monitoring to capture responses to rainfall and pumping, and 3) additional environmental tracer sampling, including the use of stable isotopes of the water molecule and water age dating

(e.g., tritium, chlorofluorocarbons and carbon−14), to differentiate water sources and establish groundwater flow paths.

9 Conclusions

The near−surface geophysical datasets collected in October and November 2024, and January 2026, provided detailed characterisation of the spatial extent of the low−salinity Elliston–Bramfield groundwater lens and the potential risk of seawater intrusion to the town water supply production bores. The data acquisition from Loupe and sTEM TEM systems were complementary with the west–east transects extending inland from the coast to characterise subsurface aquifer conditions. The Loupe system provided higher−resolution detail in the near surface to depths of approximately 50 m, while the sTEM system achieved investigation depths of up to 180 m at some locations and provided additional information in areas where the depth to groundwater exceeded 50 m.

The inverted TEM subsurface conductivity models indicate that seawater intrusion extends approximately 3.2 km inland from the coast, with the toe of the seawater wedge occurring at elevations between approximately -20 mAHD and -40 mAHD. Low subsurface conductivity features (<≈50 mS/m) identified in both the Loupe and sTEM datasets likely represent the thickness and lateral extent of the low−salinity groundwater lens within the Quaternary Limestone aquifer. Across the surveyed areas, the lens thickness is estimated to range from approximately 10 to 30 m.

The sNMR soundings provided direct measurements of water content and differentiated between mobile water (free−draining water that contributes to the specific yield of the aquifer) and bound water more tightly held within the fine−grained sedimentary material of the aquifer. Across the 14 sNMR soundings, the median total water content over the saturated thickness of the aquifer (defined here as extending from the estimated watertable depth to the depth of resolution of the NMR inversion) was 14.1%, with a median mobile water content of 5.3% and median bound water content of 2.2%. However, some locations and depths recorded substantially higher values, with total water content reaching up to 49%, mobile water up to 42%, and bound water up to 41%. The spatial distribution of the survey sites indicates significant heterogeneity both laterally and with depth across the Quaternary Limestone aquifer, reflecting the variable lithology and aquifer properties of the Bridgewater Formation.

The median estimated saturated hydraulic conductivity derived from the sNMR model inversions was 5.4 m/day (geometric mean of 3.5 m/day), with values locally exceeding 56 m/day within parts of the Quaternary Limestone aquifer.

The near−surface geophysical datasets collected in 2024 provided an initial characterisation of the spatial extent of the low−salinity Elliston–Bramfield lens and the potential threat of seawater intrusion. The additional TEM surveys undertaken in January 2026 increased confidence in these interpretations and improved vertical and horizontal resolution of the depth to the seawater wedge and inland extent of the seawater toe. The higher spatial density of the sTEM soundings verified the changes in the subsurface conductivity between the toe and the TWS bores and the likely horizontal extent of the transition zone ahead of the toe. Based on the 4 west–east transects, the seawater wedge extends approximately 3.2 km inland from the coast, with the toe located within 900 m from SA Water production bore TWS 2A (5830−258).

The forward modelling exercise validated the detection limits of the sTEM system for being able to determine the depth to the interface between low−salinity groundwater and intruding seawater. Across the 4 conceptual models tested and 2 different scenarios, the depth to the interface could be detected when the transition zone was moderately diffuse at a depth of 30 m (as was observed in this study), but not when it became highly diffuse. The modelling also showed that the interface could be determined with reasonable resolution to a depth of ≈70 m. To reduce ambiguity in future

investigations, the application of additional geophysical methods may improve characterisation of more diffuse seawater interfaces.

9.1 Future recommendations

Based on the findings from this component of the project there are several new insights that have improved our understanding of the conceptual hydrogeological model for the Elliston and Bramfield area. The project findings have also revealed other data and knowledge gaps and investigations that could be undertaken to improve the long−term management and water security of the low salinity lens.

These include:

- establishing a second monitoring well, approximately 100 to 150 m east of 5830−357 (WAD049) towards the TWS production bores. The drillhole should fully penetrate the limestone and any Tertiary sands into the basement then be partially backfilled and completed in the limestone to provide a monitoring point for the limestone aquifer. This well would serve two purposes: 1) Groundwater wells are easy to use to monitor water levels and water quality and, equipped with a level and EC logger within the production zone, would provide an effective management strategy to track the rate of seawater intrusion, and 2) provide additional geological and hydrogeological information of the Tertiary Poelpena Formation and the basement rock underlying the Bridgewater Formation in this area. The presence and absence of the Poelpena Formation as well as the Sleaford Complex and St Peter Suite basement rocks and their depositional structure and orientation are likely to influence the rate of advancement of the seawater intrusion inland. This knowledge will provide critical information about the shape of this interface and how it may influence the rate of seawater intrusion further inland under different recharge and groundwater pumping scenarios.

- combining the acquisition of hydrogeophysical data sets as part of this project with newly planned AEM surveys that are intended to traverse from the coast inland towards Bramfield. would help resolve some of the spatial and depth resolution challenges with land−based TEM. AEM surveys provide large spatial coverage and greater depth of investigation but often compromise near surface resolution. Ideally this would involve a joint/coupled inversion if manipulation of the raw data is possible; otherwise, they would be assessed separately using the same model inversion parameters and settings.

- time series monitoring of hydrogeophysics surveys along one of the TEM survey transect lines to investigate the rate of change in the movement of seawater intrusion inland towards the SA Water TWS production bores. For example, surveys could be repeated every 3 to 6 months for several years to determine if the seawater toe is migrating inland or changing in response to changes in the water balance.

- constructing a third monitoring well (preferably a nest of 2 wells completed at different depths) adjacent to the shallow wetlands near the Elliston aerodrome to investigate and monitor groundwater discharge to these low−lying surface water features that are below 0 mAHD. The deepest drillhole should fully penetrate the limestone and any Tertiary sands into the basement then be partially backfilled and completed in the limestone to provide a monitoring point for the limestone aquifer. The screen depth of the shallower well would be completed at an elevation ≈10 metres higher so that the vertical hydraulic gradient can be measured. This gradient together with an estimate of the hydraulic conductivity (for example from sNMR results) would allow for

the specific discharge to be calculated. The limited evidence of high coastal groundwater discharge at Waterloo Bay suggests that regional groundwater discharge towards these low−lying surface features may be a critical component of the water balance.

- using a numerical modelling to investigate how hydrogeological conceptualisation and setting influence the seawater interface under additional groundwater extraction. A Variable−Density Flow and Transport (VDFT) model in MODFLOW 6 would be suitable. The previously developed groundwater flow model would serve as the foundation for a two−dimensional VDFT model, aligned with a hydrogeophysical transect extending from the coast to the inland boundary. This proposed work would aim to enhance ongoing efforts by refining our understanding of the fresh water–seawater interface in the Elliston area over a much longer time scale. It would provide additional insights into changes to the groundwater quality and complement existing modelling initiatives. Groundwater salinity data from the Elliston TWS production bores indicate a rising salinity trend. While still within drinking water guidelines (TDS <1,000 mg/L), this trend suggests that the influence of saline water diffusion and dispersion within the aquifer may be more significant than previously assumed.

10 References

Auken E., Christiansen A.V., Kirkegaard C., Fiandaca G., Schamper C., Behroozmand A.A., Binley A., Nielsen E., Effersø F., Christensen N.B., Sørensen K., Foged N. & Vignoli G., (2015). An overview of a highly versatile forward and stable inverse algorithm for airborne, ground−based and borehole electromagnetic and electric data. Exploration Geophysics, 46, 223−235.

Banks, E.W. and Shanafield, M.A., (2023). Eyre Peninsula River Red Gum Groundwater Dependent Ecosystem Investigation. Report produced for the Eyre Peninsula Landscape Board, South Australian Government (Final report version 1.1. 21 July 2023).

Christiansen A.V. and Auken E., (2012). A global measure for depth of investigation. Geophysics, 77, WB171−WB177.

Costall AR, Harris BD, Teo B, Schaa R, Wagner FM & Pigois JP (2020) *Groundwater Throughflow and Seawater Intrusion in High Quality Coastal Aquifers*. Scientific Reports, 10, 9866. https://doi.org/10.1038/s41598-020-66516-6.

Davis, A.C., Munday, T.J., and Ibrahimi, T., (2025). Limestone Coast Airborne Electromagnetic Survey: Acquisition, Processing and Modelling. Goyder Institute for Water Research Technical Report Series No. 25/5.1. Goyder Institute for Water Research.

Davis, A. C., and Munday, T. J. (2025). Adaptation of the South−Eastern drainage system under a changing climate Limestone Coast Airborne Electromagnetic Survey: Conductivity−Depth Sections. Goyder Institute for Water Research.

Department for Environment and Water (DEW), (2021). Musgrave and Southern Basins Prescribed Wells Area 2019–20 water resources assessment, DEW Technical Note 2021/15, Government of South Australia, Department for Environment and Water, Adelaide.

Department for Environment and Water (DEW), (2022). Musgrave and Southern Basins Prescribed Wells Area: 2020–21 water resources assessment, DEW Technical Note 2022/18, Government of South Australia, Department for Environment and Water, Adelaide.

Department for Environment and Water (DEW), (2026). Bramfield groundwater model, DEW Technical report 2026/01, Government of South Australia, Department for Environment and Water, Adelaide.

Department for Environment, Water and Natural Resources (DEWNR), (2016). Musgrave PWA Bramfield lens 2015 Groundwater level and salinity status report, Government of South Australia, through the Department of Environment, Water and Natural Resources, Adelaide.

Duncan, A., Williams, P., Turner, G., Amann, B., Tully, T., O'Keeffe, K., Wellington, A., (1998). Examples from a new EM and electrical methods receiver system: Exploration Geophysics, 29, 347−354.

Evans, S.L., (2002). Musgrave Prescribed Wells Area groundwater monitoring status report 2002, DWLBC report 2002/23, Government of South Australia, Department of Water, Land and Biodiversity Conservation, Adelaide.

Ferguson, G. and Gleeson, T. (2012). Vulnerability of coastal aquifers to groundwater use and climate change. Nature Climate Change 2(5): 342−345. DOI: 10.1038/nclimate1413.

Flint, R.B., (1992). Explanatory notes for the ELLISTON 1:250 000 Geological Map, Government of South Australia, through Department of Mines and Energy, Geological Survey of South Australia, Adelaide.

Gholami, A., Werner, A.D., Solórzano−Rivas, C., Jazayeri, A., Kamali Maskooni, E. and Fan, H., (2025). Adaptation of the South−Eastern drainage system under a changing climate. Seawater intrusion risk. Goyder Institute for Water Research.

Ivkovic, K.M., Marshall, S.K., Carey, H., Morgan, L.K., Sundaram, B., Dixon−Jain, P, Caruana, L., Garlapati, N., and Werner, A.D., (2013). A national−scale vulnerability assessment of seawater intrusion: Coastal aquifer typology. Record 2013/04. Geoscience Australia, Canberra, and National Centre for Groundwater Research and Training, Adelaide.

Lanigan, L. (2025). Greater Bramfield Geophysical & Stratigraphic Analysis 2024−2025, DEW Technical Memo. Government of South Australia, Department for Environment and Water, Adelaide.

Lawrie, K.C., Carey, H., Christensen, N.B., Clarke, J.C., Lewis, S., Ivkovic, K.M. and Marshall, S.K., (2012). Evaluating the role of airborne electromagnetics in mapping seawater intrusion and carbonate−karstic groundwater systems in Australia. Canberra, Australia: Geoscience Australia.

Lesmes, D.P., Friedman, S.P., (2005). Relationships between the electrical and hydrogeological properties of rocks and soils. In: Rubin, Y., Hubbard, S.S. (Eds.), Hydrogeophysics. Springer Netherlands, Dordrecht, pp. 87−128. DOI:10.1007/1−4020−3102−5_4.

Ley−Cooper, A.Y., Munday, T., Gilfedder, M., Ibrahimi, T., Annetts, D. and Cahill, K., (2015). Inversion of legacy airborne electromagnetic datasets to inform the hydrogeological understanding of the northern Eyre Peninsula, South Australia, Goyder Institute for Water Research. Adelaide, Australia.

McNeill, J.D., (1980). Electromagnetic terrain conductivity measurement at low induction numbers. Technical Note 6, Geonics Limited, Ontario.

Morgan, L.K. and Werner, A.D. (2015). A national inventory of seawater intrusion vulnerability for Australia. Journal of Hydrology: Regional Studies 4: 686−698. DOI:10.1016/j.ejrh.2015.10.005.

Palacky, G.J., (1987). Resistivity Characteristics of Geologic Targets. In: Nabighian, M.N. (Ed.), Electromagnetic Methods in Applied Geophysics: Volume 1, Theory. Society of Exploration Geophysicists, pp. 0. DOI:10.1190/1.9781560802631.ch3.

Reid, A.J., et al., (2020). Resolving tectonic settings of ancient magmatic suites using structural, geochemical and isotopic constraints: the example of the St Peter Suite, southern Australia. Australian Journal of Earth Sciences, 67(1): p. 31−58.

Stewart, S., Alcoe, D. and Risby, L., (2012). Science Support for the Musgrave and Southern Basins Prescribed Wells Areas Water Allocation Plan, DFW Technical Report 2012/15, Government of South Australia, through Department for Water, Adelaide.

Street, G., Duncan, A., Fullagar, P., Tresidder, R., (2018). LOUPE − A Portable EM Profiling System. ASEG Extended Abstracts, 2018(1): 1−3. DOI:10.1071/ASEG2018abW10_3G.

Taylor, A.R., Deslandes, A., Priestley, S.C. and Shanafield, M. (2026). Characterising groundwater recharge to the Bramfield lens of the Quaternary Limestone Aquifer, Eyre Peninsula, South Australia. A technical report from CSIRO to the Department for Environment and Water. CSIRO, Australia.

Twidale, C.R. and Bourne, J.A., (2000). Dolines of the Pleistocene dune calcarenite terrain of western Eyre Peninsula, South Australia: a reflection of underprinting? Geomorphology, Volume 33, Issues 1–2, pages 89−105. DOI: 10.1016/S0169−555X(99)00112−9.

Appendix A

Summary of the forward modelling results presented in the figures below.

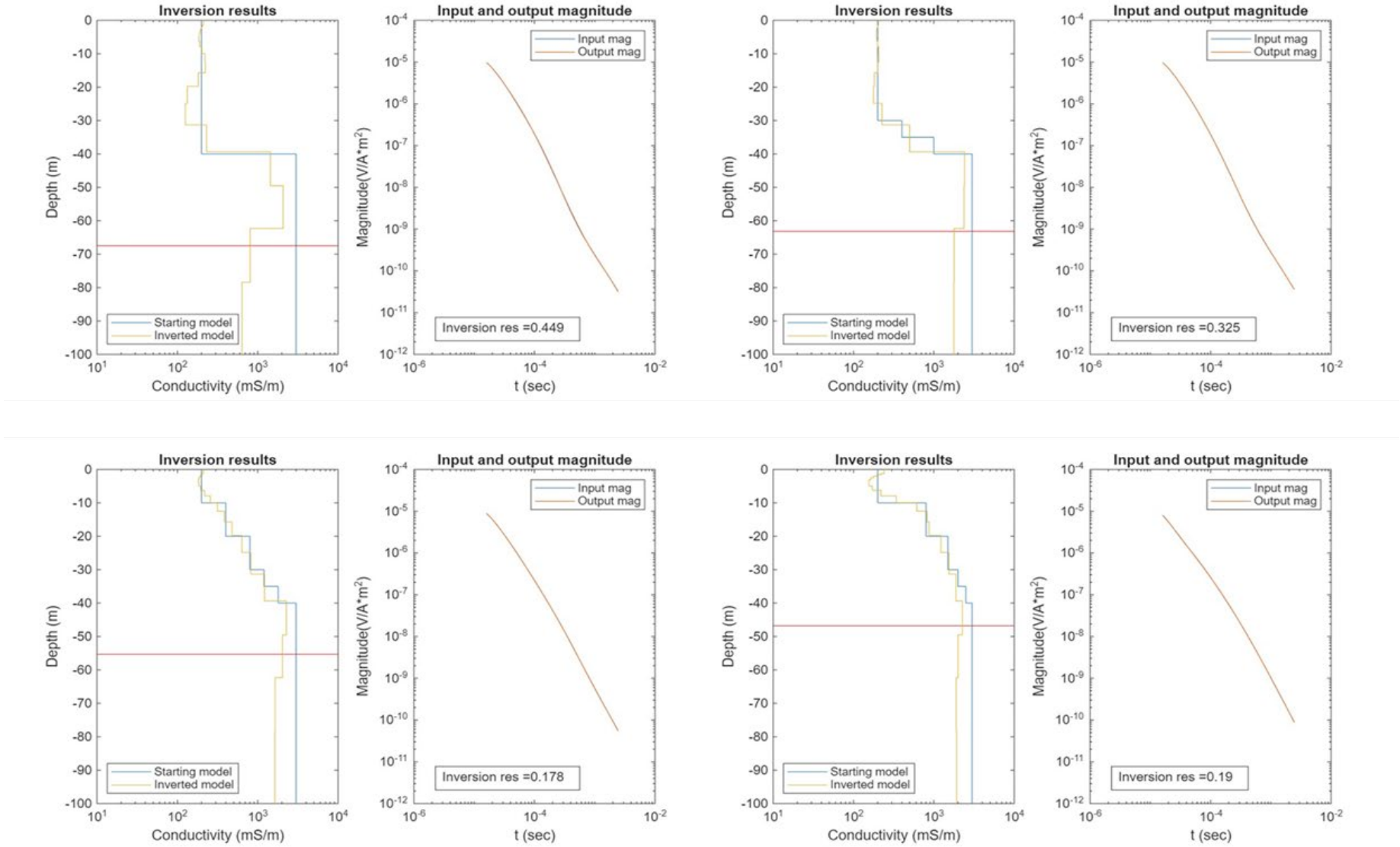


Figure 52. Scenario 1: Modelling results of the four different conceptual models of the seawater intrusion interface (very sharp, sharp, diffuse, and very diffuse) at 40 m depth. Left plot in each subfigure shows inverted results in blue and starting model in orange. Horizontal line is the depth of investigation. Right plot in each subfigure shows model fit

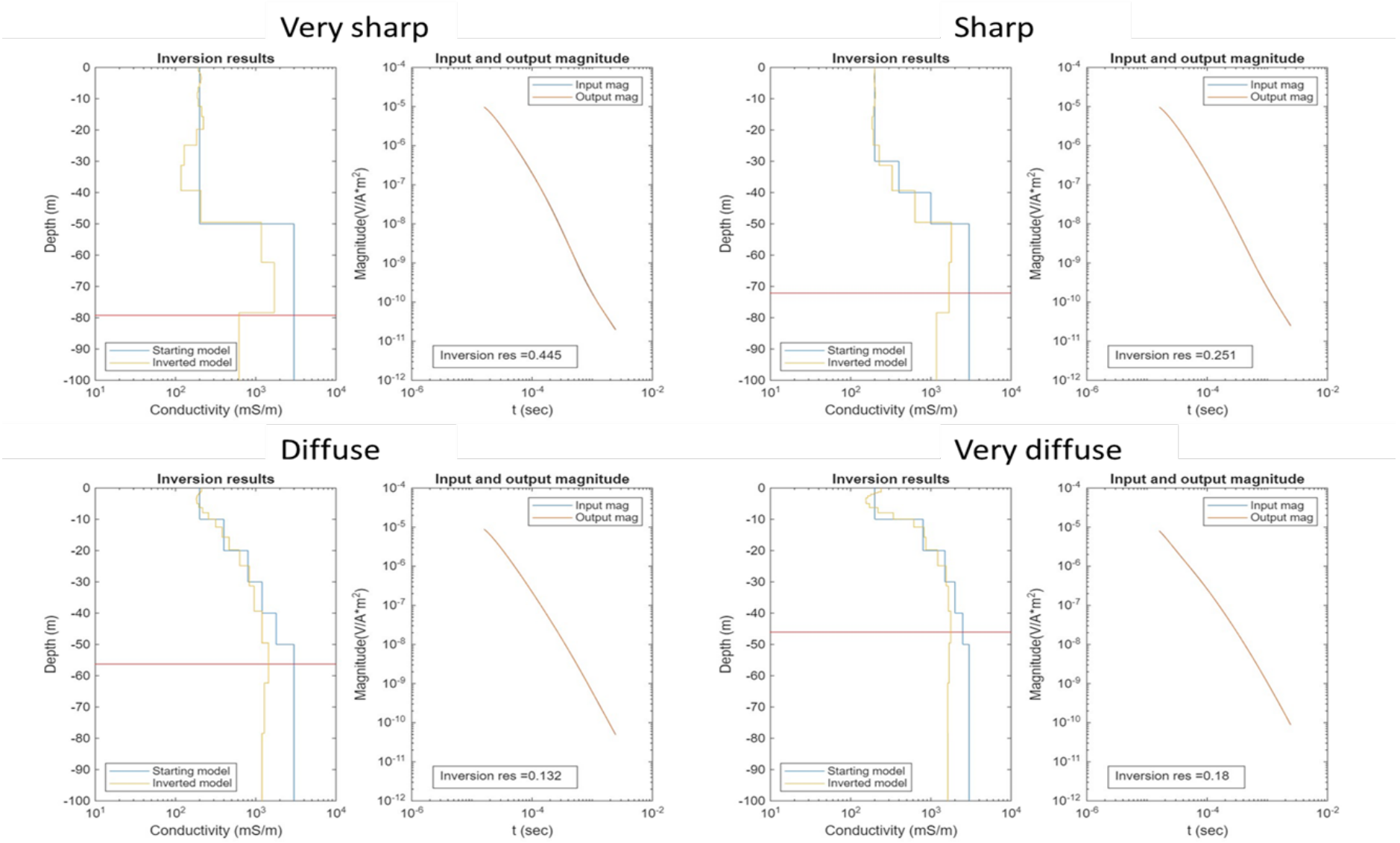


Figure 53. Scenario 1: Modelling results of the four different conceptual models of the seawater intrusion interface (very sharp, sharp, diffuse, and very diffuse) at 50 m depth. Left plot in each subfigure shows inverted results in blue and starting model in orange. Horizontal line is the depth of investigation. Right plot in each subfigure shows model fit

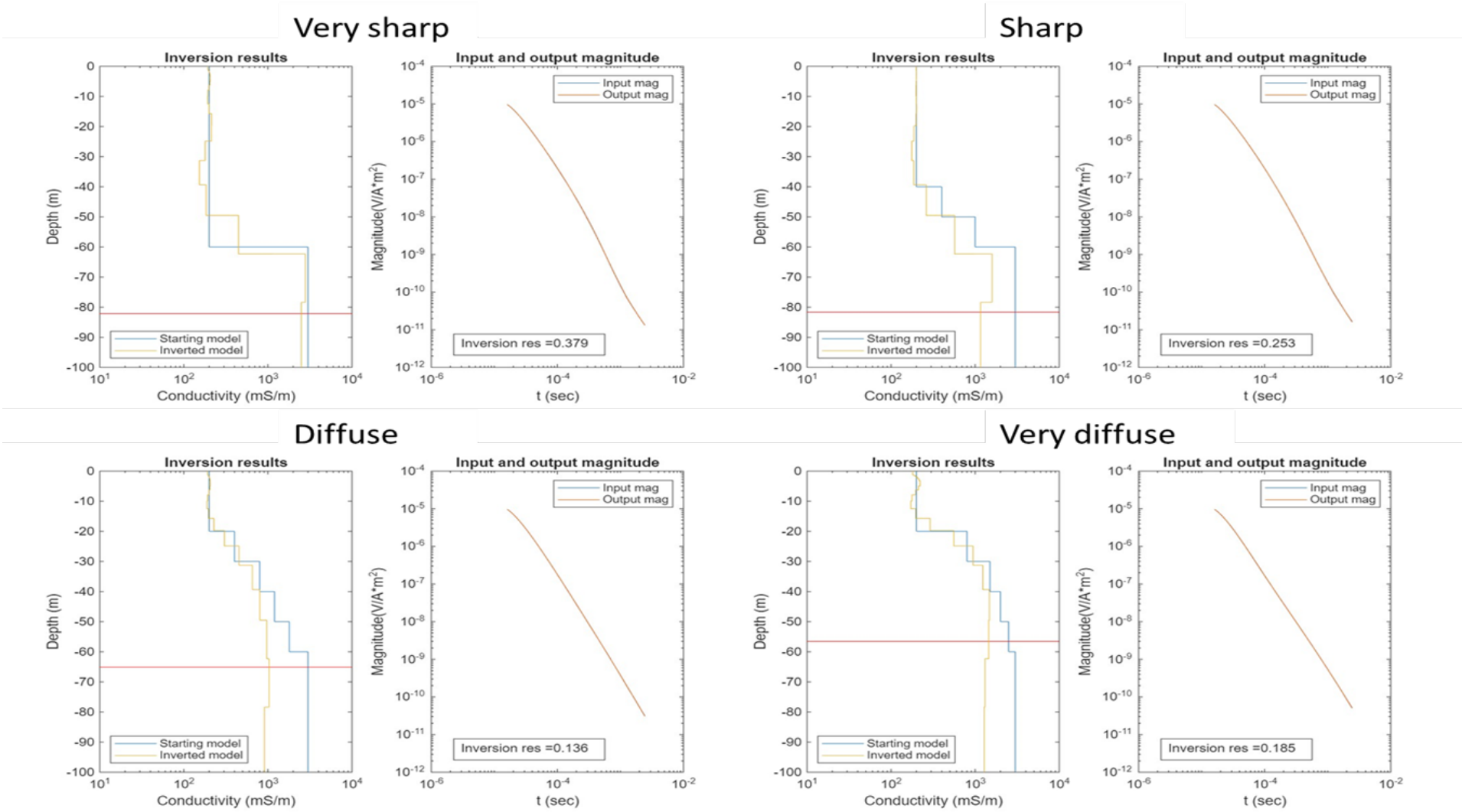


Figure 54. Scenario 1: Modelling results of the four different conceptual models of the seawater intrusion interface (very sharp, sharp, diffuse, and very diffuse) at 60 m depth. Left plot in each subfigure shows inverted results in blue and starting model in orange. Horizontal line is the depth of investigation. Right plot in each subfigure shows model fit.

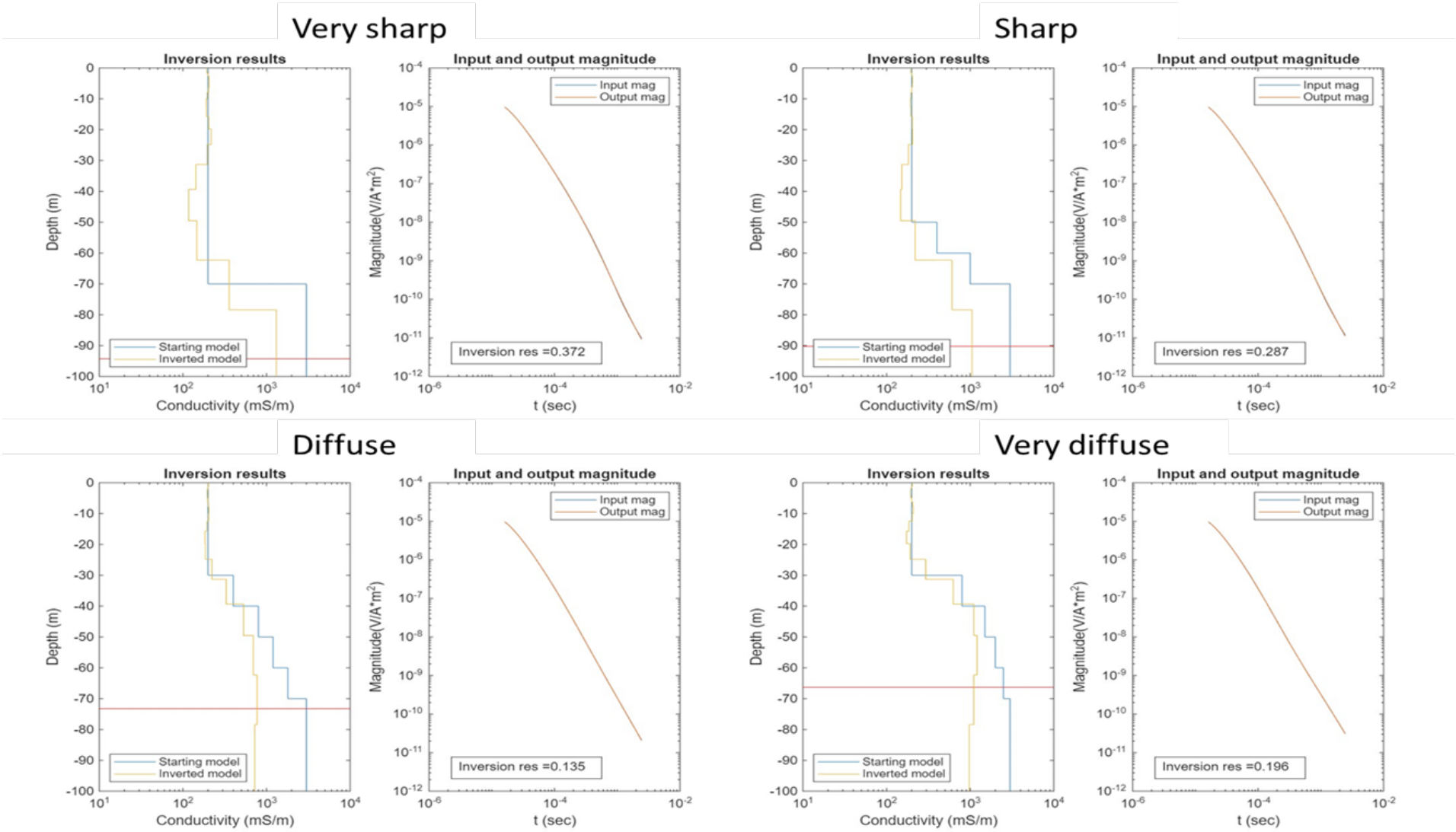


Figure 55. Scenario 1: Modelling results of the four different conceptual models of the seawater intrusion interface (very sharp, sharp, diffuse, and very diffuse) at 70 m depth. Left plot in each subfigure shows inverted results in blue and starting model in orange. Horizontal line is the depth of investigation. Right plot in each subfigure shows model fit

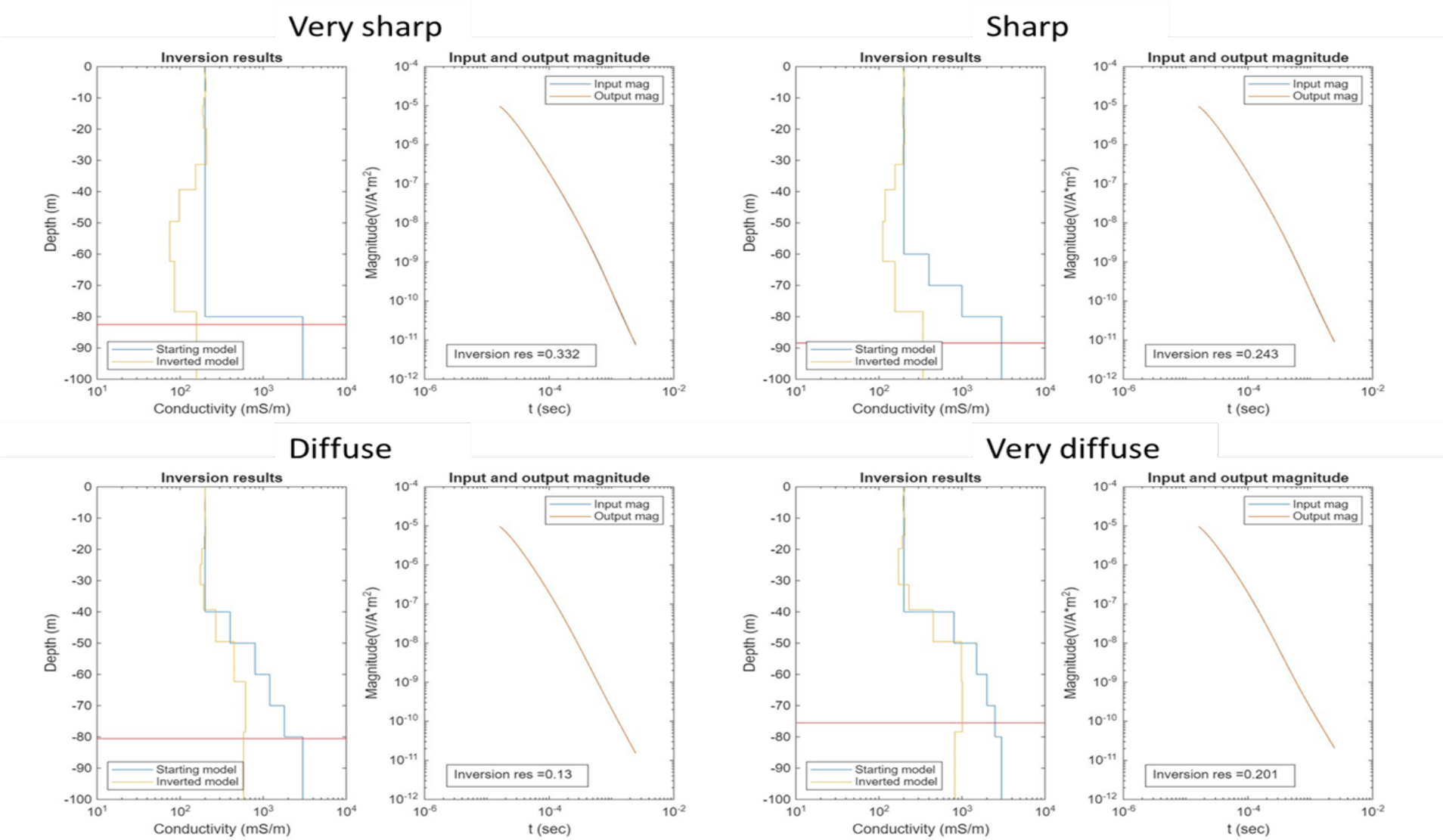


Figure 56. Scenario 1: Modelling results of the four different conceptual models of the seawater intrusion interface (very sharp, sharp, diffuse, and very diffuse) at 80 m depth. Left plot in each subfigure shows inverted results in blue and starting model in orange. Horizontal line is the depth of investigation. Right plot in each subfigure shows model fit

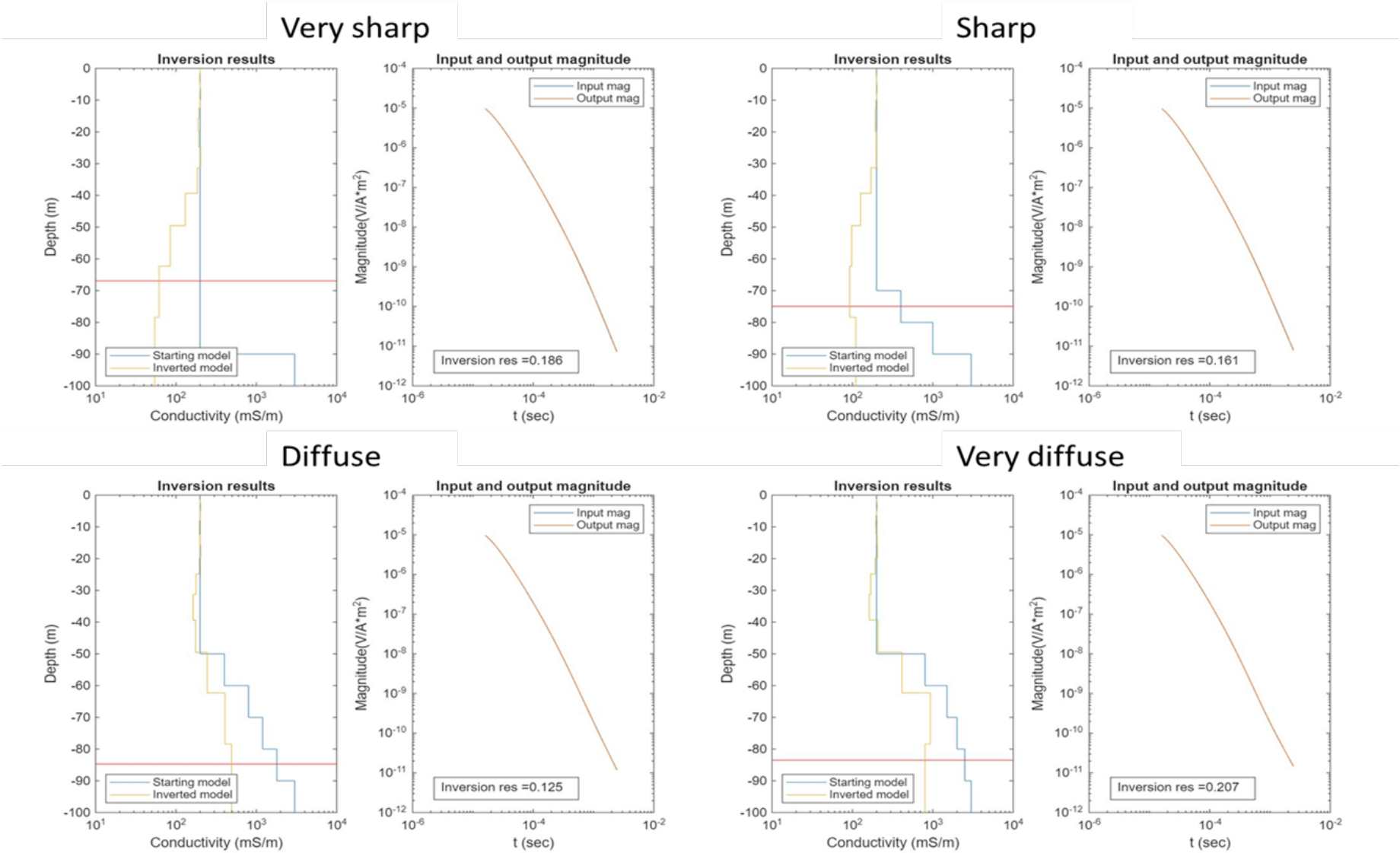


Figure 57. Scenario 1: Modelling results of the four different conceptual models of the seawater intrusion interface (very sharp, sharp, diffuse, and very diffuse) at 90 m depth. Left plot in each subfigure shows inverted results in blue and starting model in orange. Horizontal line is the depth of investigation. Right plot in each subfigure shows model fit

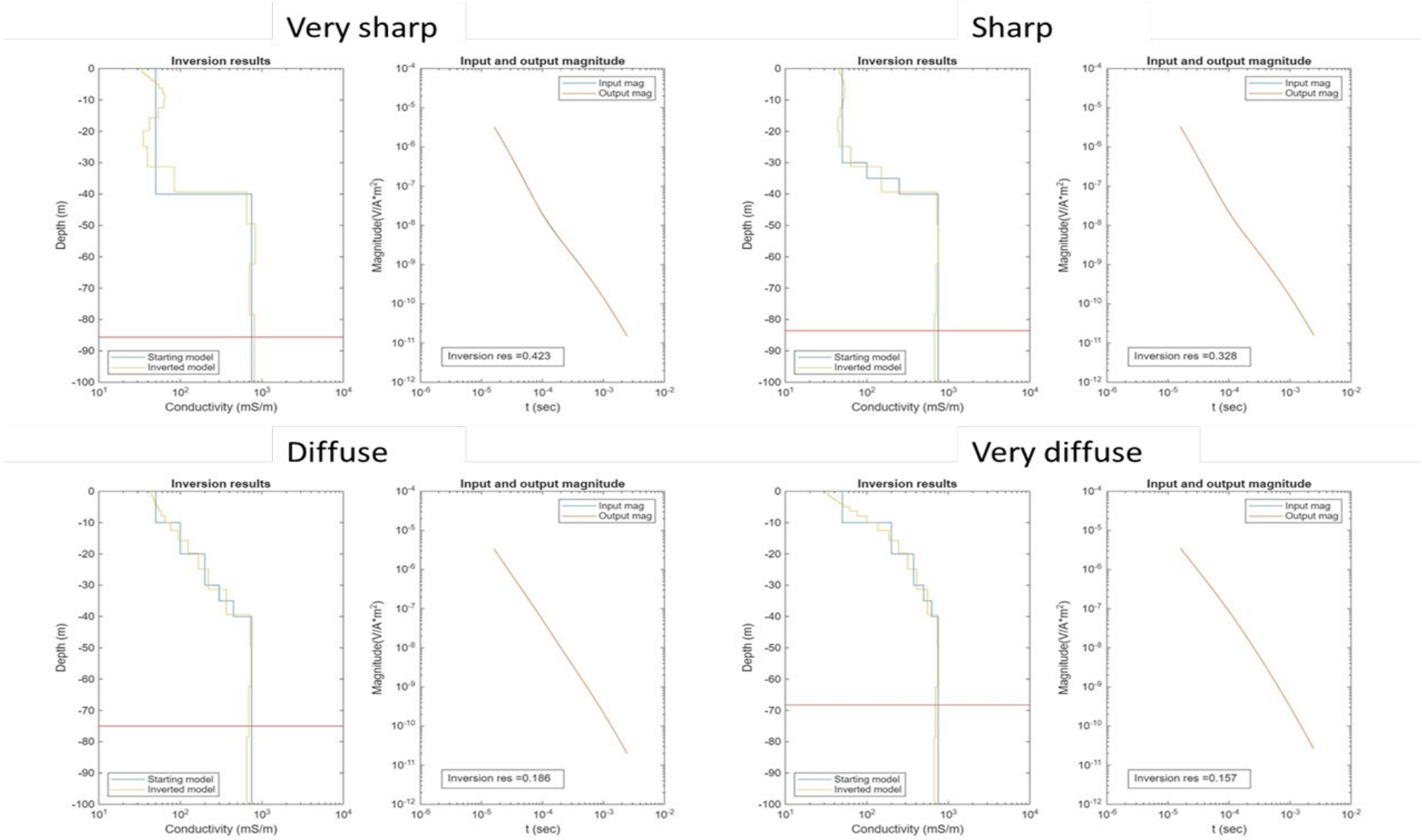


Figure 58. Scenario 2: Modelling results of the four different conceptual models of the seawater intrusion interface (very sharp, sharp, diffuse, and very diffuse) at 40 m depth. Left plot in each subfigure shows inverted results in blue and starting model in orange. Horizontal line is the depth of investigation. Right plot in each subfigure shows model fit

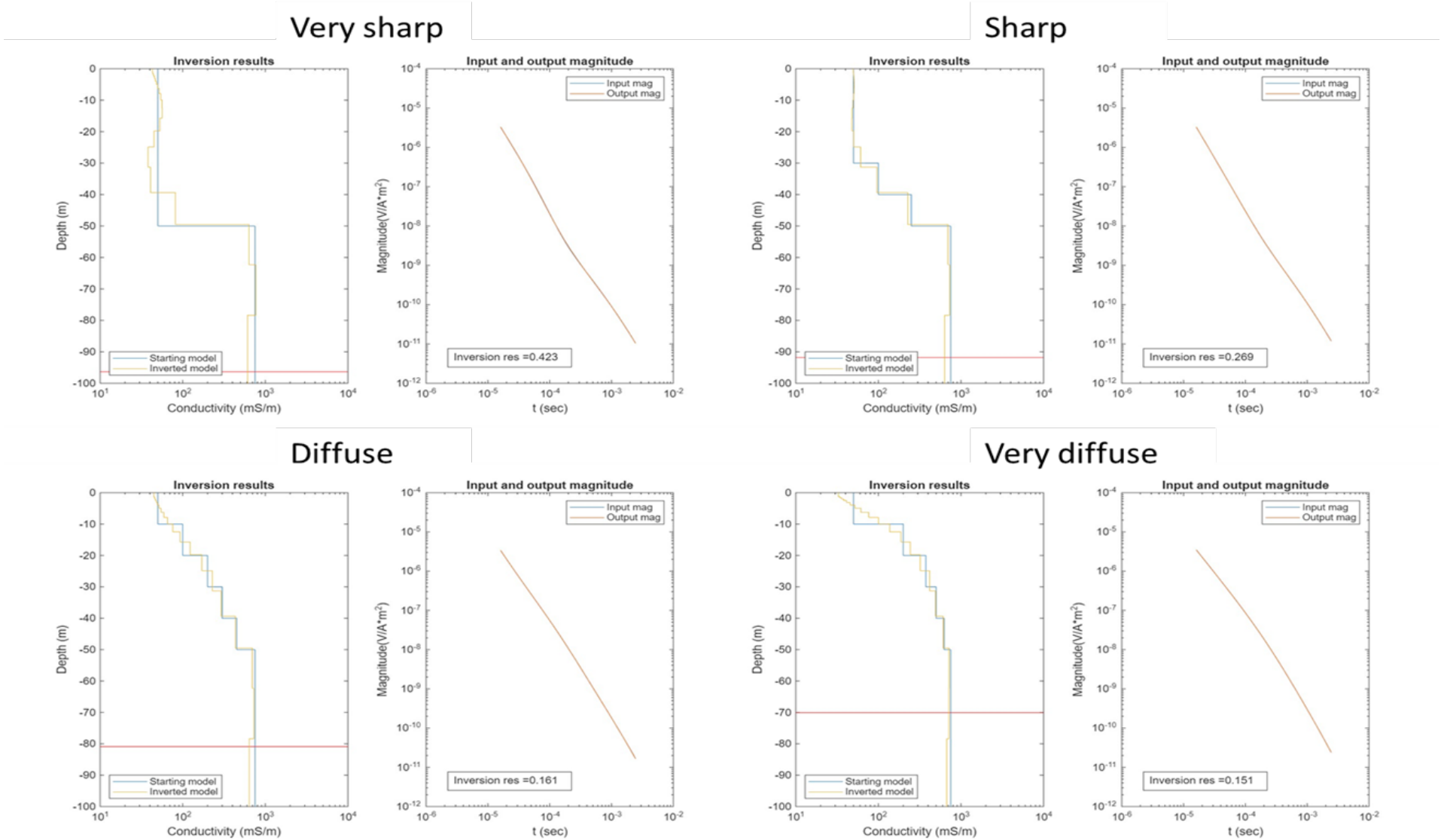


Figure 59. Scenario 2: Modelling results of the four different conceptual models of the seawater intrusion interface (very sharp, sharp, diffuse, and very diffuse) at 50 m depth. Left plot in each subfigure shows inverted results in blue and starting model in orange. Horizontal line is the depth of investigation. Right plot in each subfigure shows model fit

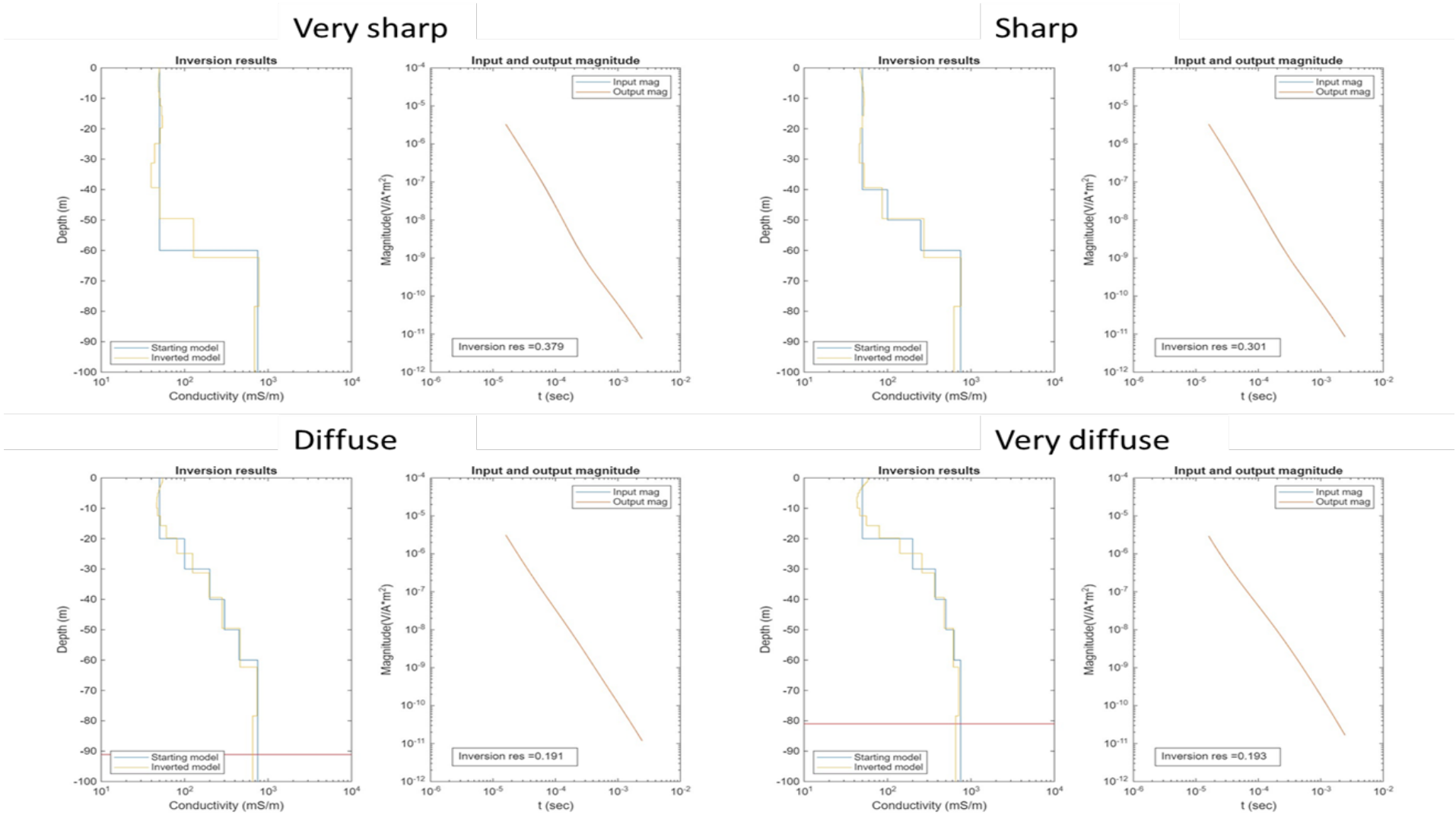


Figure 60. Scenario 2: Modelling results of the four different conceptual models of the seawater intrusion interface (very sharp, sharp, diffuse, and very diffuse) at 60 m depth. Left plot in each subfigure shows inverted results in blue and starting model in orange. Horizontal line is the depth of investigation. Right plot in each subfigure shows model fit

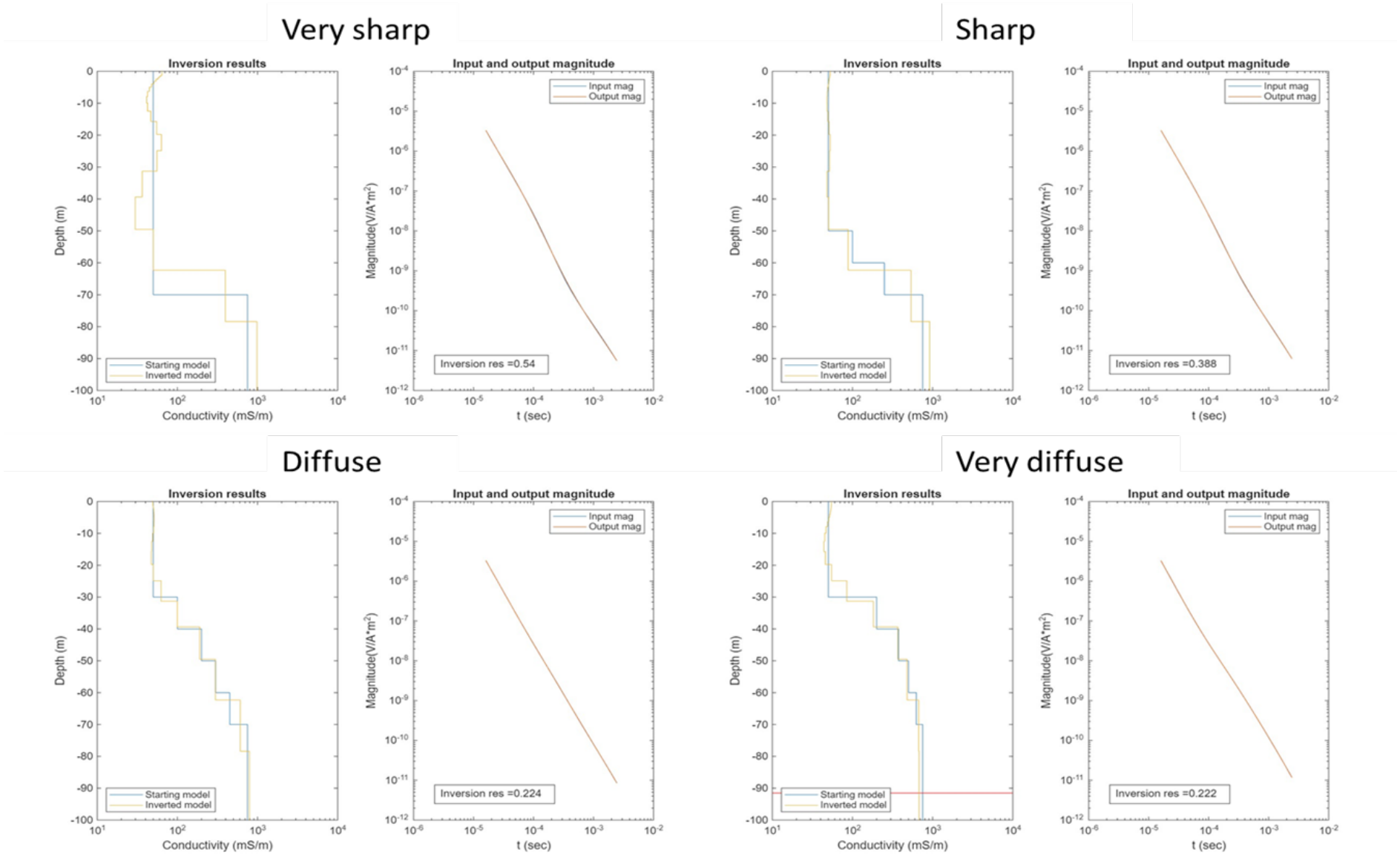


Figure 61. Scenario 2: Modelling results of the four different conceptual models of the seawater intrusion interface (very sharp, sharp, diffuse, and very diffuse) at 70 m depth. Left plot in each subfigure shows inverted results in blue and starting model in orange. Horizontal line is the depth of investigation. Right plot in each subfigure shows model fit

11 Appendix B

All hydrogeophysics data sets collected as part of the project are stored digitally and the .csv output file format makes it straight forward for the data sets to be replotted and displayed using programs such as ArcGIS Pro or QGIS. These data sets have been shared with DEW which will make the necessary arrangements for archiving the data.

1. The raw data, post−processed average raw data, and the generated data files from the Aarhus inversion for the Loupe and sTEM are contained in the following data file format:

    a. YYYY_MM_DD_site_Loupe/sTEM (All raw data)

    b. YYYY_MM_DD_site_Loupe/sTEM_processed_COND_mSm_AVG_export.xyz (All post−processed average raw data)

    c. YYYY_MM_DD_site_Loupe/sTEM_COND_mSm__MOD_dat.xyz ()

Note: The file formats include various data and model inputs. The '*_dat.xyz file' is the collected data that was used in the inversion. The '*_syn.xyz file' is the synthetic forward calculation of the final model in the model inversion. The '*_inv.xyz file' includes details describing the model. All of these are in the Aarhus Workbench XYZ format and can be opened in any text editor program.

2. sNMR outputs from the model inversion for all sites are exported as .csv files as well as figures.



Flinders University



NATIONAL CENTRE FOR GROUNDWATER RESEARCH AND TRAINING